REPORT DOCUMENTATION PAGE

Form Approved
OMB No. 0704-0188

1. AGENCY USE ONLY (Leave Blank)	2. REPORT DATE	3. REPORT TYPE AND DATES COVERED
	1/21/02	Phase I and Phase I Option Final Report, 2-1-00 to 12-30-01

4. TITLE AND SUBTITLE

Sensor System for In-Situ Soil Stress Analysis.

5. FUNDING NUMBERS

C

DAAD19-00-C-0023, 2/1/00

6. AUTHOR(S)

Jacques A Charest, Princ. Investigator & M. D. Lilly Ass. Investigator..

7. PERFORMING ORGANIZATION NAME(S) AND ADDRESS(ES)

Dynasen Inc, 20 Arnold Place , Goleta, CA, 93117, USA

8. PERFORMING ORGANIZATION REPORT NUMBER

SBIR A99-028 PIFR

9. SPONSORING/MONITORING AGENCY NAME(S) AND ADDRESS(ES)

US ARMY Research OFFICE, 4300 S. Miami BLVD; Res. Triangle Park N.C. 27009-2211

10. SPONSORING/MONITORING AGENCY REPORT NUMBER

11. SUPPLEMENTARY NOTES

12a. DISTRIBUTION/AVAILABILITY STATEMENT (see Section 5.3b of this solicitation)

Distribution Unlimited

20020201 058

13. ABSTRACT (Maximum 200 words)

The goal of this investigation is to develop a sensor system capable of measuring 3D In-Situ 0-200 PSI principal stresses in soil resulting from vehicle-terrain interactions. Emphasis is to be given to lateral loads and methods of sensor emplacements that cause minimum disturbance to the surrounding soil. Three prototype 3D sensors were designed and constructed during Phase I and Phase I Option and tested in mock-geological media under controlled uni-directional loading environment, σ_x. They produced highly- encouraging results of measurements of the three states of stress to which they were exposed to. Two types of sensor designs were investigated. They were the solid-coupled and the fluid-coupled arrangements. Of all the three sensor designs evaluated, the symmetrical fluid-coupled arrangement was found to yield the most promising results for their long-term application to Phase II. Indeed, fluid-coupled stress sensors are by design inherently immune to shear stress effects and have been found to produce the most accurate lateral loads σ_y and σ_z when tested in isotropic mock geological media. It is anticipated that the symmetrical fluid-coupled arrangement will meet all requirements set by the Army for this investigation and that many practical applications will follow.

14. SUBJECT TERMS	15. NUMBER OF PAGES
3D In-Situ Stress Sensor for Soil Stress analysis	46
	16. PRICE CODE

17. SECURITY CLASSIFICTION OF REPORT	18. SECURITY CLASSIFICATION OF THIS PAGE	19. SECURITY CLASSIFICATION OF ABSTRACT	20. LIMITATION OF ABSTRACT
UNCLASSIFIED	UNCLASSIFIED	UNCLASSIFIED	SAR

SENSOR SYSTEM FOR IN-SITU 3D SOIL STRESS ANALYSIS

SBIR Solicitation # A99-028

1 INTRODUCTION.

This document summarizes the work done under phase I and Phase I Option of this contract as an effort to design, construct and test sensor arrangements that can be used to measure 3D in-situ states of stresses in soils created by the interaction of moving Army vehicles. Twelve progress letters (*6 Each for Phase I and 6 each for Phase I Option*) were forwarded to the Army Research Organization of Research Triangle Park, North Carolina, describing in details all the efforts produced by both phases of this investigation. Both progress letters # 6 for Phase I and Phase I Option summarized the work done during each phase respectively. Only the important findings of Phase I are discussed in this report, whereas the entire progress report # 6 for Phase I Option is presented here because of the highly encouraging results reported and the major impact they may have on the remainder of this program.

2 PRIME OBJECTIVE OF INVESTIGATION.

The prime objective originally set by the Army at the onset of this investigation was to construct a field-portable prototype system and demonstrate its capability for producing credible in-situ 3D stress data in distended geological media, with emphasis to be given to the measurements of lateral loads and emplacement in soils causing minimum disturbance. See Fig. 1 for the constituents of the system. They comprise a 3D stress sensor unit, a field-portable excitation/interface arrangement and a Lap Top PC recorder. Discussions on the work done for Phase I and Phase I Option are discussed next in Sections 3 and 4 respectively.

3 EFFORTS AND RESULTS SUMMARY FOR PHASE I INVESTIGATION.

3.1 Meeting at WES at Onset of Phase I.

At the onset of Phase I, a kick-off meeting was held at WES under ARO's auspices to discuss with the Army's mobility group Dynasen's first approach to the development of the 3D stress sensor,to gather relevant information on Army's application and the pressure ranges of interest, and the main trust of efforts to be implemented during Phase I.

3.1.1 Dynasen-Proposed Approach to 3D stress Sensor

In our original proposal to the Army, we proposed to develop a 3D stress sensor using three thin-film carbon stress element solid that were cemented on three orthogonal surfaces of a solid rectangular substrate. See Fig. 1. As we were proceeding in our early design efforts of the 3D sensor, it became apparent that the use of a solid rectangular arrangement would create a large " localized inclusion effect" to the stress field when used in distended soil. An inclusion effect can be defined as the change imparted to a given local stress field when a rigid object of a finite size is emplaced in a highly compressible medium. Because of our concerns about such inclusion effect, we deviated from our original proposal in the design of the 3D stress sensor choosing instead a technique we had successfully used earlier to measure the lateral loads in shock-loaded geological media. Such technique is called the " Knife-Edge approach". See Fig. 2 for the basic concept of a 3D Knife-Edge stress sensor arrangement which we investigated and tested during Phase I.

3.1.2 Stress Range and Other Concerns of Interest. Scope Limitation.

In our discussions with the Army's Mobility group, it was established that the levels of interest for the applications of the 3D stress sensors were 0-30 PSI for military vehicle-terrain interactions and 0-200 PSI for the load generated beneath the pavement of a landing strip upon the touch-down of an aircraft. One important issue raised by a member of the group was the effect of the 3D sensor's orientation during a series of measurements. Finally. it was suggested by the ARO representative that the efforts afforded to Phase I investigation should be limited to investigating the 3D sensor itself.

3.2 Test Equipment Designs and Constructions.

Part of the essential efforts to be devoted to Phase I were the designs and constructions of dedicated equipment needed at Dynasen to test prototypes of 3D stress sensors in controlled laboratory environments. Such equipment consisted in a loading apparatus to test 3D sensor prototypes in mock geological media, an hydro-static chamber to establish calibration of 3D sensors and a four-channel bridge/excitation source to excite individual carbon stress elements.

3.2.1 3D Sensor Loading Apparatus.

Figure 3 show the basic design of the loading apparatus that was constructed during Phase I to test 3D stress sensor prototypes. This apparatus was assembled using an existing piece of equipment that had been constructed in an earlier program to reconstitute geological samples for gas gun testing. The dedicated components constructed during Phase I for the loading apparatus consisted in a 6-Inch-diam. test cavity, and hydraulic operating valve and plumbing system and a loading hydraulic reservoir. Later on during Phase I, a second test cavity having 12 inches in diameter and 41/2- Inch in depth was constructed, as our 6 inch cavity was deemed too small to adequately test prototypes.

3.2.2 Hydro-Static Test Chamber.

Figure 4 shows the hydro-static test chamber we constructed during Phase I to produce the individual calibrations of the three carbon stress elements of a given 3D sensor arrangement. Indeed, once a 3D sensor package is completed, it is no longer sufficient to use the stress calibration of the carbon elements themselves to infer stress data because of the effect produced by protective layer needed to insure survival of the thin film sensors. Thus an hydro-static apparatus was deemed needed to establish the over all calibration of a finished 3D stress sensor.

3.2.3 Bridge/Excitation Source.

Figure 5 shown the schematics of a four-channel bridge/excitation source we constructed to excite the carbon gauge elements of the prototype 3D sensors constructed during Phase I.

3.3 3D Knife-Edge Stress Sensor prototype.

Figures 2 and 6 show the two types of 3D knife sensor prototypes we constructed and tested during Phase I. As one can see, our first prototype (see Fig. 2, which we named Charlie, was constructed from a solid Aluminum block producing a gauge mounting wall thickness of approximately .1 Inch whereas two prototypes as per Fig. 6 were constructed using .020 Inch -thick stainless steel for gauge mounting wall. The main idea for reducing the wall thickness with the stainless steel sensors was to minimize the inclusion effect which we discussed earlier. Indeed, our thinking then was ,"the thinner the gauge mounting wall was the lesser the inclusion effect would be."

3.3.1 Thin-Film Carbon Stress Gauge Elements.

The thin-film carbon stress elements used in this project were of the type C300-50-EKRTE which are commercially-produced by Dynasen having a 50Ω nominal resistance. Such gauge element was developed (see Fig. 7 for strip type element) was developed thirty years ago for UGT tests and has been used ever since in many applications of stress measurements in solids. To minimize the excitation current and of increase outputs, we decided to use the grid-type arrangement of the C300-50-EKRTE gauge , centering its nominal resistance at around 1,500 Ω. The carbon elements were mounted on the outside faces of the 3D sensors using epoxy resin as the cementing agent. The carbon elements of the Aluminum 3D sensor were covered with .005 Inch-thick copper shield whereas with the elements of the stainless steel sensors were covered with .006 Inch-thick stainless steel protection. Figure 8 is a photograph of the three knife edge 3D sensors produced during Phase I.

3.3 Test Results and Discussions.

3.3.2 3D Aluminum Knife-Edge ' Charlie"

At mid-point of Phase I, we were invited by the Army to submit a Phase II proposal on the subject of 3D stress sensor. As we felt awkward to respond to such invitation, of course not knowing at that time, that such sensor could be constructed and be shown to work, we pressed-on on our Phase I work to assemble as quickly as possible our first prototype 3D stress sensor which we named " Charlie". We then proceeded to test our first prototype using our loading apparatus shown on Fig. 2 and sifted #40 Silica sand as the working medium. The results of these tests are shown on Fig.9. Seemingly, the data produced by our first prototype 3D sensor prototype appeared to be reasonable, showing however unexpected differences between the two lateral principal stresses σ_y and σ_z and a value of σ_x greater than expected for the 0^0 orientation of the 3D sensor package. Our first prototype did survive the tests without showing any visible or measurable substantial damage. Of course as we know it now from our tests of Phase I Option, there was considerable stress gradient within the test cavity when using Silica sand as the working medium. Limitations imposed by its construction features prevented us from calibrating the unit using our hydro-calibration apparatus. Finally, it had not been established then that shear forces were acting along the vertical walls of the sensors, thus adding an extra load component to the σ_x gauge

3.3.3 3D Stainless Steel Prototypes.

After completion of our two stainless prototype units, we subjected them to hydro-static calibration, the only method which we knew could be used to truly calibrate the 3D sensor arrangement. Unfortunately, both stainless steel units produced a malfunction in one of their carbon elements during the hydro-calibration. However, from the results of the two other gauges these hydro-calibration tests clearly showed that the method was a powerful approach to establish calibration of a finish 3D sensor. Figure 10 shows the results of hydro-calibration of our stainless steel unit #2, producing nearly identical results for the two good elements σ_x and σ_z at 50 and 100 PSI loading and output levels that were very similar to the carbon elements' calibrations. For unexplained reasons σ_y gauge of stainless steel unit#2 produced a higher calibration output. Figure 11 shows typical test results of stainless unit #2 in #90 Silica sand, using this time our 12 Inch-diam. test cavity. As one can see, the data produced by our #2 stainless 3D sensor also appeared to be reasonable.

Although our Aluminum and stainless 3D stress sensor prototypes did not produce perfect results, the trend of the data produced was strongly suggesting that such devices could be made to work by implementing further improvements. However because of the asymmetry of the 3D knife-edge improvements needed to be implemented to improve its performance were deemed very challenging and perhaps found to be prohibitively to extensive, considering that other design avenues were possible. Thus testing of arrangements other than the knife-edge concept appeared to be a more logical step forward for this work a decision that was greatly rewarded by our work of phase I Option.

4 EFFORTS AND RESULTS OF PHASE I OPTION

In this section we will discuss those issues we have addressed during Phase I Option which we feel are most relevant to future work and, of course, to the success of this investigation. Thus, details of work accomplishments of lesser relevance can be found in our progress letters # 1 to #5.

In the course of Phase I Option work, we have identified and partially addressed the following areas of investigation that are key to this work. They are as follows and will be discussed in their respective listed order.

Determination of Stress Field in 12 Inch Test Cavity Using Mini Flat Packs.

Visit at WES, in June, 2001, and discussions of results of Phase I and Discussions on aspects of 3D Knife-Edge sensors and design and support Calculations to back-up future basic measurements at Dynasen's facility.

Establish the need to reinforce components of test cavity for reducing tension strain effects on critically-located reference stress sensors.

Investigate other carbon sensor's excitation sources to circumvent difficulties experienced full bridge arrangement.

Meeting and discussions at Dynasen on Dec. 10, 01,with ARO and WES' Personnel on accomplishment during Phase I Option and direction of direction of future work during Phase II.

Construction and Testing of one prototype each symmetrical solid- and fluid-couple 3D stress sensor packages.

4.1 Determination of Stress Field in Test Cavity.

As we stated in our previous progress letters #5, it was deemed essential for future development work of 3D stress sensors that the stress field near the center of our 12-inch test cavity be known in order to benchmark the results produced by future 3D stress sensor arrangements. To do so, we conducted two series of tests using the so-called mini-flat packs stress sensing arrangement using 40-60 glass bead work medium. 40-60 glass bead is a fine sand-like medium consisting in tiny solid glass spheres showing an fluid-like behavior. The main objective of these tests was to determine the vertical downward load around the center of the test cavity. Our tests with the mini flat packs showed approximately a 50 PSI downward stress around the center of the cavity , as one would expect from simple calculations considering the physical parameters of the test apparatus at 200 PSI loading, assuming that the stress field is to be nearly uniform across the cavity when using glass beads. Minor stress gradients of the vertical load were detected at about 2 inch away from the center.

An example of stress field measurements is presented here on Fig. 12 showing typical results obtained with mini flat packs in #40-60 glass bead work medium along with a schematics of the test arrangement. Our few attempts to mount three mini flat packs to mimic the 3D knife edge arrangement failed to produce any valid or interpretable data of lateral loads. The individual tests were discussed in our progress letters #2 and #3. Reverse side of Fig. 12 is a sketch of mini flat pack.

4.2 Visit at WES in June, 2001.

The purpose of our visit at WES in late June 2001 was primarily to review Dynasen's work and important findings during Phase I with the 3D knife-edge stress sensor and to discuss some critical aspects of the design approach used by Dynasen in its original work. These critical aspects primarily centered around 1) the concerns by Dynasen about the asymmetrical geometry of the Knife-edge arrangement and 2) the concerns by WES' technical personnel about that peculiarity of such design and the effects of shear stresses on the response of such type of arrangement. Also discussed were the need by Dynasen to have

WES' personnel perform computer simulations calculations to back up Dynasen's calibration and side yard experiments. Other issues were also discussed such as the need to map the stress field in our test cavity, investigate other excitation sources for the carbon stress elements and the possibility of increasing the stiffness of the stationary pusher plate of our calibration apparatus.

The critical points raised by WES about the 3D knife-edge arrangement were well taken into considerations by Dynasen and prompted us upon returning to our facility at directing much of our research efforts to re-examine the design features of our test apparatus and at exploring symmetrical arrangements of the solid-coupled and fluid-coupled 3D stress gauge arrangements.

4.3 _Need to Reinforce Components of Test Cavity.

While mapping the stress field of our 12-Inch test cavity, we were getting unreliable results with the stress gauges that was mounted at the bottom center of the stationary pusher plate of the test apparatus. Indeed, we felt that it was necessary to have one reference gauge mounted at the center of the stationary plate and also one gauge mounted at the center of the bottom plate to provide additional information to our the stress field measurements. Indeed, we went from a solid-mounted gauge to a fluid-coupled mounted gauge on the stationary pusher plate and saw no improvement in our measurements.

Again remembering comments made earlier by WES on the possibly-insufficient stiffness of the Aluminum pusher plate, we investigated the existence of tension strain effects to develop while loading the working medium. A dedicated test was conducted (See Fig. 13 here) which unequivocally demonstrated that tension strain is present at the center of the stationary pusher plate while loading the working medium. That dedicated test consisted in placing wedges around the container to prevent the pusher plate from touching the test medium and in applying a 200 PSI load to the test apparatus. As one can see, no pressure is registered by the three mini flat packs as one would expect. However, a large positive output is developed by the stress gauge G_t thus indicating a large level of tension strain at the center of the bottom face of the pusher plate.

Immediately following the above dedicated test, we re-designed our 12-inch test cavity and had constructed a 2-Inch thick steel plate to back up the Aluminum pusher plate and a 2-Inch thick plate steel plate for the bottom of the test cavity. These components have already been fabricated and we are awaiting for the beginning of Phase II efforts to install them on our test apparatus. These two add-on plates should stiffen by a large factor the pusher and bottom plates of our test cavity and thus eliminating any tension strain effect on either plates.

4.4 Investigate Other carbon sensor's excitation sources.

One major operational problems we have experienced while testing our 3D stress sensors has been the drift in output by the circuit arrangement used in Phase I and part of Phase I Option. See Fig. 5 for the bridge/amplification circuit we built during Phase I to excite the carbon sensors of the 3D stress sensors. The drift in output was caused by to thermal resistivity coefficient of the carbon stress element combined to the Joule Heating Effect RI^2t and the 100:1 amplification of the bridge output. Such drift made it very difficult for us to capture the sensors' output signals using our recording oscilloscope. Of course, one possible approach to remedy the drift problem is to use a carbon element of same value in the opposite arm of the active gauge of the Wheatstone bridge used for the excitation circuit. That technique is called temperature effect self-canceling approach which requires a compensating stress carbon element of same resistance as the active gauge and be made part of the bridge as we said above. We intend to explore this approach as part as our Phase II effort as a bridge arrangement offers some advantages over other excitation techniques.

A second approach which we have explored and used during Phase I Option has been the so-called large-capacitor coupling technique. Such technique can be easily understood in Fig. 14 A here. Figure 14 B is the Wheatstone Bridge arrangement. The large-capacitor coupling is equivalent to the bridge arrangement providing the time scale of the event measured is substantially shorter than the RC constant of the product "viewing coupling capacitor times the viewing resistor". Furthermore the above technique is greatly simplified in interpretation when used with a constant current source. Indeed, we found that once current equilibrium was reached within the circuit, data recording was very easy. Of course, we did not use any

amplification with the large-coupling capacitor. Further work on the capacitor-coupling method is anticipated during Phase II.

4.5 Meeting at Dynasen with ARO and WES'.

A meeting was held at Dynasen on December 10, 01, to review our work progress during Phase I Option with ARO and WES personnel. Our meeting primarily consisted in a brief overall review of Phase I Option work and its recent efforts with solid- and fluid-coupled stress gauge which are discussed in the next section. The review by Dynasen of its most recent work was of course marked by our great excitement from our part due to recent encouraging findings with the fluid-coupled stress gauge. The other areas covered were 1) the submission of an abstracts for an up-coming meeting to be held at WES in late October, 2002, on Dynasen's work with the 3D stress sensor, 2) the desirability for ARO to have at hand a prototype 3D stress sensor to show to other Government or non-Government groups the Army's efforts and the potential application of such sensor by others, and 3) the extended interactions needed between Dynasen and WES' technical personnel during Phase II to assure that the Army's specific needs are met.

4.6 Testing of symmetrical solid- and fluid-couple 3D stress sensor.

Figure 15 shows the basic designs of the symmetrical solid- and fluid-coupled 3D stress sensors we constructed and tested during the past two months of Phase I Option efforts. As shown on Fig. 15, each package consisted in four carbon elements. One gauge, σ_{xt} ,was dedicated to measure the vertical (downward) stress being applied to the top of the arrangement whereas a second gauge, σ_{xb}, was mounted at the bottom of the arrangement to measure the downward stress produced by the package against the working medium. The two other gauges were dedicated to measure the lateral loads σ_y and σ_z . The main idea for gauges σ_{xt} and σ_{xb} was to find out if frictional forces were acting along the walls of the lateral load gauges and causing secondary forces to act upon the bottom download gauge σ_{xb}. One may remember that we discussed this issue during our work with the Knife-edge stress sensor. Indeed, pre-empting on discussions of results presented later in this section, we did unequivocally find out with our fluid-coupled stress gauges that such shear forces are acting the vertical wall of the 3D sensors causing the bottom gauge σ_{xb} to experience larger stresses than gauge σ_{xt}.

4.6.1- TESTING SOLID-COUPLED SYMMETRICAL 3D STRESS SENSOR. Prototype #1 .

Our first symmetrical solid-coupled 3D stress sensor prototype was tested in two ways. The first way consisted in establishing its hydrostatic calibration whereas the second way consisted in testing the unit in #40-60 glass bead medium. Figures 16 to 20 show the results of the individual calibration tests whereas Fig. 21 shows plots of the individual hydro-calibrations for the four stress sensors of the unit. The basic design of the hydrostatic calibration apparatus built during Phase I is shown on the upper part of each test data sheet. As we discussed it in past work, the hydro-calibration method is the only method we know that can be used reliably , given the low stress range (0-30 PSI) the 3D stress sensor is to be exposed to. As one can on Fig.21, there is substantial variation in output sensitivity shown by the four stress elements, suggesting small deviations in construction may influence the response of each individual stress sensor.

Figures 22 to 25 are the actual results in tests conducted in the glass-bead medium with our first solid-coupled prototype. As one can see on Fig. 22 the data produced by σ_{xt} carbon element is very close to the data produced earlier with the mini-flat packs whereas the σ_{xb} gauge produced a slightly higher pressure. The higher data of σ_{xb} gauge was our first evidence that indeed there were frictional forces acting along the vertical wall of the sensor arrangement. The data produced by the σ_y sensor appear to be reasonable, of course, without having any calculation to support such measurement. On the other hand the data of σ_z gauge is not really evident. In one test, see Fig.25 we reverse the orientation of the 3D sensor placing the σ_{xt} gauge at the bottom as shown on the upper right hand side of the testing arrangement. Again, the sensor placed at the bottom showed greater stress measurements, thus furthering the evidence of shear stresses acting along the wall of the 3D package.

One important aspect which we could not detect from our tests with the solid-coupled 3D sensor was the influence of shear stresses upon the output of the lateral stress elements. Having no immediate support to resolve such issue, we did proceed to evaluate the fluid-couple 3D sensor, as potentially it was thought to be immune shear stresses.

4.6.2 TESTING FLUID-COUPLED SYMMETRICAL SENSOR. Prototype #1. (σ_y gauge Damaged)

Upon completion of our first prototype fluid-coupled 3D stress gauge, we accidentally damaged its σ_y gauge element by causing the coupling silicone fluid to partially escape from the cavity. Indeed, until now we have used epoxy resin to cement the coupling/sensing diaphragm to sensor housing, thus making the package vulnerable to tension tears. Of course, spot welding of the diaphragm to the sensor housing will used in future units to avoid such problem. As we were very anxious to get information with our first fluid-coupled prototype prior to our meeting at Dynasen on Dec. 10, 01, we proceeded to the hydro-calibration and testing of the unit knowing of course that the σ_y gauge would not function properly.

Figures 26 to 28 are the individual hydro-calibration tests of our first fluid-coupled prototype (remembering that σ_y was damaged) whereas Fig. 29 is a plot of the data. Figures 30 and 31 are actual tests in glass bead medium. As one can see on Fig. 29, the calibration of stress elements σ_{xt}, σ_{xb} and σ_z appear to be relatively similar to one another as a result, we believe, of the no-shear stress transmission across the .005 Inch thick stainless steel diaphragm. Indeed, any gauge at the bottom of a fluid-coupled cavity can only sense the normal stress acting upon the diaphragm, thus rendering it immune to shear stress effects. By examining the results of Fig. 30, one can see that the bottom gauge σ_{xb} produces a stress that is higher than gauge σ_{xt} thus confirming once more that shear stresses are acting along the vertical walls of the 3D stress sensor.

A second test,(see Fig.3 1), was conducted with the fluid-coupled unit, this time placing the damaged σ_y on top and of course a no-gauge arrangement at the bottom, leaving the σ_{xt}, σ_{xb} and σ_z gauges to measure the lateral stresses only. In an isotropic material , such as #40-60 glass bead medium, one should expect to measure the same stress with the three above good sensors. As one can see on Fig. 31, the three gauges σ_{xt}, σ_{xb} and σ_z did produce nearly identical measurements as isotropic material behavior predicts. This in our views is a very strong indication that a fluid-coupled stress gauge arrangement is the way to approach 3D stress measurements or principal lateral loads in geological media. To further increase our excitement, we used our scope to superimpose the three records produced by σ_{xt}, σ_{xb} and σ_z gauges. See back side of Fig. 31. As far as we are concerned, the three sets of data lay on top of each other." This is very exciting data??????, we think.....

4.6.3 TESTING FLUID -COUPLED SYMMETRICAL 3D STRESS SENSOR. Prototype #1. (after σ_y and σ_z gauges were rebuilt)

Immediately after our Dec. 10, 01, meeting with ARO and WES, we proceeded to repair the σ_y and σ_z gauges of our first symmetrical fluid-coupled arrangement. With great precaution, we managed not to inflict any damage to the unit the second time around and proceeded with a second round of hydro-calibrations of its four sensing elements and in testing the 3D unit in #40-60 glass bead and #90 Silica sand using the same loading pressure as our previous tests. As one may remember, a 200 PSI loading pressure of the test apparatus produces a download vertical pressure of about 50 PSI in the center of the test cavity when using #40-60 glass bead working medium. The information produced by this second of testing with our rebuilt fluid-coupled unit is presented on Figs. 32 to 41.

As one can see on Fig. 35, the hydro-calibration of the rebuilt fluid-coupled unit dated 12-17-01 appears to yield very similar output sensitivity of the four sensing elements. Furthermore the data presented in Figs. 26-28 confirm one more time what we said earlier: that the bottom gauge produces higher stress level due to the frictional forces acting along the vertical walls of the 3D sensors and that both lateral gauges σ_y andσ_z produce the same lateral loads. In test of Fig. 39, the unit was rotated to 45 degrees with respect to

andσ_z produce the same lateral loads. In test of Fig. 39, the unit was rotated to 45 degrees with respect to the line of loading. A simple vector summation of the vertical and lateral loads is well in line with the actual measurements produced by the σ_{xt} and σ_y gauges, a fact that further raises our confidence in the operational capability of the fluid-couple 3D sensor.

It is interesting to note here that our tests with #90 Si sand (see Figs. 40 and 41) produced much larger stress data than with #40-60 glass bead, a finding which is not surprising considering the larger pressure-induced inter-granular shear strength that develops within the sand itself. Otherwise we observed the same stress pattern in Sand as we did in #40-60 glass beads. Without any hesitation, the data produced with the rebuilt fluid-coupled unit is re-affirming our earlier excitement , leaving no doubt in our mind, at the cost of repeating ourselves, that the fluid-coupled approach will be the way to proceed in Phase II.

As we are about to begin Phase II on the 3D stress sensor, we can summarize our key findings so far as follows:

1- Shear stresses acting along the vertical walls of the 3D sensors cause additional forces to be imparted upon the bottom gauge thus making its stress measurement larger than the top gauge.

2- The fluid-coupled arrangement renders the 3D stress sensors to be insensitive to shear stress effects, and thus permits direct measurements of principal lateral loads.

3- Each type of mock geological test medium seems to produced its unique stress field in a given test arrangement as a result of the pressure-induced inter-granular shear strength produced .

4- The fluid-couple arrangement is the approach to be used in future work for its demonstrated capability to yield information from which in situ 3D stress data can be inferred.

5. ANTICIPATED WORK FOR BEGINNINING AND THROUGHOUT PHASE II.

From the results of work done Phase I and Phase I Option, we have identified four important areas which need to be concurrently investigated at the beginning or in the course of Phase II. These areas are: 1- the completion of needed laboratory testing equipment and the streamlining of test procedures, 2- the improvement of design and performance of our 3D stress sensor, 3- the construction of a versatile and easy-to-use multi-channel battery-powered gauge excitation source for laboratory and field work, and 4- the extensive testing and evaluation of prototypes as they are produced. As one can imagine, each of the above tasks may require different amount of time for their investigations. Thus, our general approach will be that each improvement made on any of the above-mentioned areas will be implemented in a 3D sensor prototype and consequently fully evaluated by testing.

5.1-Complete or Add features on Testing Equipment and Streamline Test Procedures.

As we were searching during Phase I and specially during Phase I Option to define the type of 3D stress sensor which would most likely succeed over a long term, our efforts at designing and constructing needed tests equipment were kept to a minimum level, stressing only on those basic features required to properly evaluate prototype sensors. Needless-to-say that such testing apparatuses were not optimized in many respects and made capable of efficient testing nor were testing procedures standardized.

Having seemingly established that the fluid-coupled 3D stress sensor concept is our best design approach for succeeding in this program, one of the very first task we are planning to address early-on during Phase II is to strengthen our 12-Inch test cavity system as we said earlier and add a few key valves and controls and operational safety features to streamline its operation and provide the operator with a safe work environment. Indeed, we found that dealing with fine materials such #90 Silica sand dust can damage equipment or be a health hazard , thus mandating that adequate protection features be used on around testing area. We plan to extend an adjacent existing ventilation system used for our gas gun facility to achieve the above. Also, as part of the above efforts, we plan to standardize or streamline testing and logging information in order to maximize the return of our efforts.

5.2-improvement of design and performance of Fluid-Coupled 3D stress sensor.

As we were constructing and testing the 3D fluid-coupled stress sensor, several improvements became obvious to us to be added to construction approach or to characteristics its features. The following are improvements we are currently seeking for our 3D stress sensor.

A-The use of separate fluid-coupled pressure sensing modules instead of integrated built-in pressure sensors. Indeed, we found out that building the fluid-coupling cavity out of the 3D sensor's main body makes it difficult to spot weld the coupling stainless steel diaphragm, a feature which is needed to preserve its attachment to the sensor arrangement. The course of action we intend to take is to build thin flat small-diameter fluid coupled pressure modules that can be spot welded, calibrated individually and thereafter cemented to the 3D sensor's housing.

B- The increase in sensitivity of the individual carbon sensing elements. In views of the low pressure (1-30 PSI) to be resolved by the 3D stress sensor, we feel very strongly that an increase in pressure sensitivity and a reduction of thermal resistivity coefficient are two highly desirable features to be added to the pressure sensing elements. Indeed, although our carbon element type C300-50-EKRTE has produce reasonable data so far, an improvement of these two above-mentioned characteristics would constitute a great achievement over our past work , particularly as far as excitation and recording schemes are concerned.

There are three avenues we intend to explore. They are 1) The improvement of our current carbon stress element, 2) the further exploration of the 5 Mil carbon-loaded polyethylene film (an approach briefly explored during Phase I), and 3) The evaluation of an inexpensive commercially-available High-Resistance Dime-Size contact resistance pressure device capable of high output. These three avenues will be explored in the order presented above. It is anticipated that the above task will cover a substantial amount of time of Phase II.

5.3- Multi-Channel Battery-Powered Gauge Excitation Source.

In our work so far we have used two excitation methods to energize our carbon stress elements. They were the full bridge arrangement with 100:1 amplification and the large capacitor coupling method with no amplification. The full bridge method was marred by output drift whereas the coupling capacitor was limited to low output. As of this writing, we believe that the key to achieving high-amplitude low-noise output data rests primarily upon reducing the resistivity coefficient of the sensing element and in using the self-canceling arrangement that makes use of a second element that is placed in the bridge itself.

Another aspect to the excitation source which needs to be investigated is the acquisition of an arrangement that permits the downloading of data directly into a Lap-Top computer instead of an oscilloscope. Such arrangement is readily available from Lab View Systems, the most important matter being the selection of the right hardware/software system capable of meeting our requirements.

5.4- Testing and Evaluation of Prototype 3D Sensors.

As we said earlier, for each major improvement achieved in the above described tasks planned for early on Phase II, prototype(s) will be constructed reflecting such improvement and fully tested in representative geological media. It is our plan to remain in continuous contact with WES technical personnel and to report verbally or by informal FAX or e mail on all of our work progress, discuss and seek advice about unforeseeable problems and whenever possible have computer calculations performed to support our laboratory and down-the-road side yard tests.

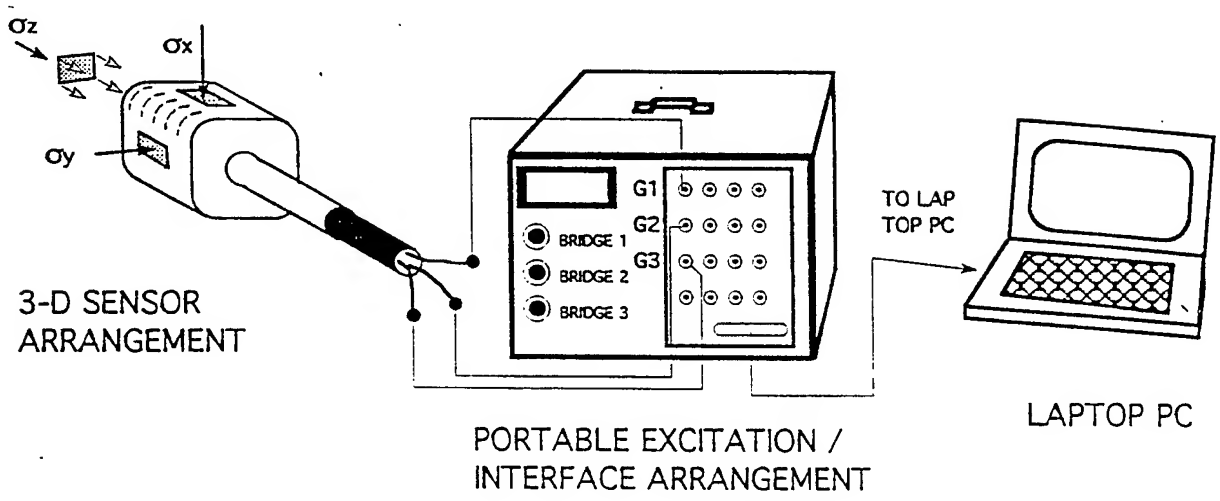

Fig. 1. Field-Portable 3D In-situ Sress Measurement System.

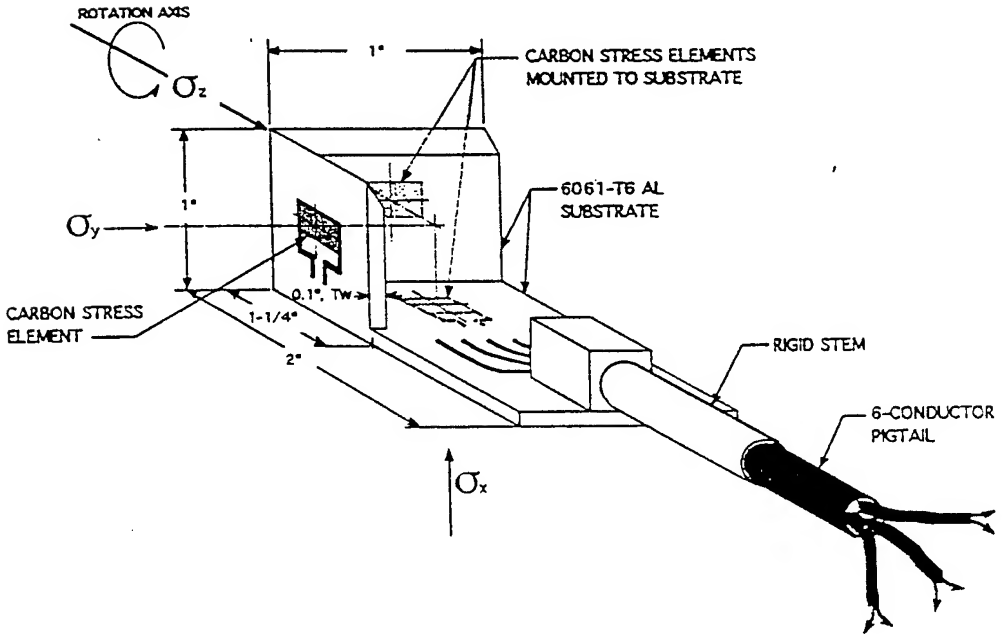

Fig. 2. Knife-Edge 3D Stress Sensor.

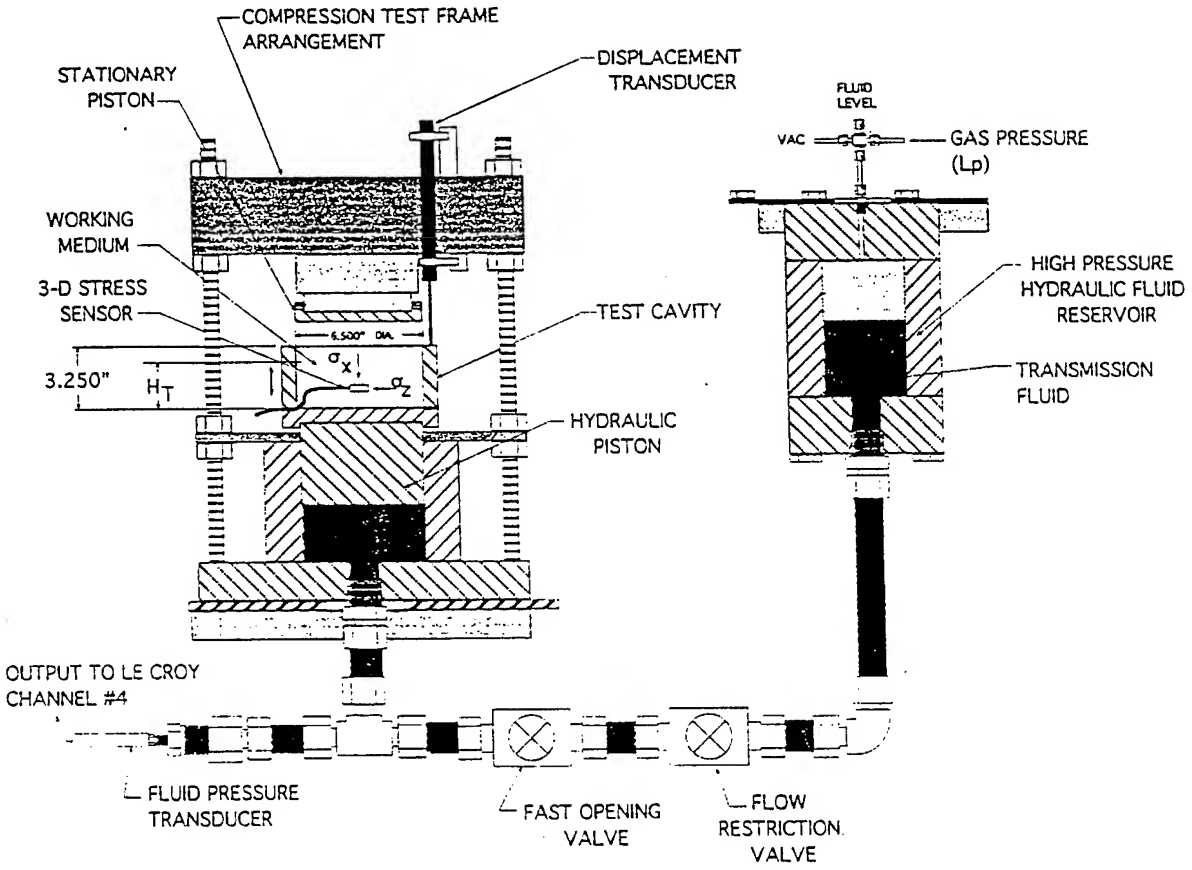

Fig.3. 3D Sensor Loading Apparatus

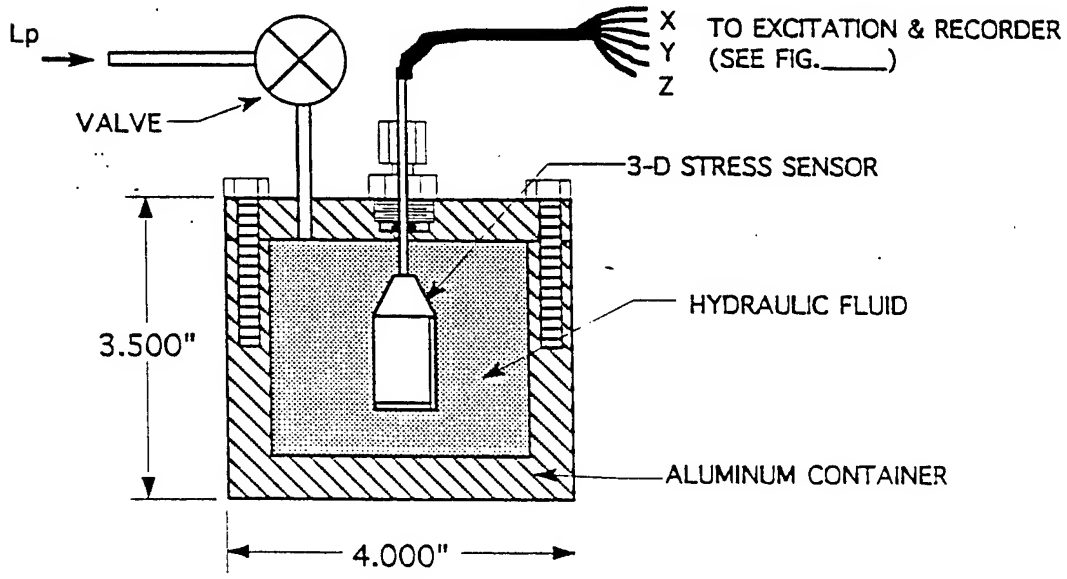

Fig. 4. Hydro-Static Calibration Chamber.

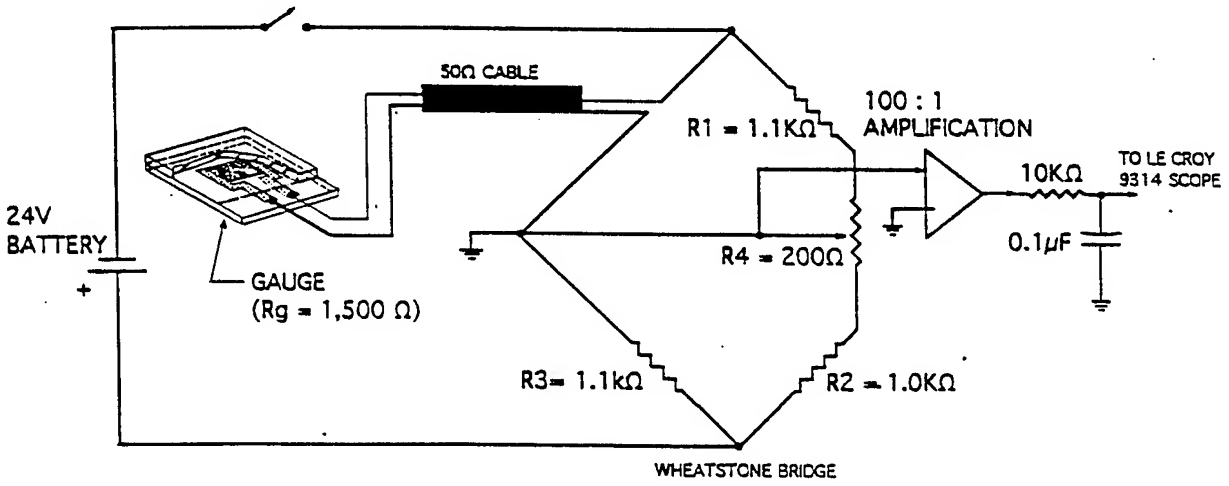

Fig. 5 Battery-Powered Bridge/Amplification Arrangement.

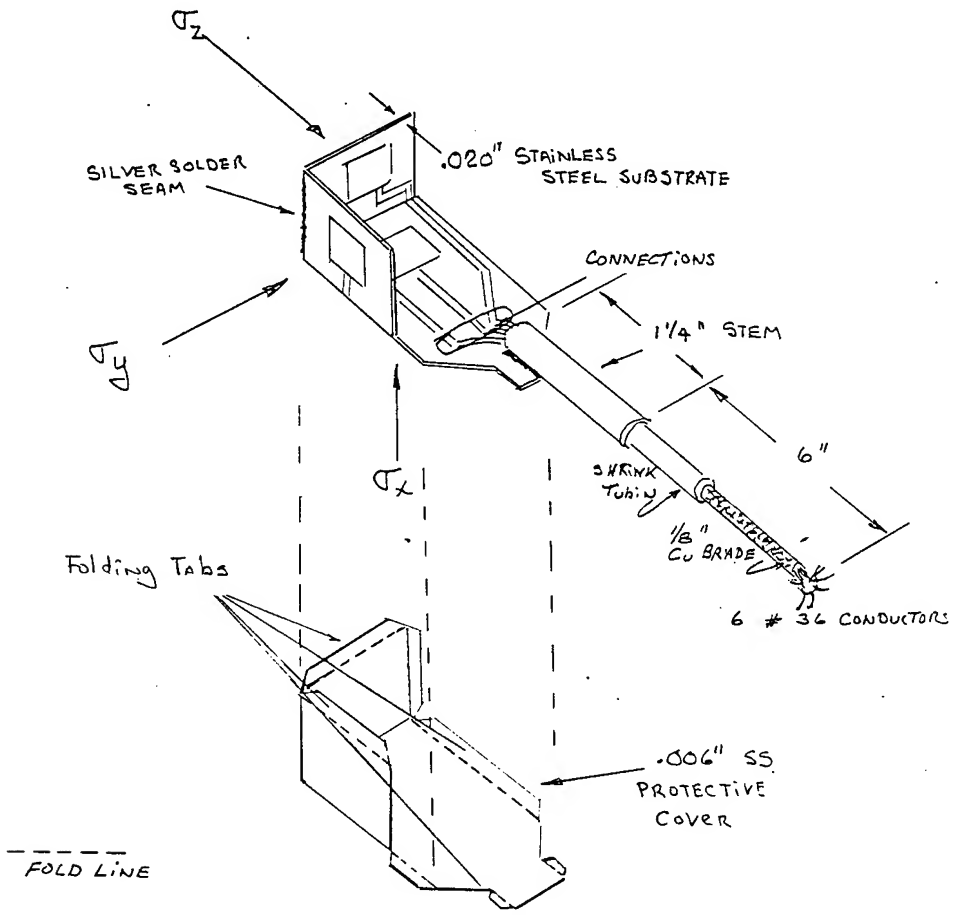

Fig. 6. 3D Knife-Edge Stainless Steel Sensor

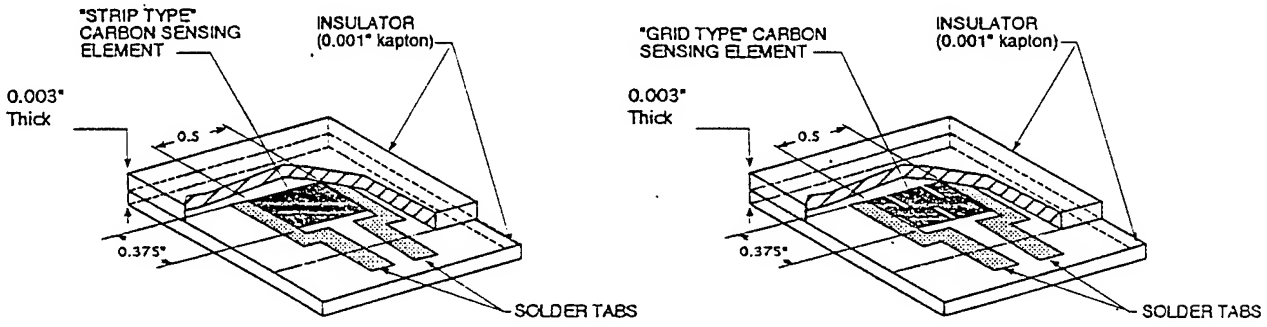

Fig. 7. Thin-Film Strip and Grid Type Carbon Stress Elements.

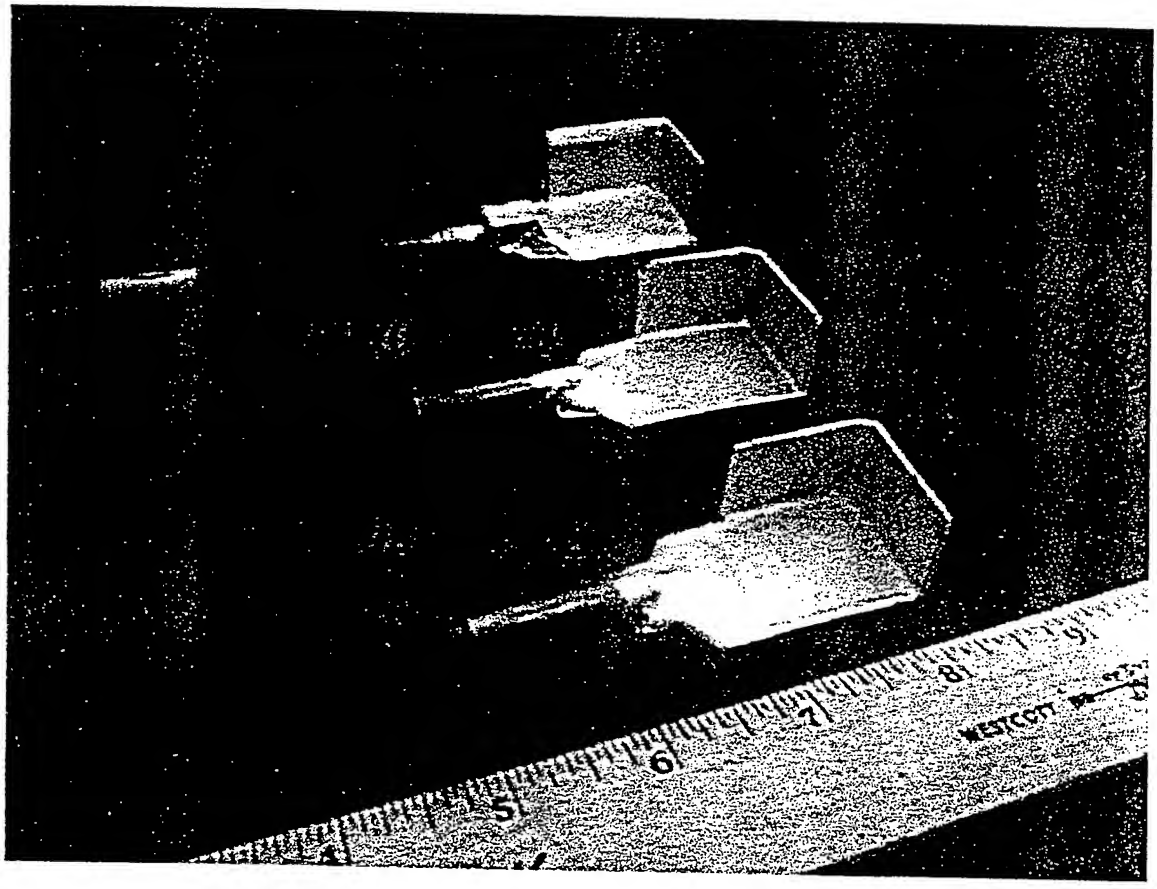

Fig. 8. Photographs of 3D Knife-Edge Produced in Phase I.

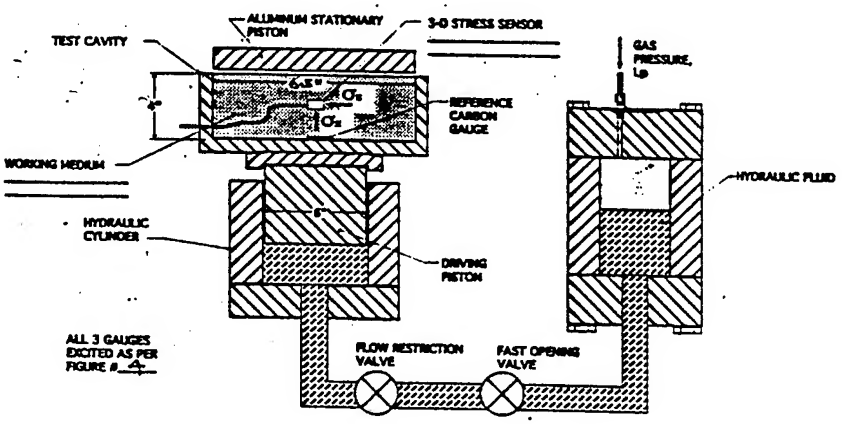

TEST ARRANGEMENT

TEST # 1 Work Medium Loose Si Sand
Orientation 0 Degrees
Load Pressure 100 PSI
Carbon Gauge Calibration 2.1 MV/PSI
Gauge Resistance.

	Before Test Ω	After Test Ω
σ_x	1,523.5	1,534.8
σ_y	1,507.6	1,518.6
σ_z	1,554.0	1,565.2

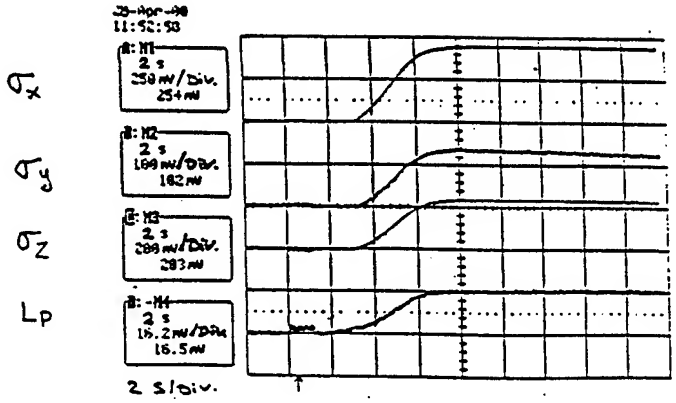

OUTPUTS OF PROTOTYPE AT 100 PSI LOADING

TEST # 2 Work Medium TAMPED Si SAND
Orientation 0 Degrees
Load Pressure 50 PSI
Carbon Gauge Calibration 2.1 MV/PSI
Gauge Resistance.

	Before Test Ω	After Test Ω
σ_x	1,528.0	1,525.0
σ_y	1,512.0	1,509.0
σ_z	1,558.0	1,556.0

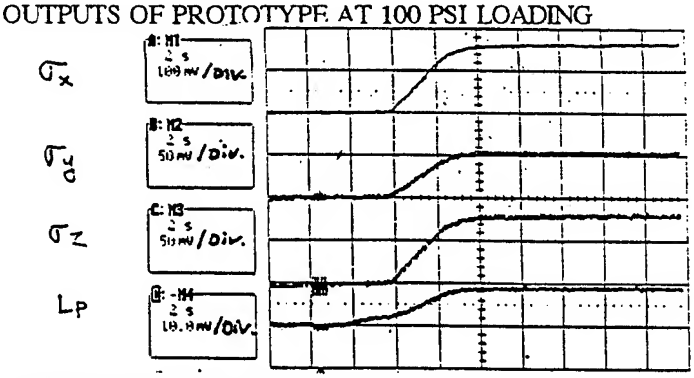

OUTPUTS OF PROTOTYPE AT 50 PSI LOADING

TEST # 4 Work Medium TAMPED Si SAND
Orientation -45 Degrees
Load Pressure 50 PSI
Carbon Gauge Calibration 2.1 MV/PSI
Gauge Resistance.

	Before Test Ω	After Test Ω
σ_x	1,531.0	1,527.0
σ_y	1,515.0	1,512.0
σ_z	1,561.0	1,558.0

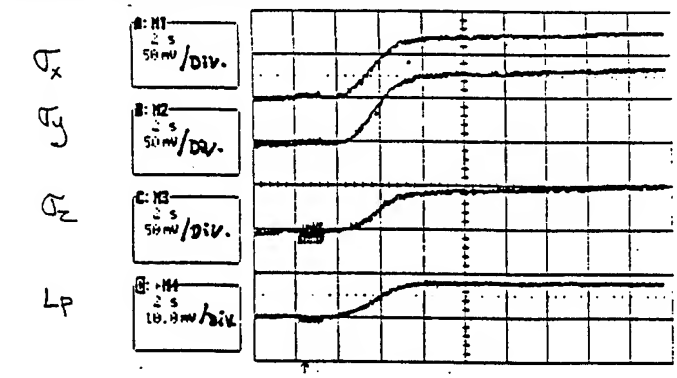

OUTPUT OF PROTOTYPE AT 50 PSI LOADING AND – 45°

FIG. 9 Representative Results With First Prototype 3D Stress Sensor.

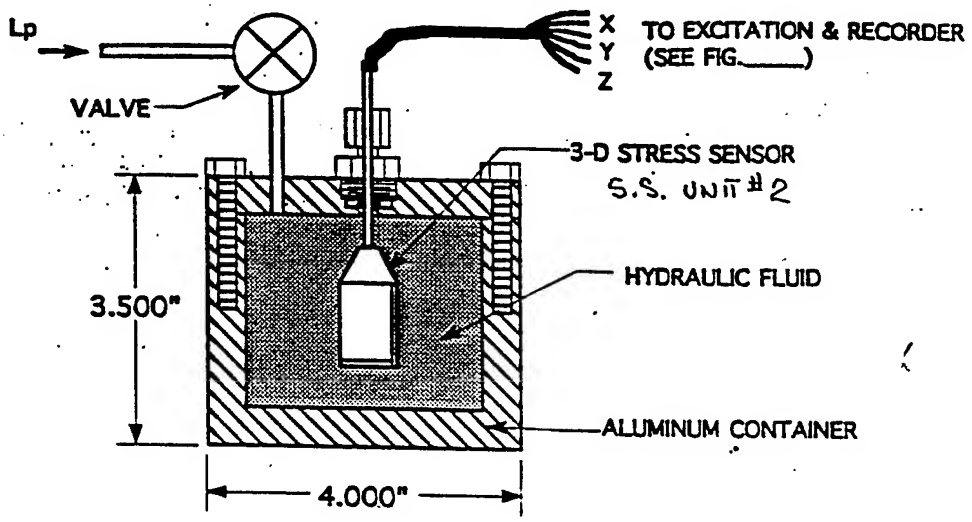

TEST ARRANGEMENT

SS PROTOTYPE 3D STRESS SENSOR #2

TEST # S-4510 T1 7/25/00

LOAD PRESSURE, Lp 50 PSI

Carbon Gauge Cal. 2.0 MV/PSI

Gauge Resistance,

	Before Test Ω	After Test Ω
σ_x	1,550.5	1,550.5
σ_y	1,565.4	1,565.4
σ_z	1,560.0	1,560.6

COMMENTS: VERY SMALL CHANGES OF RESISTANCE

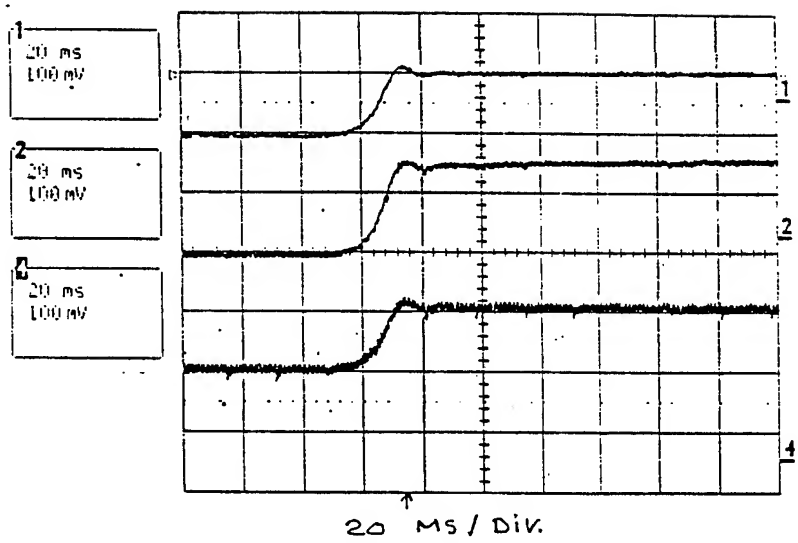

SS PROTOTYPE 3D STRESS SENSOR #2

TEST # S-4510 T2 7/25/00

LOAD PRESSURE, Lp 100 PSI

Carbon Gauge Cal. 2.0 MV/PSI
EXCEPT σ_y is 3.0 MV/PSI

Gauge Resistance,

	Before Test Ω	After Test Ω
σ_x	1,551.2	1,549.7
σ_y	1,566.2	1,564.5
σ_z	1,560.0	1,558.7

COMMENTS: RELATIVELY SMALL CHANGES OF RESISTANCE

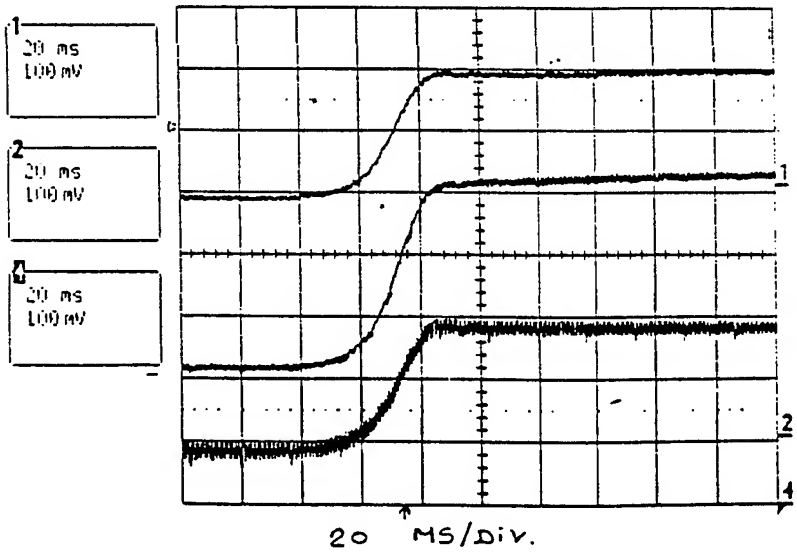

Fig. 10. Hydrostatic Calibration Outputs of Stainless Steel 3D Sensor.

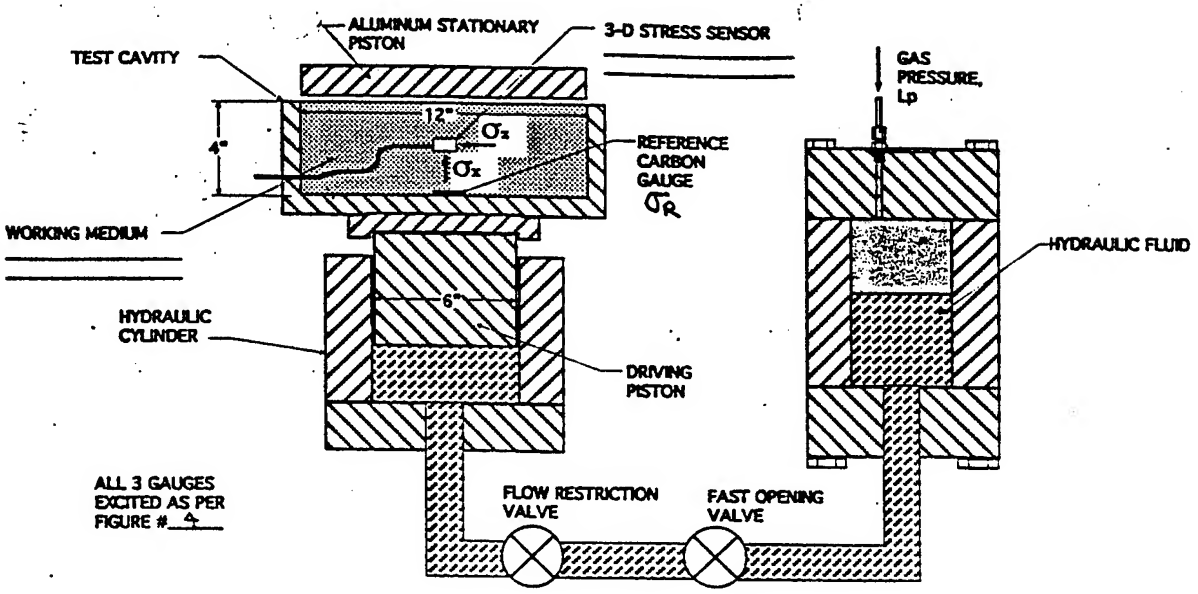

TEST ARRANGEMENT

Test # S-4510 T2 7/29/00

Unit # 2 Stainless Steel

Work Medium #90 UNTAMPED Si SAND
Orientation 0 Degrees
Load Pressure 180 PSI
Carbon Gauge Calibration 2.0 MV/PSI
Gauge Resistance. EXCEPT σ_y IS 3.0 MV/PSI

	Before Test Ω	After Test Ω
σ_x	1,553.1	1,549.1
σ_y	1,571.2	1,567.4
σ_z	1,562.4	1,559.0

Comments SMALL CHANGES OF RESISTANCE

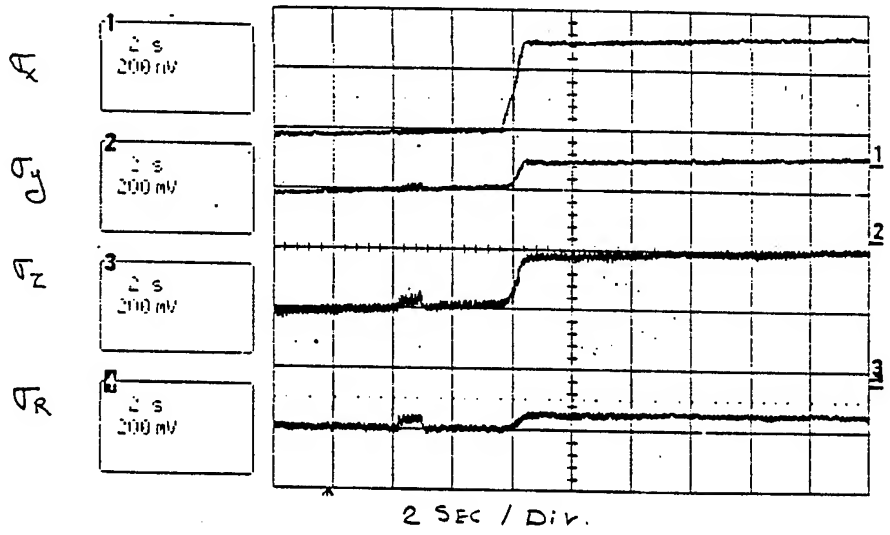

Test # S-4510 T2 7/29/00

Unit # 2 Stainless Steel

Work Medium #90 UNTAMPED Si SAND.
Orientation 0 Degrees
Load Pressure 375 PSI
Carbon Gauge Calibration 2.0 MV/PSI
Gauge Resistance. EXCEPT σ_y IS 3.0 MV/PSI

	Before Test Ω	After Test Ω
σ_x	1,549.0	1,547.3
σ_y	1,568.0	1,566.2
σ_z	1,560.0	1,558.4

Comments SMALL CHANGES OF RESISTANCE

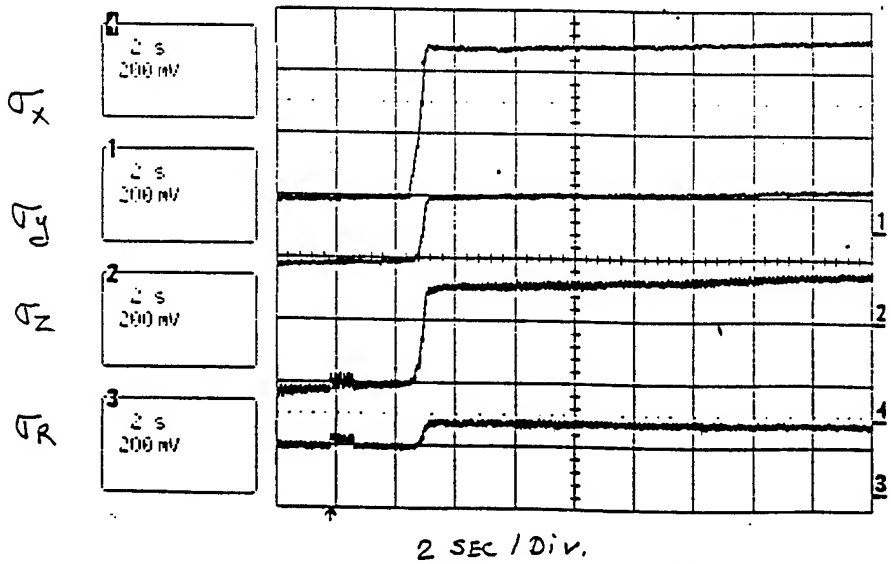

Fig. 11. Test Results with Stainless Steel Unit #2 in #90 Si Sand.

TESTING

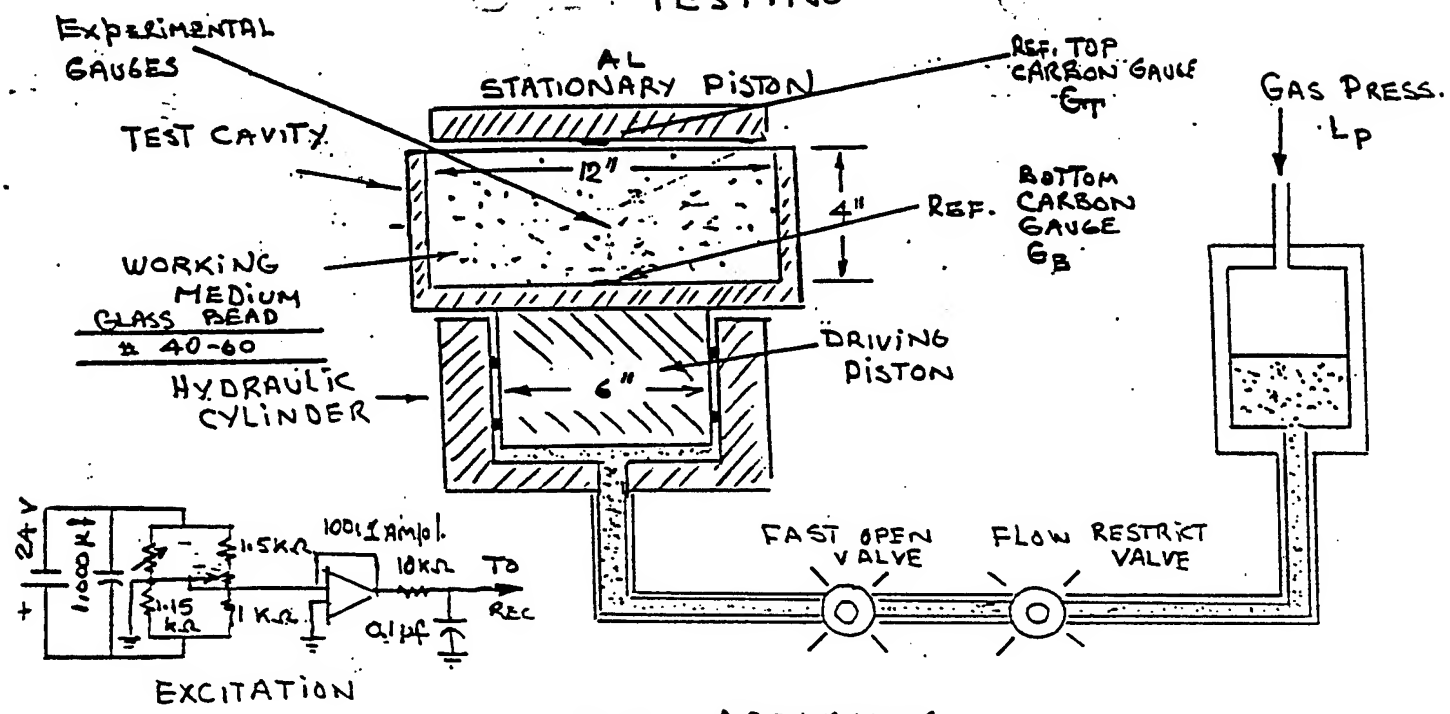

TEST APPARATUS

TEST DATE 6/3/01 SALE NO 4787 TEST NO 6-3-01 T1 TEMP. 20 °C

TEST PURPOSE TO DETERMINE STRESS FIELD IN TEST CAVITY.

GAUGES: SENSITIVITY : 2.1 MV/PSI

G_T : C300-1,500-EKRTE : CEMENTED TO BOTTOM OF STATIONARY PISTON. COVERED WITH .034" S.S. SHIM — BEFORE TEST: — Ω AFTER TEST: ~~1,615.2~~ Ω

G_B : C300-1,500-EKRTE : CEMENTED TO BOTTOM OF TEST CAVITY COVERED WITH .004" SS SHIM — BEFORE TEST 1,615.5 Ω AFT. TEST 1615.2 Ω

G : C300-1,500-EKRTE Flat Pack #1 — BEFORE TEST 1,460.3 Ω AFT TEST 1,458.4 Ω

G : C300-1,500-EKRTE Flat Pack #2 — BEFORE TEST 1,470.7 Ω AFT. TEST 1,468.8 Ω

G 3: C300-1,500-EKRTE Flat Pack #3 — BEFORE TEST 1,503.8 Ω AFT TEST 1,501.9 Ω

SCOPE 9314

LOAD PRESS 200 PSI

GAUGE EMPLACEMENT : σ_x: SEE OTHER SIDE

TEST RESULTS

FP#1, 100 MV, 47.6 PSI

σ_x: FP#2, 125 MV, 59.5 PSI

σ_x: FP#3, 113 MV, 53.8 PSI

G_B, 70 MV, 33.3 PSI

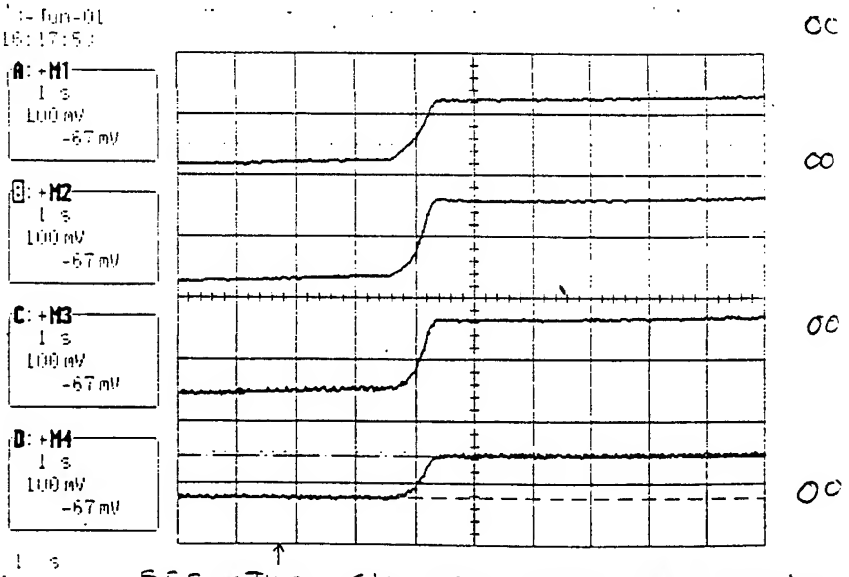

Fig. 12.

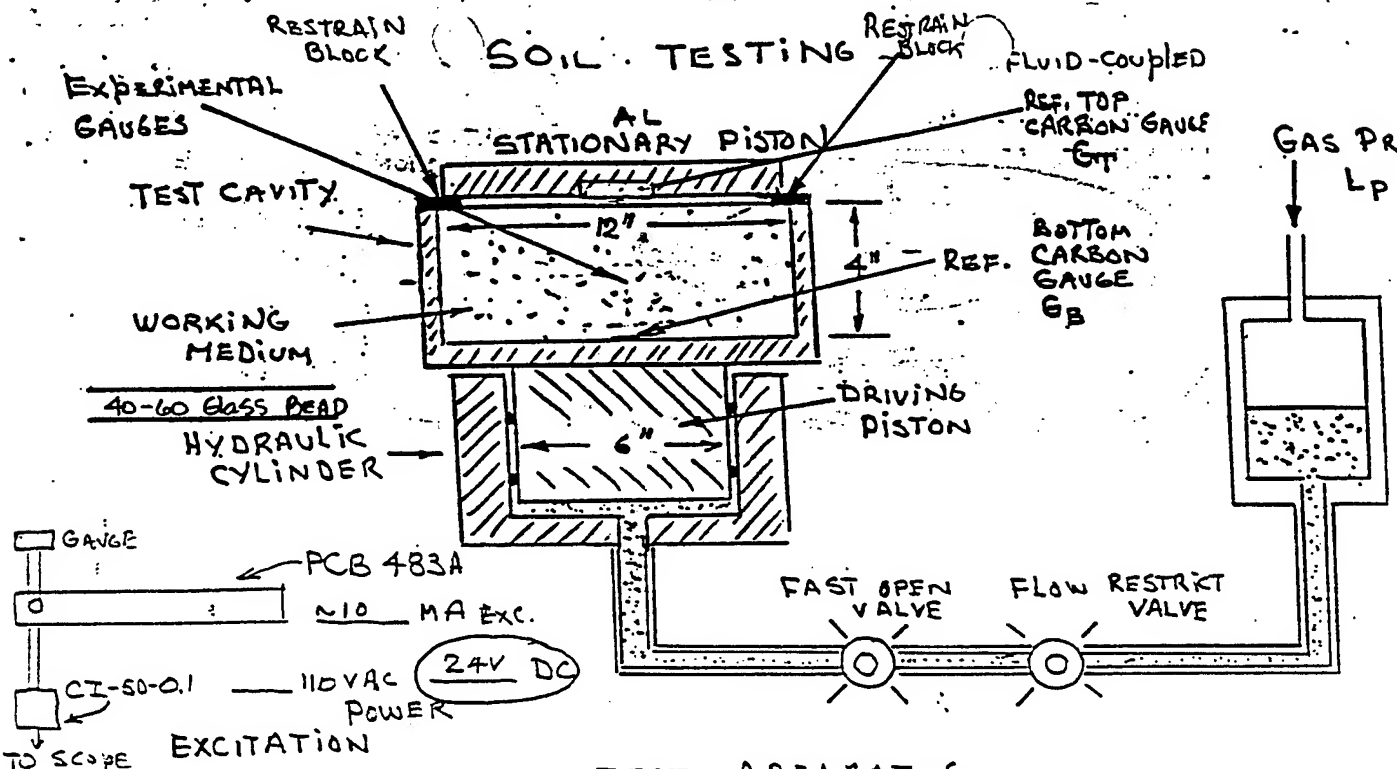

TEST APPARATUS

TEST DATE 10/14/01 SALE NO S-4787 TEST NO 10/14/01 TEMP. ~22 °C

TEST PURPOSE REPEAT TEST 10/13/01 AND PREVENT STATIONARY PISTON TO TOUCH 40-60 GLASS BEADS USING 3 RESTRAIN STEEL BLOCK

GAUGES:

G_T: C300-1,500-EKRTE ; CEMENTED TO BOTTOM OF STATIONARY PISTON. BEFORE TEST: 1,590.8 Ω AFTER TEST: 1,590.7 Ω
COVERED WITH .004" S.S. SHIM

G_B: C300-1,500-EKRTE: CEMENTED TO BOTTOM OF TEST CAVITY BEFORE TEST Ω AFT. TEST Ω
COVERED WITH .004" SS SHIM

G : C300-1,500-EKRTE FP #4 BEFORE TEST 1817.8 Ω AFT TEST 1817.8 Ω

G : C300-1,500-EKRTE FP #5 BEFORE TEST 1,764.5 Ω AFT. TEST 1,764.5 Ω

G 3: C300-1,500-EKRTE FP # 6 BEFORE TEST Ω AFT TEST Ω

SCOPE LT 344

LOAD PRESS 200 PSI

GAUGE EMPLACEMENT : SEE OTHER SIDE

TEST RESULTS

G_T V_A = 15.71V	.009	$\%\frac{\Delta R}{R}$ = 5.74% $\%\varepsilon$ = 1.0%
FP#4 V_A = 17.82V	0 V	0 PSI
FP#5 V_A = 17.30V	0 V	0 PSI
FP#6 V_A = 16.63V	0 V	0 PSI

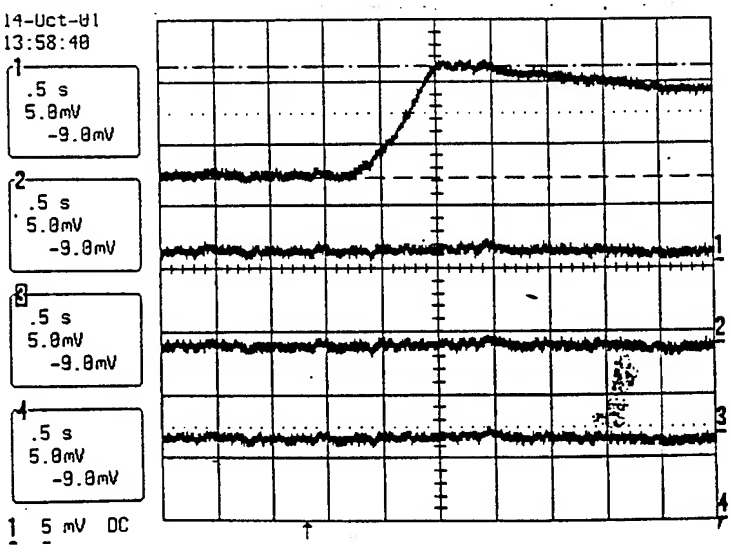

COMMENT: APPROXIMATE CALCULATIONS SHOW 1% STRAIN!!!

SEE OTHER SIDE FOR MINI FLAT PACK LOCATIONS

Fig. 13

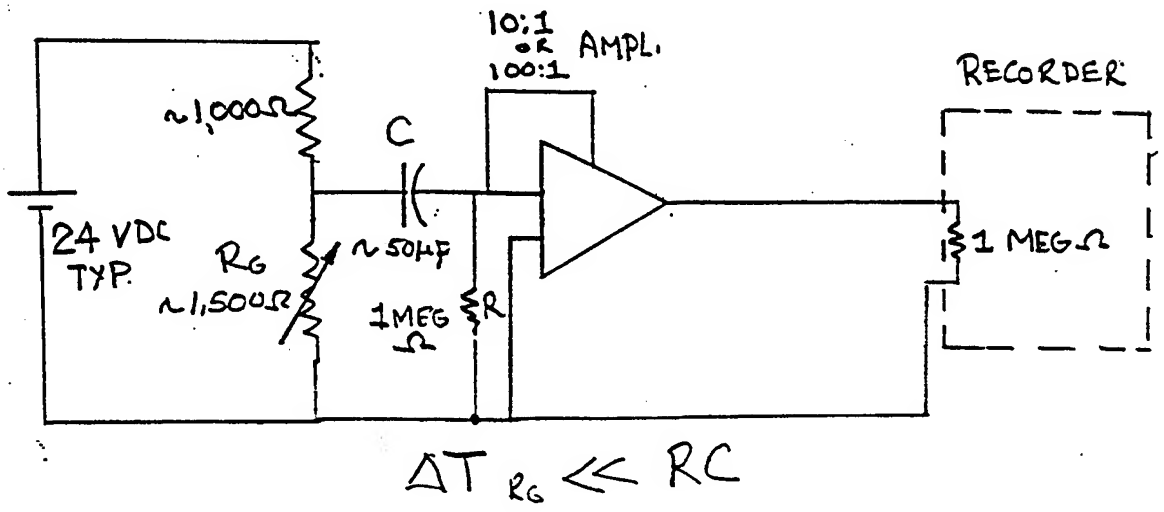

-A- Large Capacitor Coupling Method

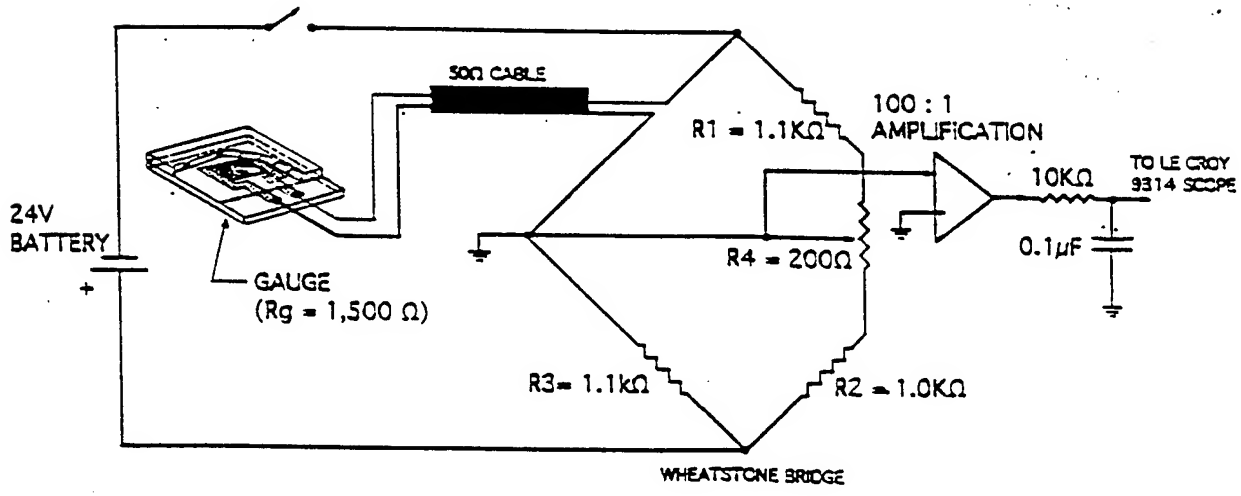

-B- Bridge/Amplification Excitation Method

Fig. 14. Carbon Elements Excitation Techniques.

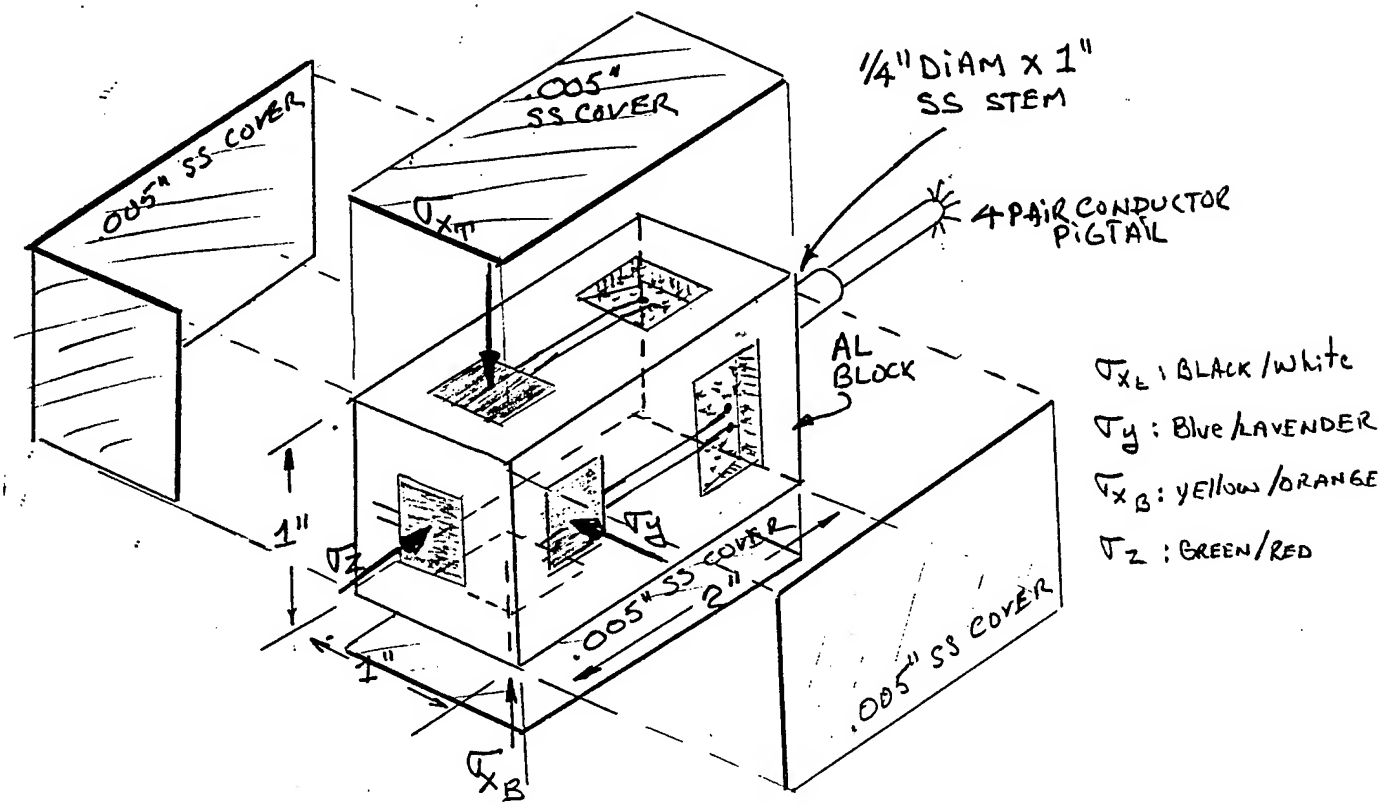

-A- Solid-Coupled Arrangement.

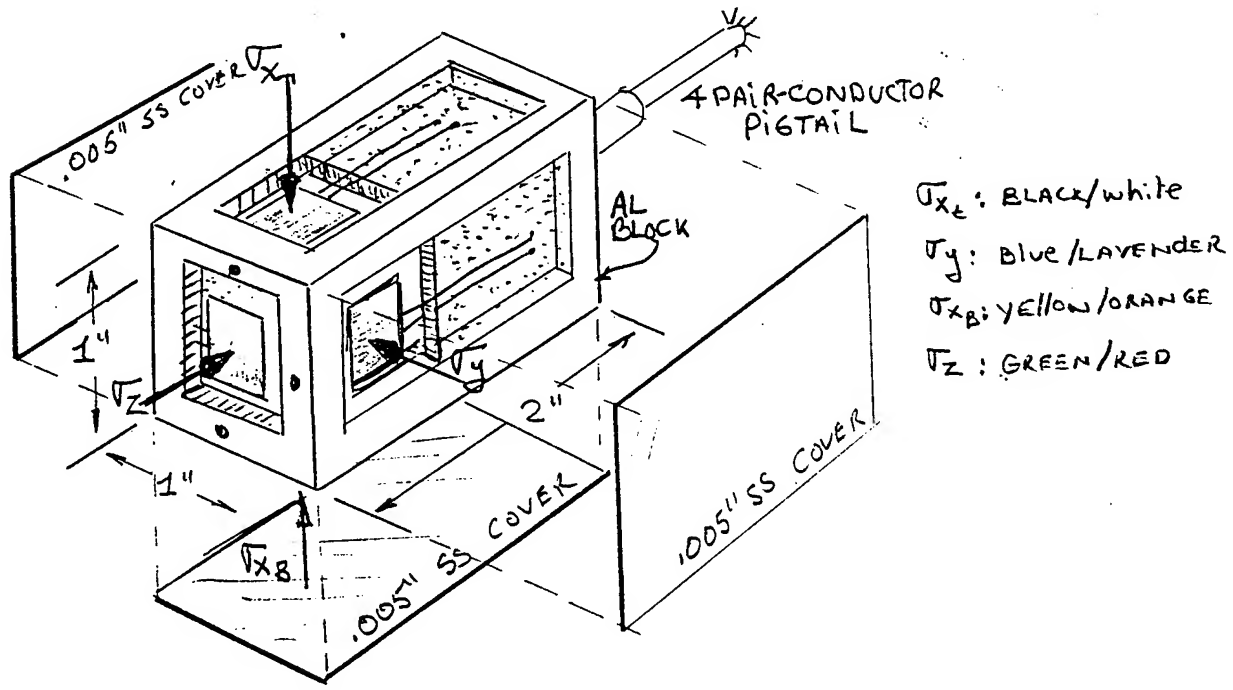

-B- Fluid-Coupled Arrangement.

Fig. 15. Symmetrical Rectangular 3D Stress Sensors.

H.V.D.P. STATIC CAL. TEST

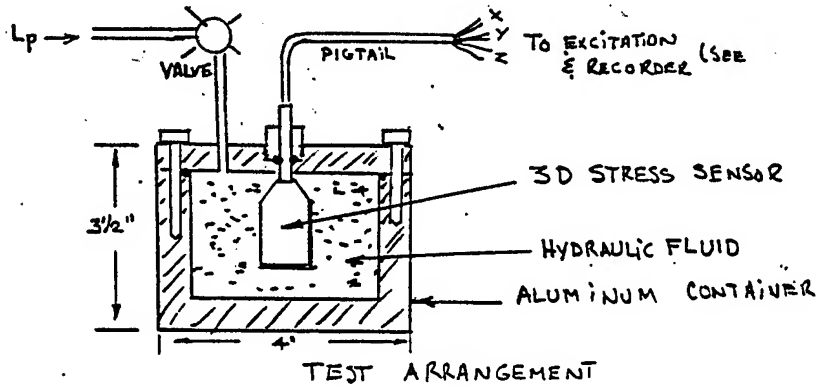

TEST ARRANGEMENT

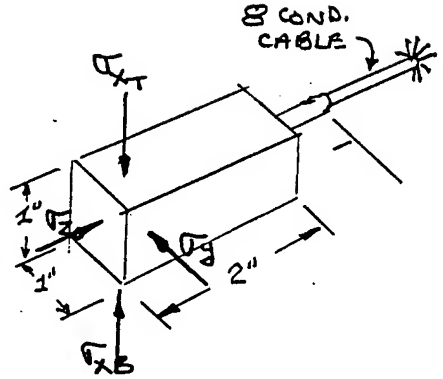

3D SENSOR SOLID-COUPLED #1

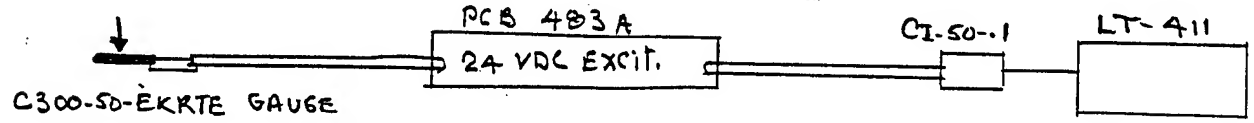

EXCITATION & RECORDING

DATE 12/4/01 Temp: 15°C TEST #: 12/4/01 T1 TEST PRESS 25 PSI

GAUGE	R, Ω BEFORE TEST	R, Ω AFTER TEST	ΔV, EXCIT. BEFORE TEST	ΔV, EXCIT. AFT. TEST	ΔV, SIGNAL	
σ_{xT} BLACK/WHITE	2,328.0	2,328.0	21.46	21.48	.00072 V	
σ_y BLUE/LAVENDER	2,003.0	2,003.0	18.84	18.86	.00072 V	
σ_{xB} YELLOW/ORANGE	1,821.0	1,820.0	17.21	17.22	.00072 V	
σ_z GREEN/RED	2,343.0	2,342.0	21.64	21.67	?	

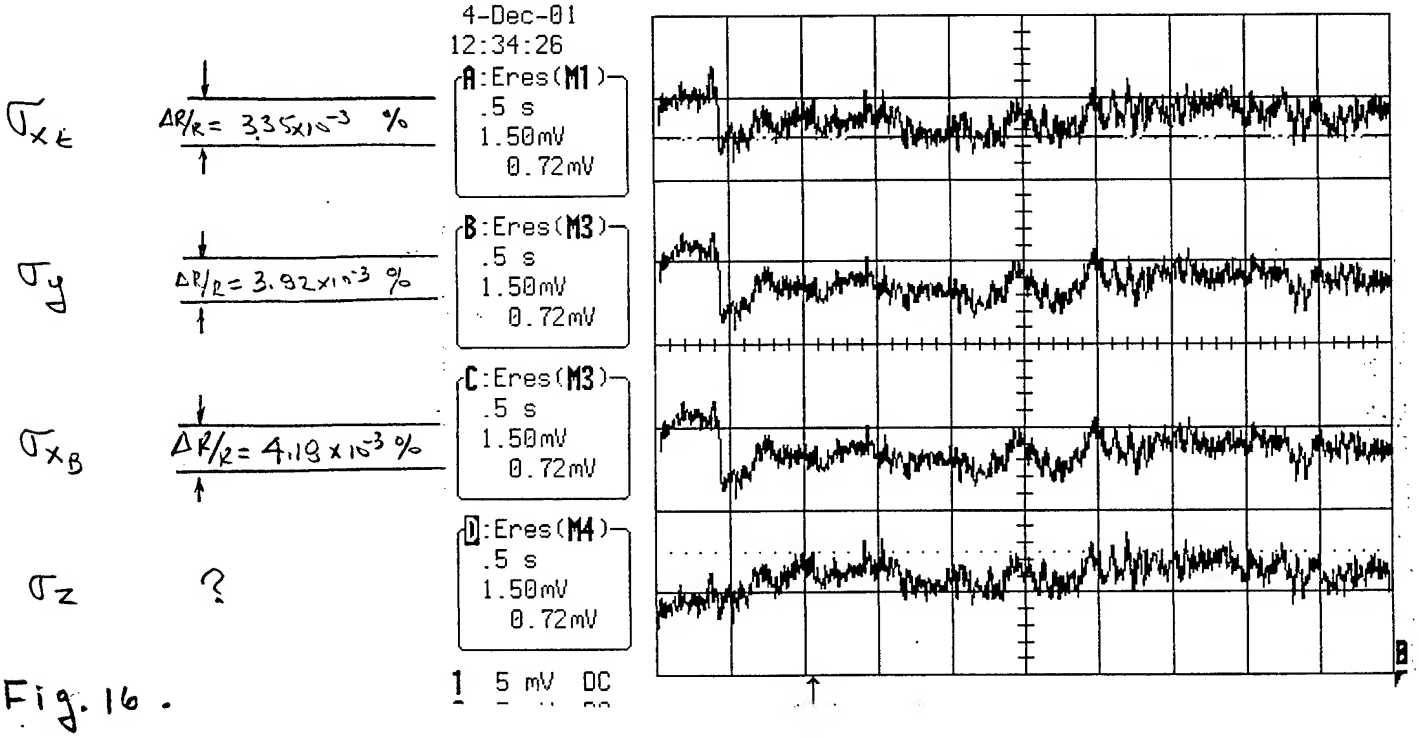

σ_{xT} $\Delta R/R = 3.35 \times 10^{-3}$ %

σ_y $\Delta R/R = 3.92 \times 10^{-3}$ %

σ_{xB} $\Delta R/R = 4.18 \times 10^{-3}$ %

σ_z ?

Fig. 16.

HYDROSTATIC CAL. TEST

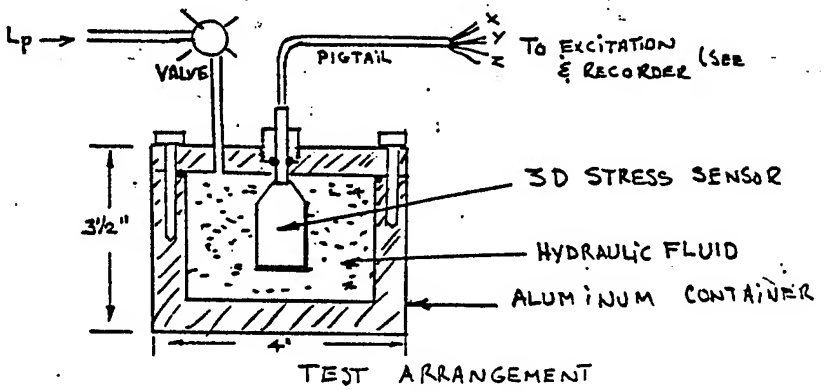

TEST ARRANGEMENT

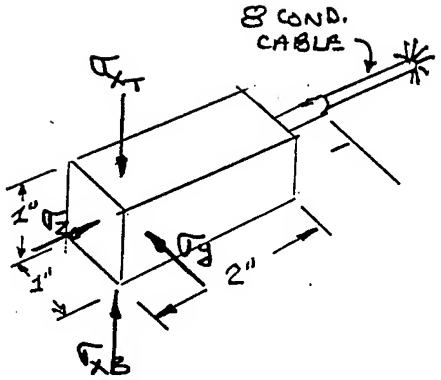

3D SENSOR SOLID-COUPLED #1

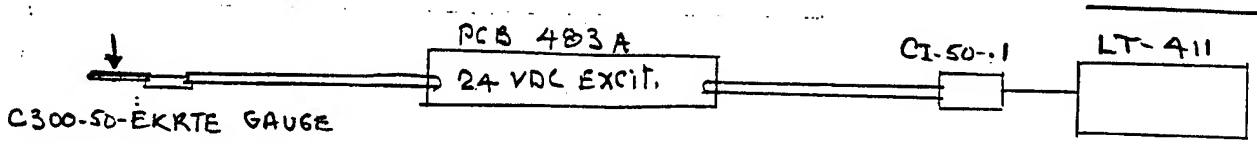

EXCITATION & RECORDING

DATE 12/03/01 17°C TEST #: 12/03/01 T2 ___ TEST PRESS 50 PSI

GAUGE	R, Ω BEFORE TEST	R, Ω AFTER TEST	ΔV, EXCIT. BEFORE TEST	ΔV, EXCIT. AFT. TEST	ΔV. SIGNAL	
σ_{xT} BLACK-WHITE	2,322.0	2,321.0	21.61	21.65	.00201	
σ_y BLUE LAVENDER	1,999.0	1,997.0	18.98	19.02	.00196	
σ_{xB} YELLOW ORANGE	1,816.0	1,815.0	17.34	17.39	.00205	
σ_z GREEN RED	2,339.0	2,339.0	21.80	21.85	.00093	

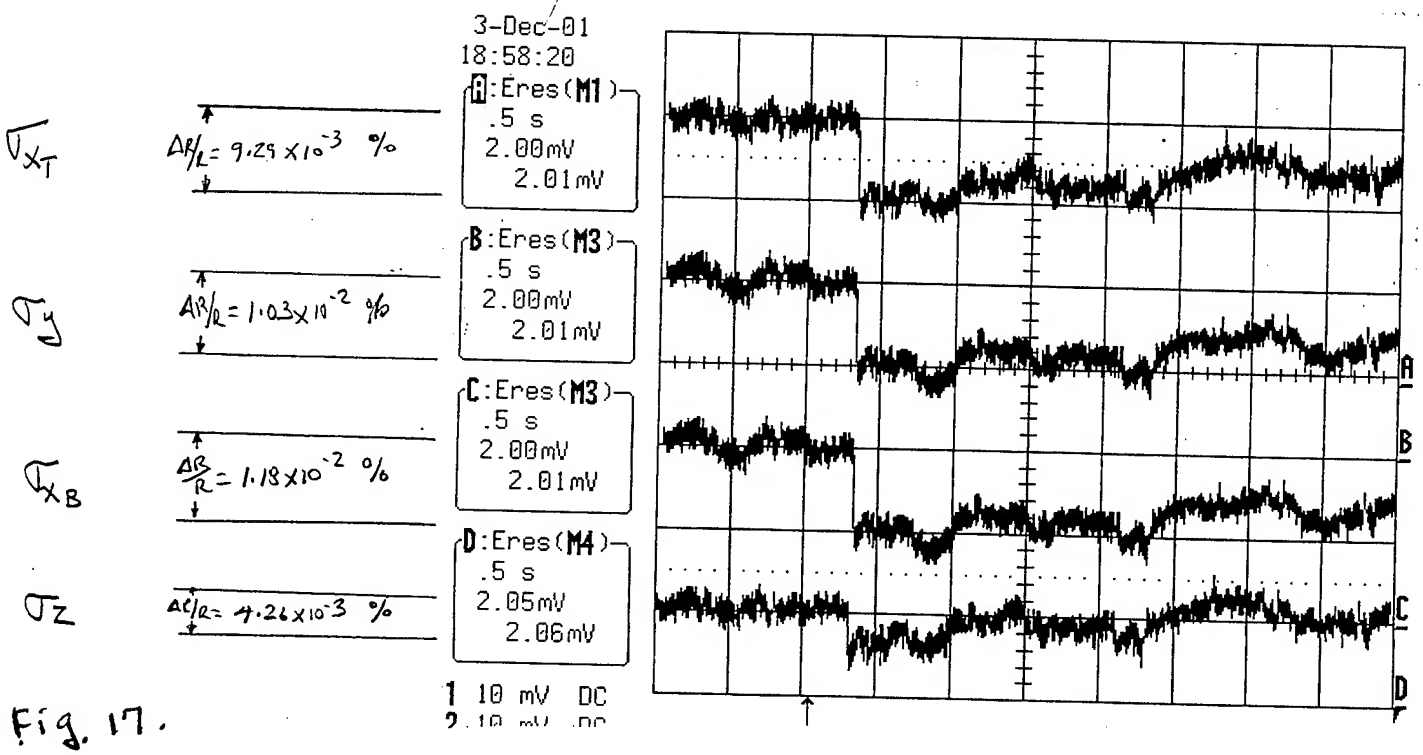

Fig. 17.

HYDROSTATIC CAL. TEST

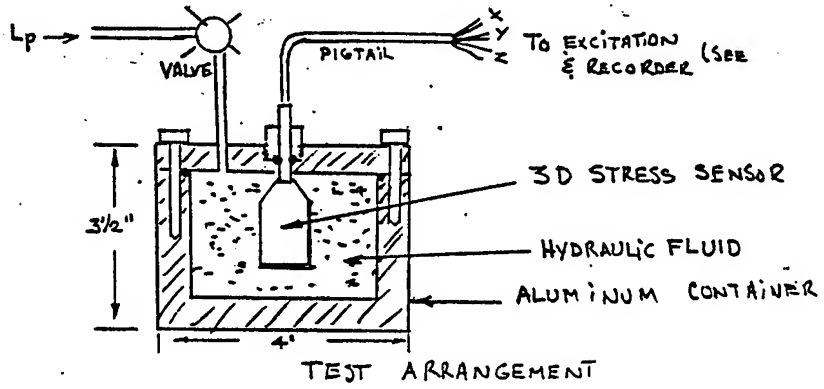

TEST ARRANGEMENT

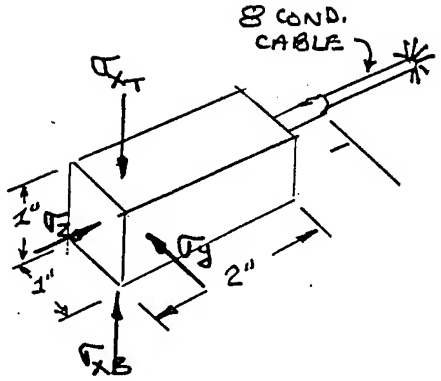

3D SENSOR SOLID-COUPLED #1

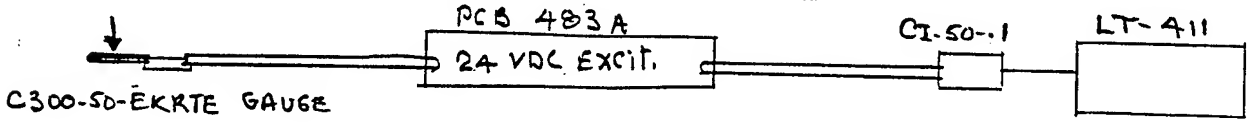

EXCITATION & RECORDING

DATE 12/3/01 17°C TEST#: 12/3/01 T 1 TEST PRESS 50 PSI

GAUGE	R, Ω BEFORE TEST	R, Ω AFTER TEST	ΔV, EXCIT. BEFORE TEST	ΔV, EXCIT. AFT. TEST	ΔV. SIGNAL	
σ_{xT} BLACK-WHITE	2,322.0	2,321.0	21.56 V	21.62 V	.00205 V	
σ_y BLUE/LAVENDER	1,998.0	1,997.0	18.93 V	18.99 V	.00228 V	
σ_{xB} YELLOW/ORANGE	1,816.0	1,815.0	17.30 V	17.36 V	.00232 V	
σ_z GREEN/RED	2,339.0	2,338.0	21.75 V	21.82 V	.00117 V	

σ_{xT} $\Delta R/R = 9.49 \times 10^{-3}$ %

σ_y $\Delta R/R = 1.32 \times 10^{-2}$ %

σ_{xB} $\Delta R/R = 1.34 \times 10^{-2}$ %

σ_z $\Delta R/R = 5.37 \times 10^{-3}$ %

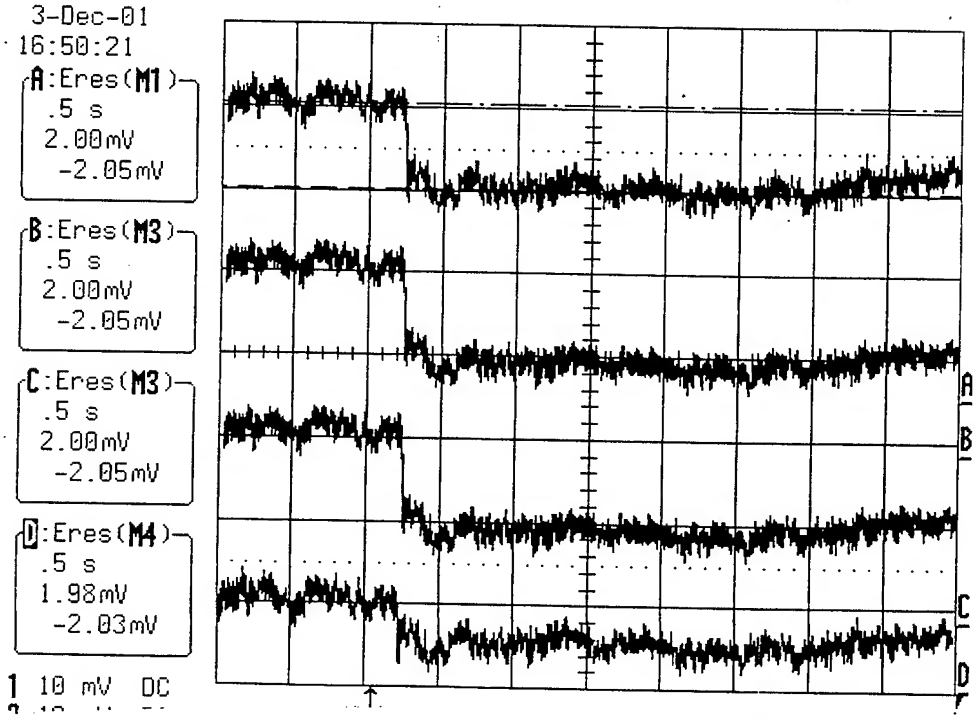

Fig. 18.

H.V.DR. STATIC CAL. TEST

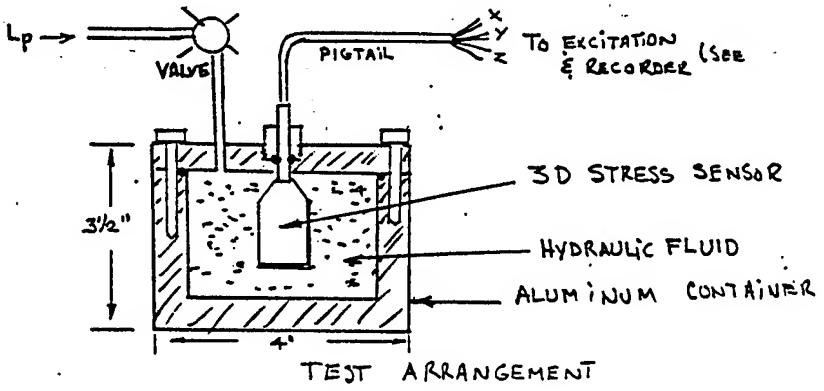

TEST ARRANGEMENT

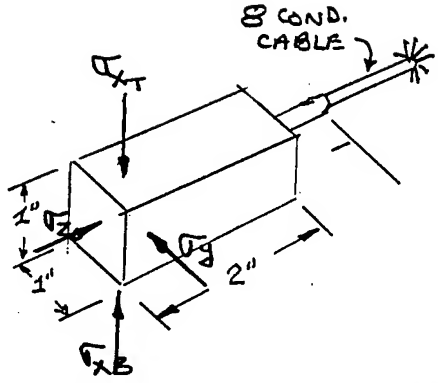

3D SENSOR SOLID-COUPLED #1

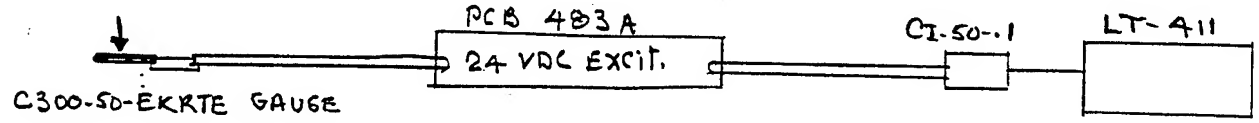

EXCITATION & RECORDING

DATE 12/14/01 15°C TEST#: 12/14/01 T2 Test Press 50 PSI

GAUGE	R, Ω BEFORE TEST	R, Ω AFTER TEST	ΔV, EXCIT. BEFORE TEST	ΔV, EXCIT. AFT. TEST	ΔV, SIGNAL	
σ_{xT} BLACK-WHITE	2,328.0	2,328.0	21.53	21.53	.00179 V	
σ_y BLUE/LAVENDER	2,003.0	2,003.0	18.90	18.91	.00210 V	
σ_{xB} YELLOW/ORANGE	1,821.0	1,820.0	17.28	17.28	.00187 V	
σ_z GREEN/RED	2,343.0	2,342.0	21.73	21.74	.00096 V	

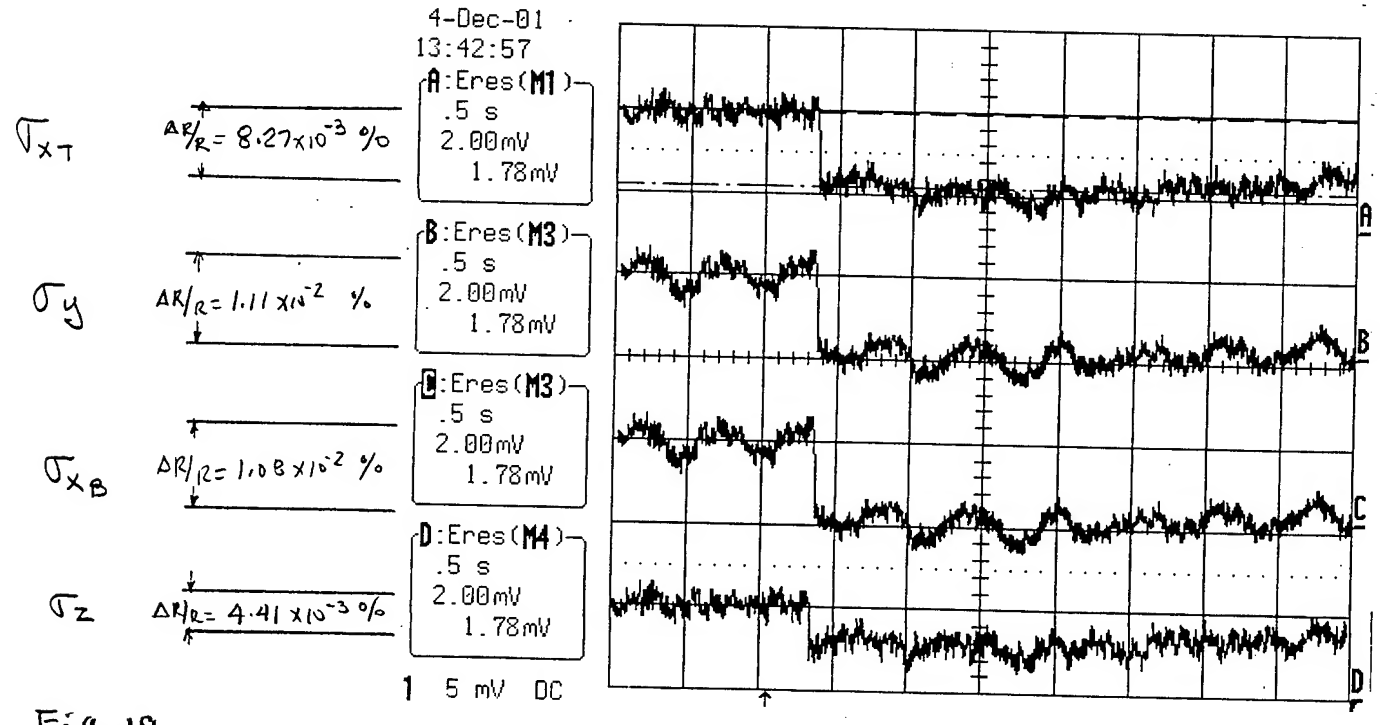

Fig. 19.

HYDROSTATIC CAL. TEST

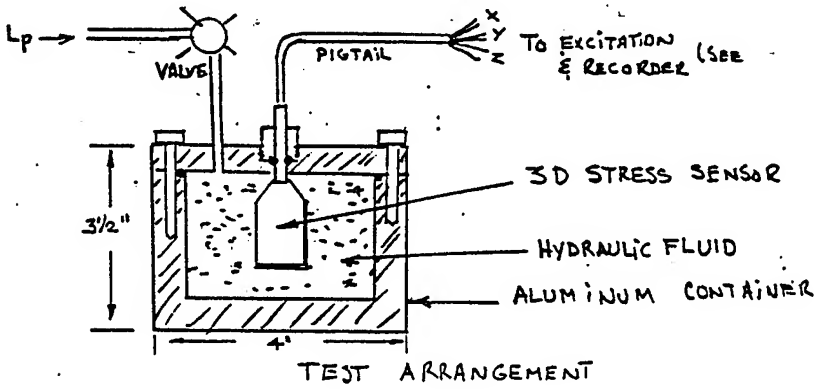

TEST ARRANGEMENT

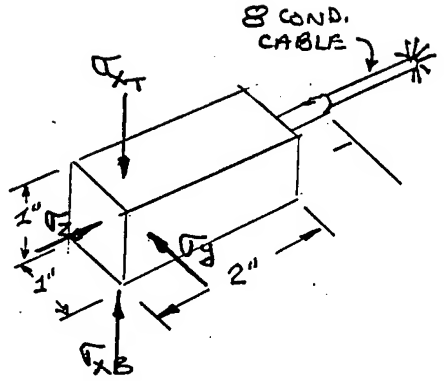

3D SENSOR SOLID-COUPLED #1

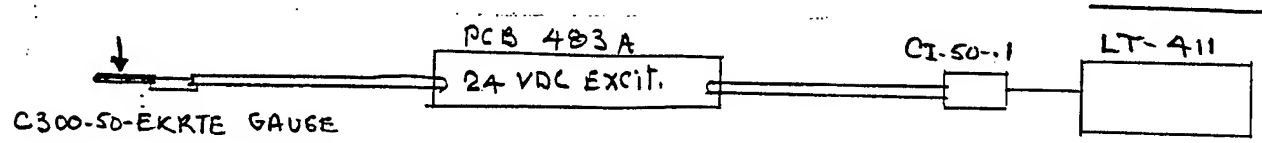

EXCITATION & RECORDING

DATE 12/03/01 17°C TEST# 12/03/01 T3 ___ TEST PRESS 100 PSI

GAUGE	R, Ω BEFORE TEST	R, Ω AFTER TEST	ΔV, EXCIT. BEFORE TEST	ΔV, EXCIT. AFT. TEST	ΔV, SIGNAL	
σ_{xT} BLACK-WHITE	2,382.0	2,321.0	21.45	21.48	.00376	
σ_y BLUE LAVENDER	1,998.0	1,997.0	18.93	19.87	.00393	
σ_{xB} YELLOW ORANGE	1816.0	1,815.0	17.19	17.24	.00376	
σ_z GREEN RED	2,338.0	2,337.0	21.63 ✓	21.68	.00329	

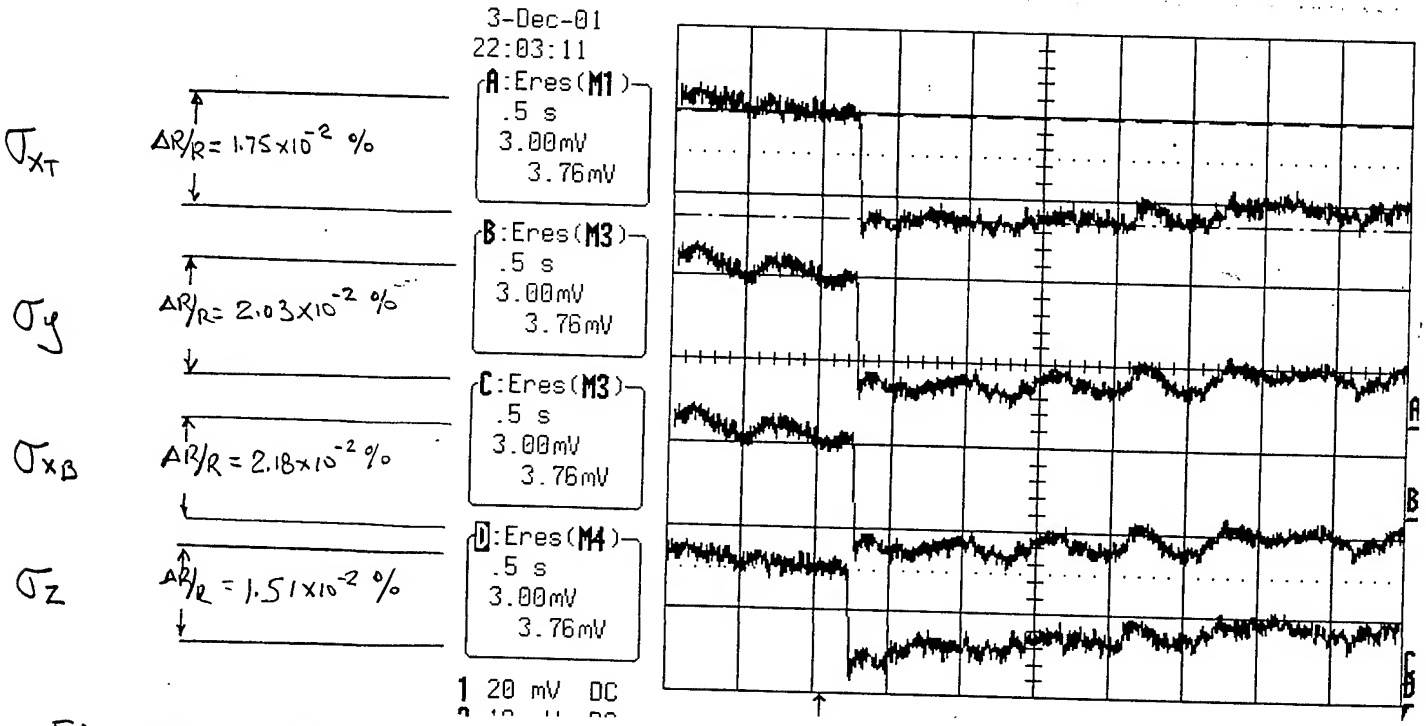

Fig. 20.

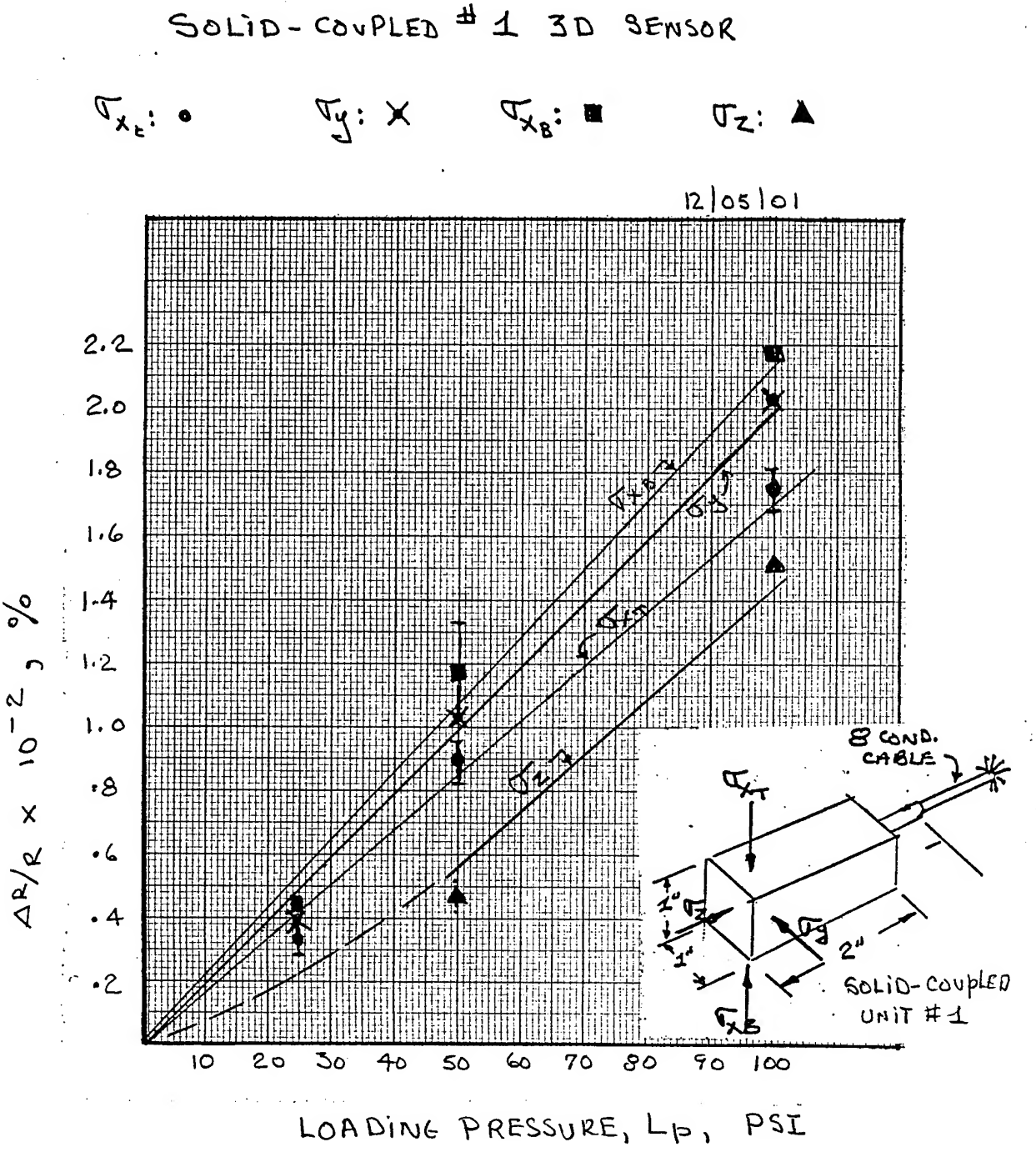

Fig. 21. Hydro-Static Calibration of Symmetrical Solid-Coupled 3D Sensor.

SOIL TRANSDUCER TESTING

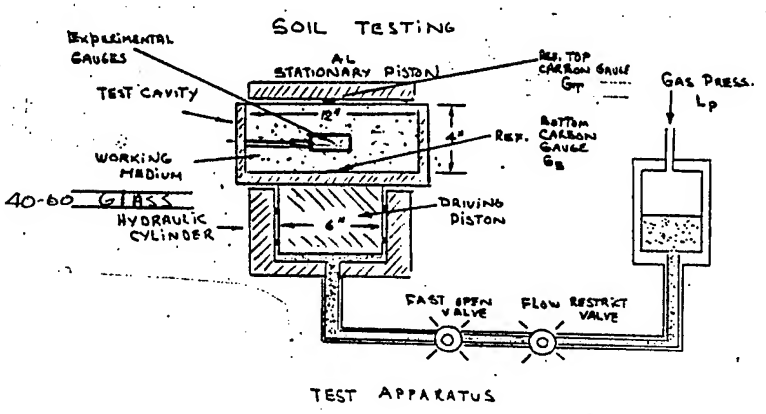

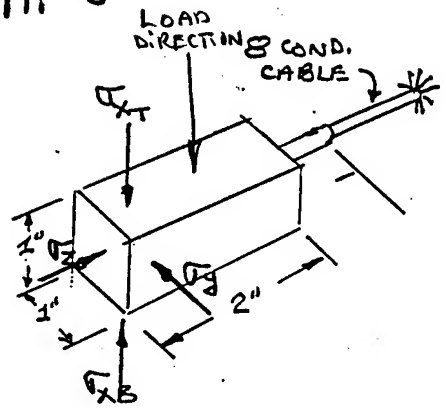

3D SENSOR SOLID-COUPLED #1

σ_{xt} Pointing UPWARD

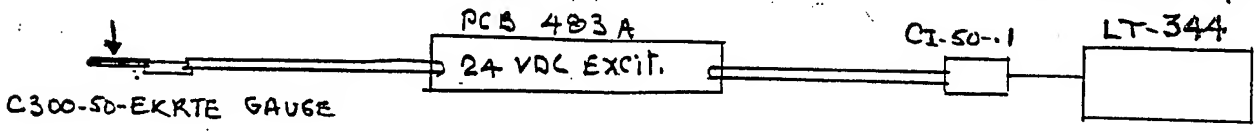

EXCITATION & RECORDING

DATE 12/4/01 TEMP. 17 °C TEST #: 12/4/01 T1 TEST PRESS L_P: 200 PSI

1ST TEST AFTER TEST BED FILL

GAUGE	R_1 Ω BEFORE TEST	R_1 Ω AFTER TEST	ΔV_E EXCIT. BEFORE TEST	ΔV_E EXCIT. AFT. TEST	ΔV_S SIGNAL	
σ_{xT} BLACK-WHITE	2,325.0		21.59 V	21.65 V	.00178 V	
σ_y BLUE/LAVENDER	1,999.0		17.17 V	17.24 V	.00105 V	
σ_{xB} YELLOW/ORANGE	1,816.0		18.80 V	18.87 V	.00219 V	
σ_z GREEN/RED	2,339.0		21.44 V	21.49 V	.00073 V	

$\frac{\Delta R}{R} = \frac{\Delta V_S}{\Delta V_E} \times 100$ %

CAL: 12/05/01

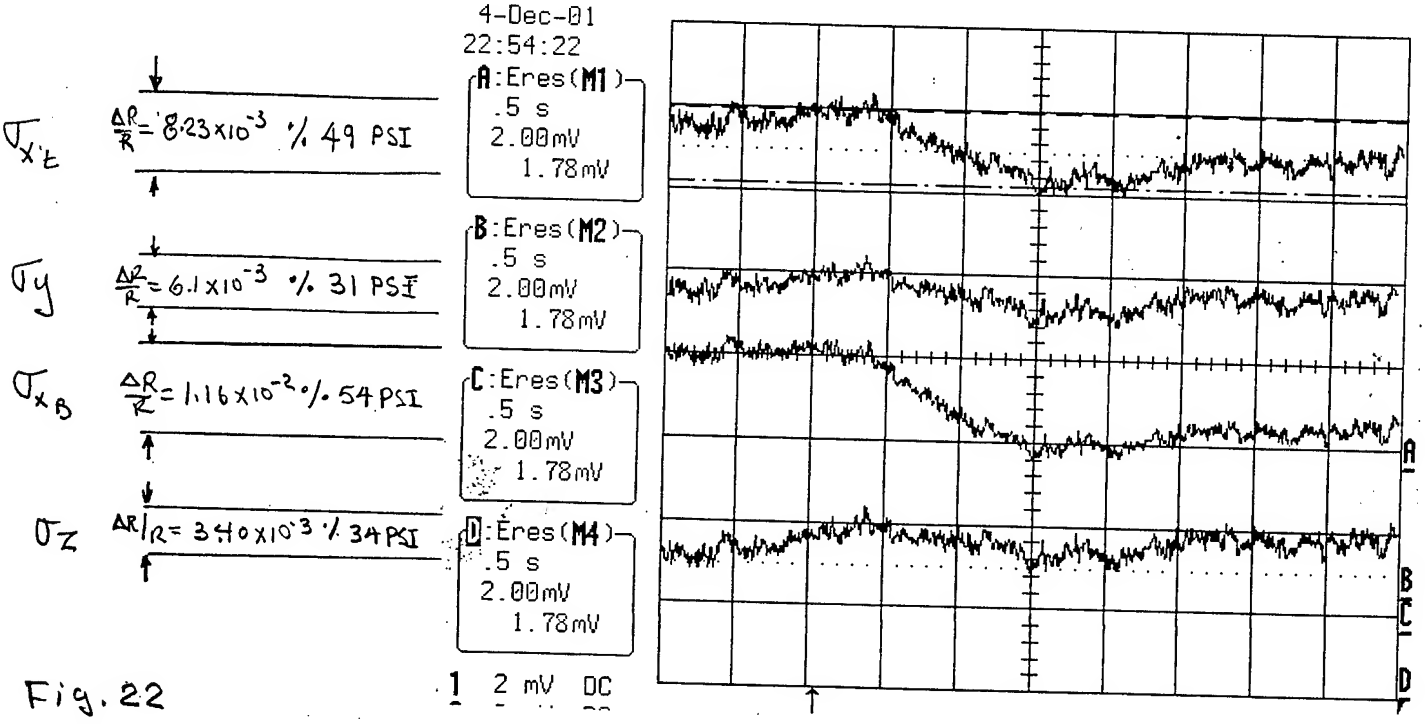

Fig. 22

SEE OTHER SIDE FOR ACTUAL REC.

SOIL TRANSDUCER TESTING

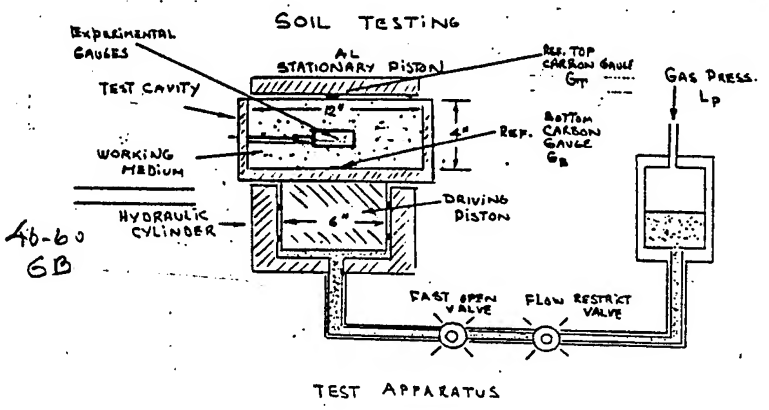

46-60
6B

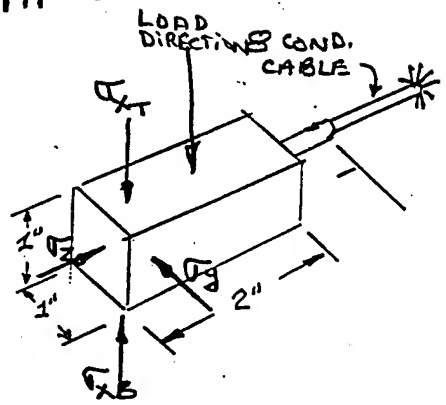

3D SENSOR SOLID-COUPLED #1

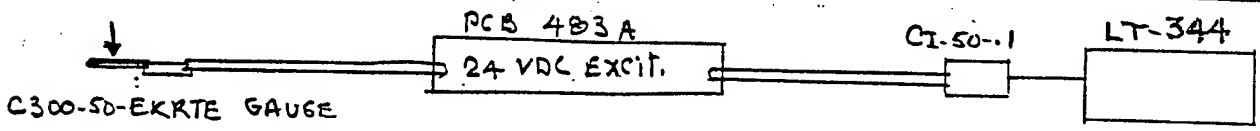

EXCITATION & RECORDING

DATE 12/05/01 TEMP. 15 °C TEST #: 12/05/01 T1 TEST PRESS L_p: 200 PSI → (120)

2nd TEST AFTER TEST #12/04/01T1 BED LEFT UNDISTURBED

GAUGE	R, Ω BEFORE TEST	R, Ω AFTER TEST	ΔV, EXCIT. BEFORE TEST	ΔV, EXCIT. AFT. TEST	ΔV, SIGNAL	
σ_{xT} BLACK-WHITE	2,329.0	2,326.0	21.36 V	21.39 V	.00251	
σ_y BLUE/LAVENDER	2004.0	2,001.0	18.75 V	18.79 V	.00118	
σ_{xB} YELLOW/ORANGE	1821.0	1,819.0	17.13 V	17.16 V	.00324	
σ_z GREEN/RED	2,343.0	2,341.0	21.54 V	21.58 V	.001/0007	

$$\frac{\Delta R}{R} = \frac{\Delta V_S}{\Delta V_E} \times 100$$

CAL: 12/05/01

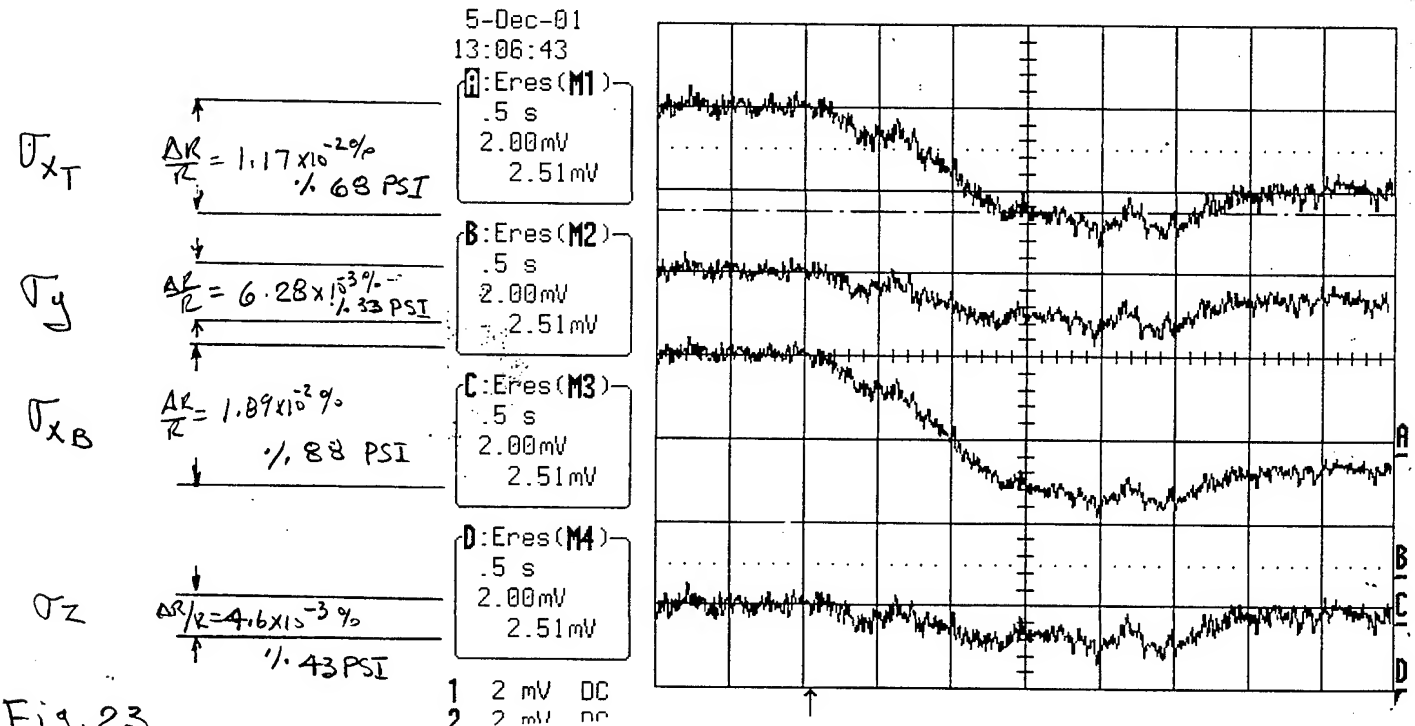

Fig. 23

SEE OTHER SIDE FOR ACTUAL RECORDING

50" TRANSDUCER TESTING

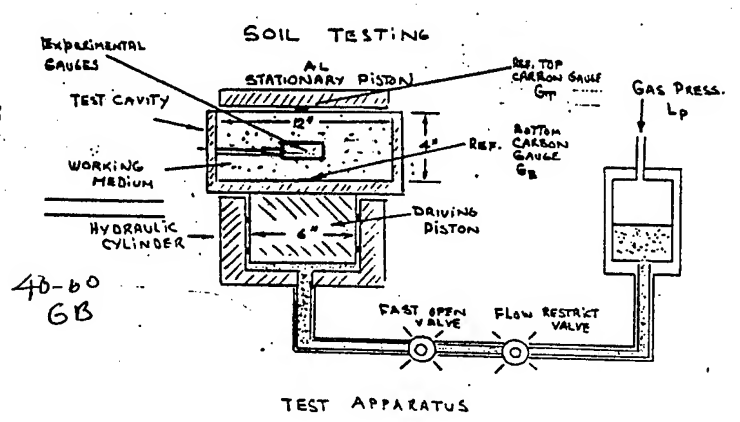

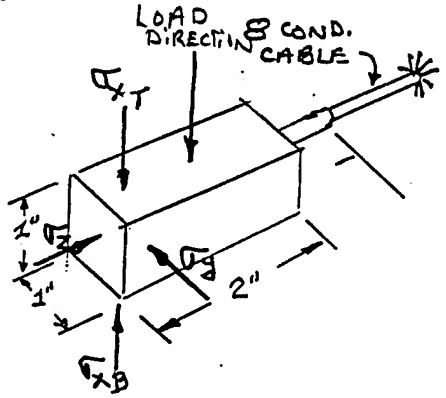

3D SENSOR SOLID-COUPLED #1

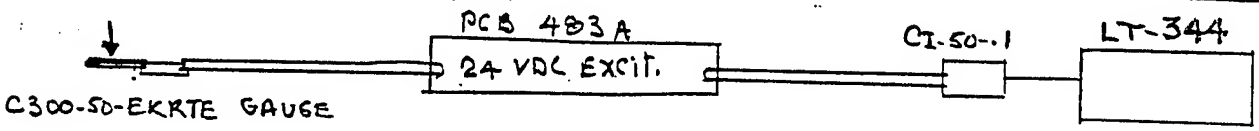

EXCITATION & RECORDING

DATE 12/05/01 TEMP. 17°C TEST #: 12/05/01 T2 TEST PRESS L_P: 200 PSI

3RD TEST AFTER TEST # 12/04/01 T1, BED LEFT UNDISTURBED

GAUGE	R_1 Ω BEFORE TEST	R_1 Ω AFTER TEST	ΔV_E EXCIT. BEFORE TEST	ΔV_E EXCIT. AFT. TEST	ΔV_S SIGNAL	
σ_{XT} BLACK-WHITE	2,329.0		21.51 V	21.58 V	.00242 V	
σ_y BLUE LAVENDER	2,004.0		18.97 V	18.96 V	.00109 V	
σ_{XB} YELLOW ORANGE	1,821.0		17.25 V	17.32 V	.00283 V	
σ_Z GREEN RED	2343.0		21.69 V	21.78	.001 V	

$$\frac{\Delta R}{R} = \frac{\Delta V_S}{\Delta V_E} \times 100$$

CAL: 12/05/01

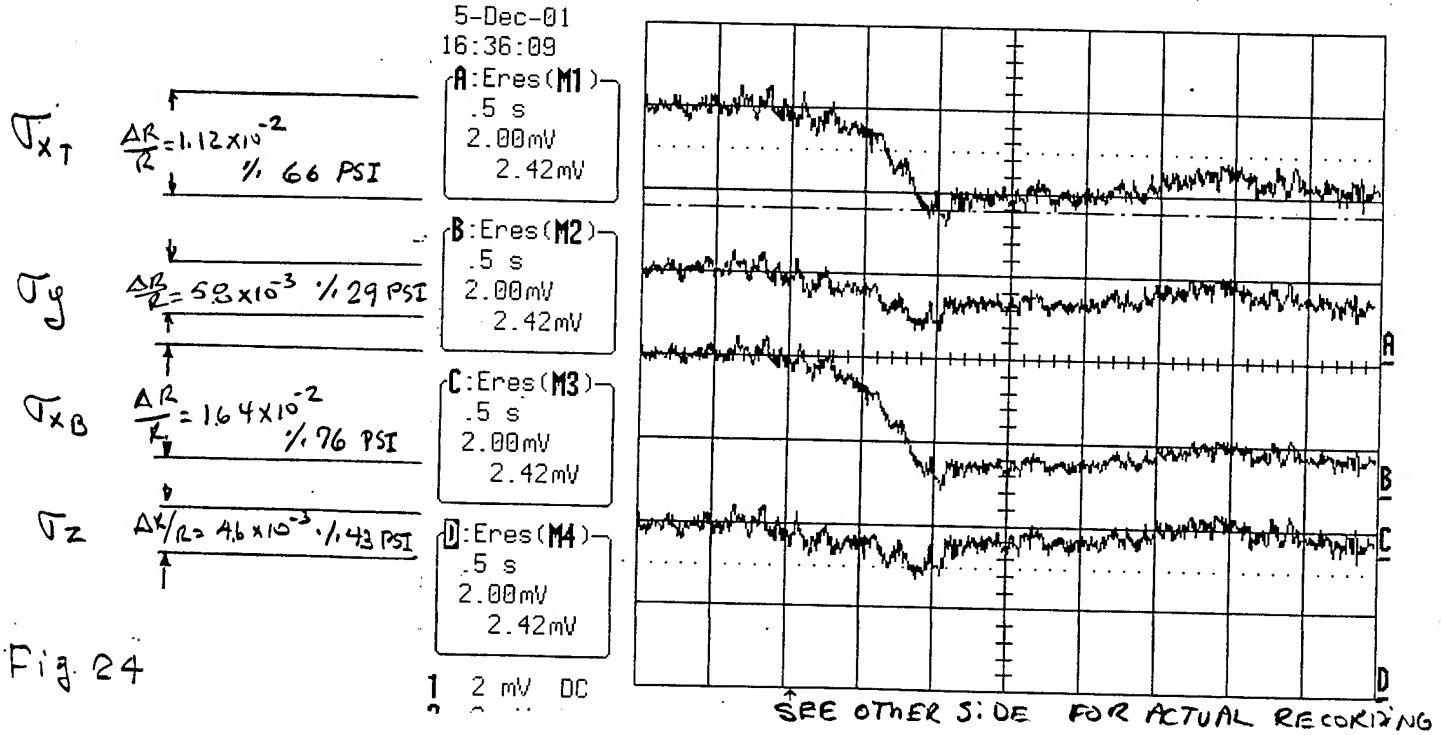

Fig. 24

SEE OTHER SIDE FOR ACTUAL RECORDING

50" TRANSDUCER TESTING

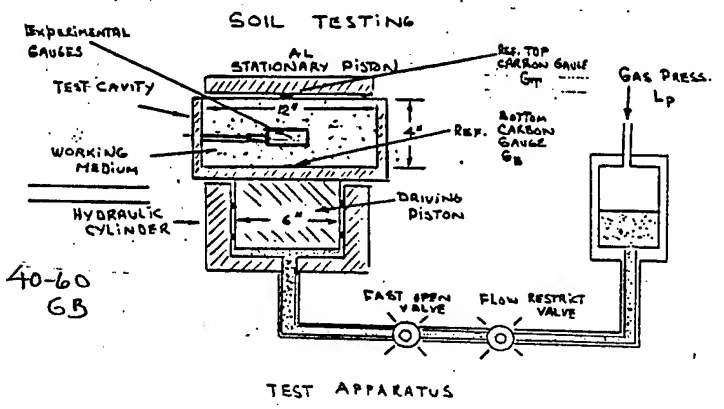

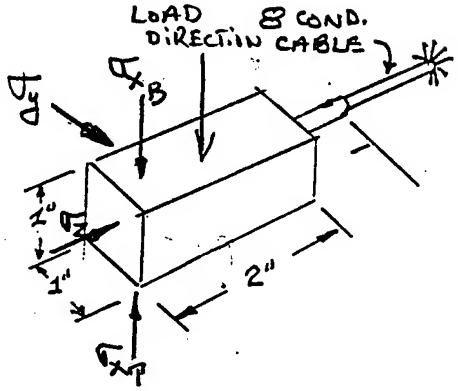

3D SENSOR SOLID-COUPLED #1

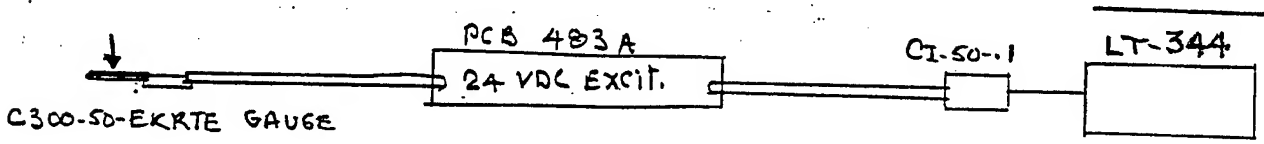

EXCITATION & RECORDING

DATE 12/05/01 TEMP. 17°C TEST #: 12/05/01 T3 TEST PRESS, L_P: 200 PSI

RE did TEST BEC GAUGE UP-SIDE DOWN

GAUGE	R, Ω BEFORE TEST	R, Ω AFTER TEST	ΔV_E, EXCIT. BEFORE TEST	ΔV_E, EXCIT. AFT. TEST	ΔV_S, SIGNAL	
σ_{xT} BLACK-WHITE	2,325.0		21.53 V	21.57 V	.00255	
σ_y BLUE/LAVENDER	2,001.0		18.90 V	18.96 V	.00068	
σ_{xB} YELLOW/ORANGE	1,819.0		17.27 V	17.27 V	.00201	
σ_z GREEN/RED	2340.0		21.71 V	21.71 V	.00036	

$$\frac{\Delta R}{R} = \frac{\Delta V_S}{\Delta V_E} \times 100\ \%$$

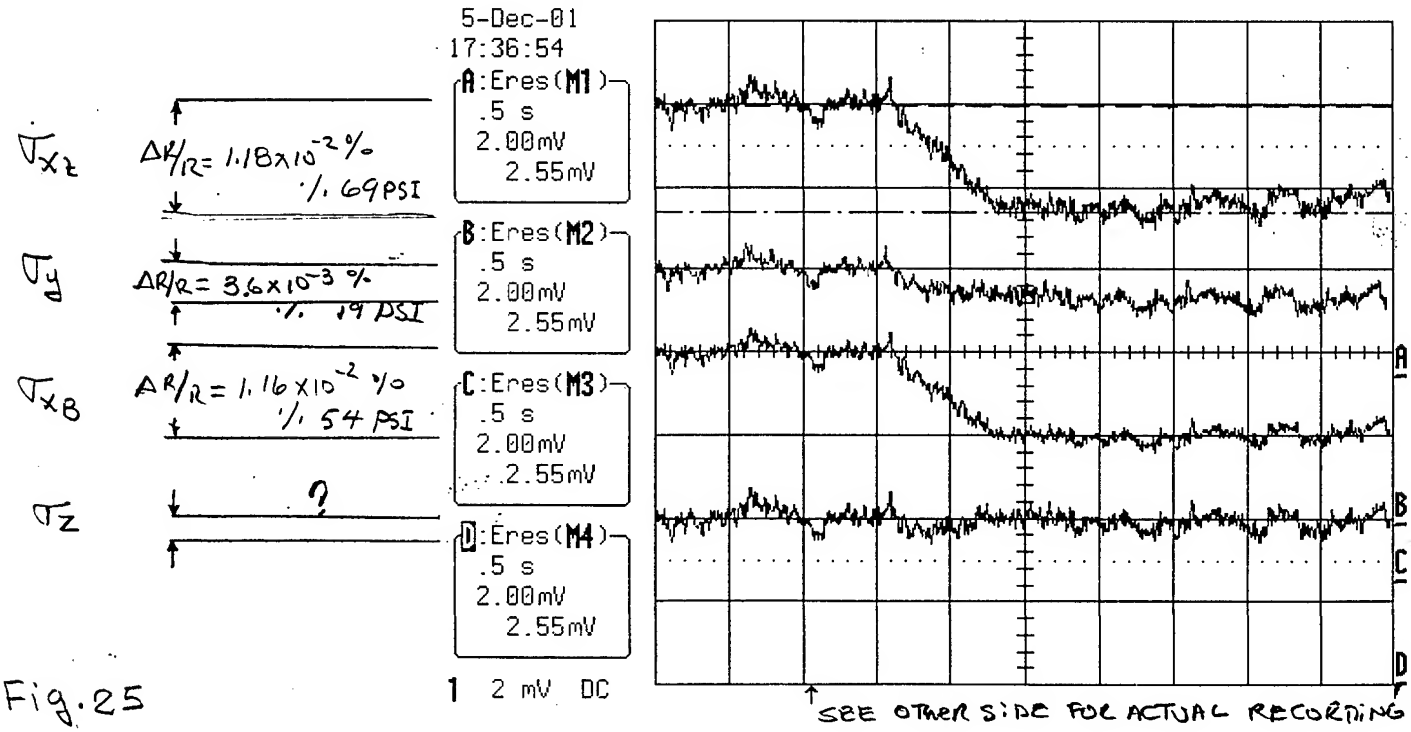

Fig. 25

H.V.D.P. STATIC CAL. TEST

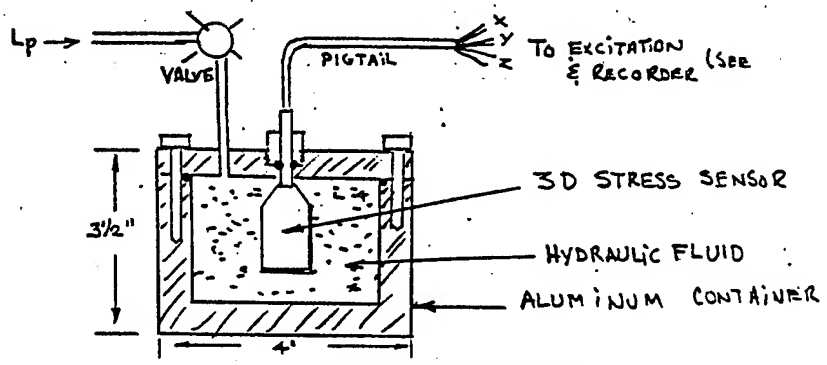

TEST ARRANGEMENT

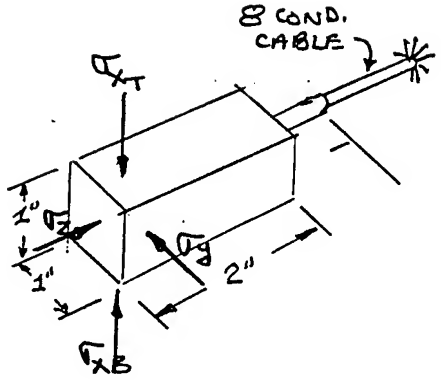

3D SENSOR FLUID-COUPLED #1

σy GAUGE DAMAGED

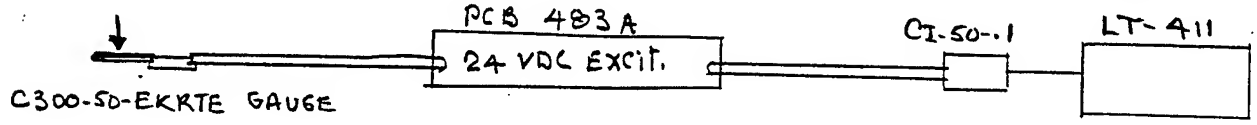

EXCITATION & RECORDING

DATE 12/06/01 Temp. 17°C TEST #: 12/06/01 TT TEST PRESS 25 PSI

GAUGE	R, Ω BEFORE TEST	R, Ω AFTER TEST	ΔV_E, EXCIT. BEFORE TEST	ΔV_E, EXCIT. AFT. TEST	ΔV_S, SIGNAL	
σ_{xT} BLACK-WHITE	1,837.1	1833.7	17.410 V	17.519	.00159	
σ_y BLUE LAVENDER	1,769.1	1,766.0	16.959 V	17.015	.00109	
σ_{xB} YELLOW ORANGE	1,849.7	1,845.6	17.640 V	17.688	.00164	
σ_z GREEN RED	1,643.8	1,640.9	15.730 V	15.782	.00155	

$$\frac{\Delta R}{R} = \frac{\Delta V_S}{\Delta V_E} \times 100\ \%$$

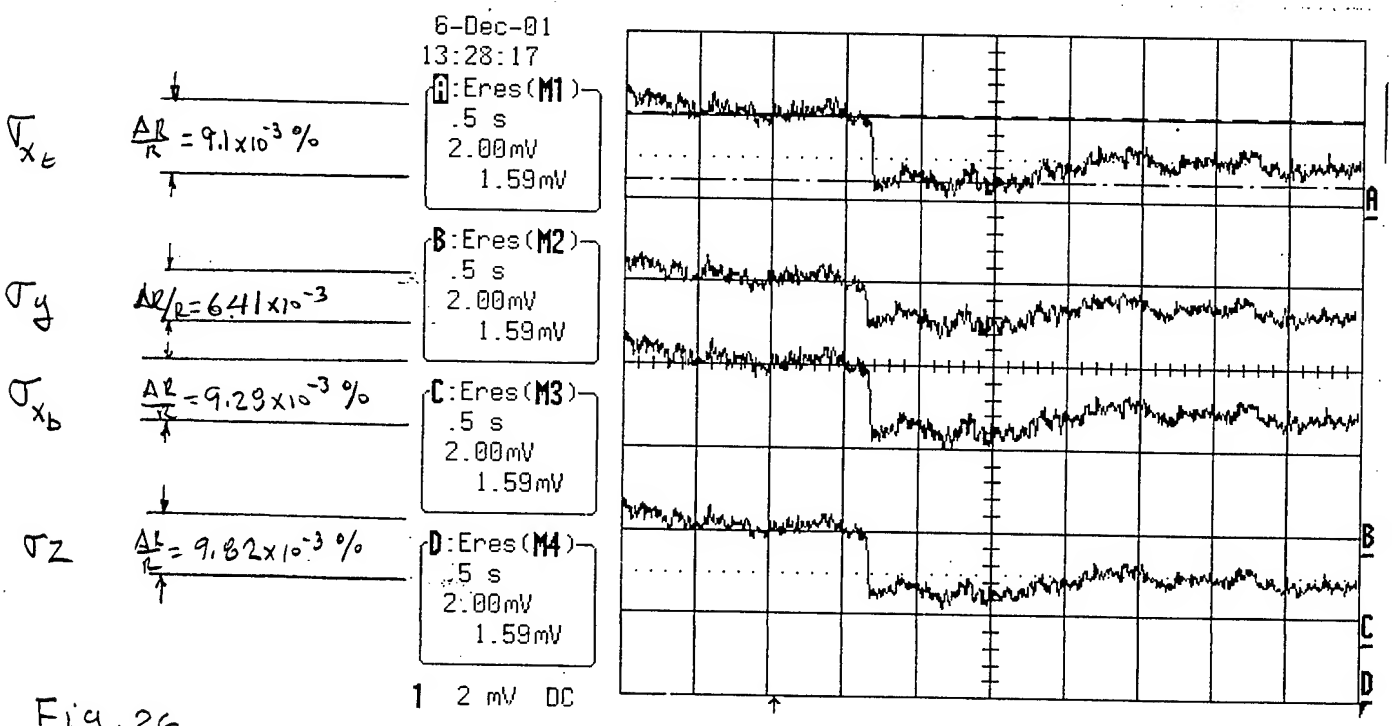

Fig. 26

H.V.D.P. STATIC CAL. TEST

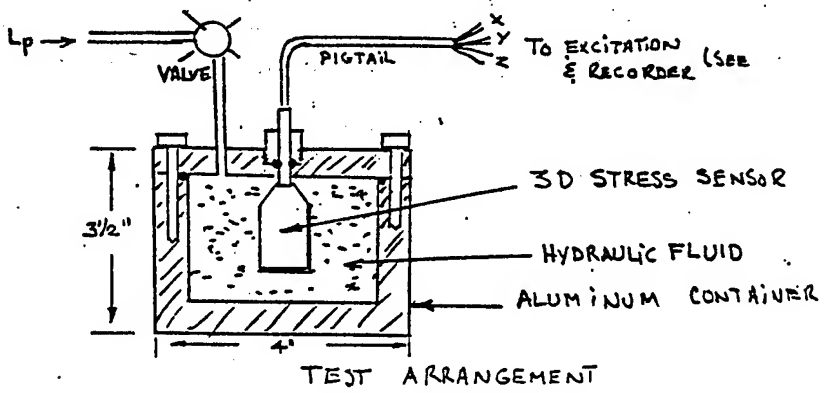

TEST ARRANGEMENT

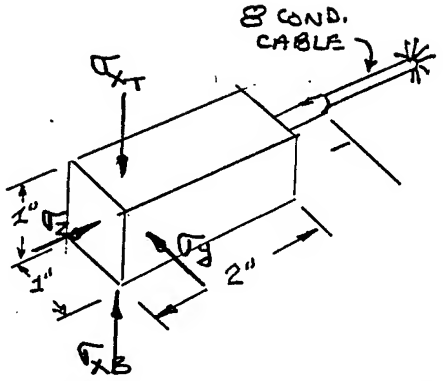

3D SENSOR

FLUID-COUPLED #1
σ_Y GAUGE DAMAGED

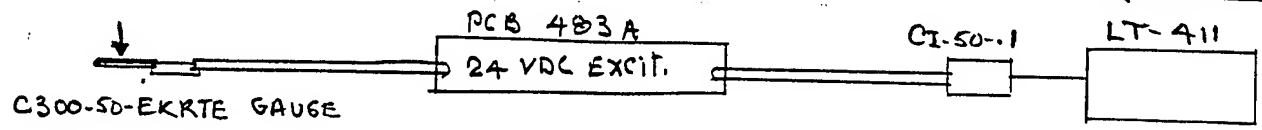

EXCITATION & RECORDING

DATE 12/06/01 TEMP. 17°C TEST #: 12/06/01A TZ TEST PRESS Lp: 50 PSI

GAUGE	R, Ω BEFORE TEST	R, Ω AFTER TEST	ΔV, EXCIT. BEFORE TEST	ΔV, EXCIT. AFT. TEST	ΔV, SIGNAL	
σ_{XT} BLACK-WHITE		1,833.2	17.540 V	17.549	.00287	
σ_Y BLUE/LAVENDER		1.765.4	17.037 V	17.046	.00205	
σ_{XB} YELLOW/ORANGE		1,844.9	17.713 V	17.720	.00296	
σ_Z GREEN/RED		1,6402	15.849	15.854	.00296	

$$\frac{\Delta R}{R} = \frac{\Delta V_S}{\Delta V_E} \times 100, \%$$

σ_{XT} $\frac{\Delta R}{R} = 1.64 \times 10^{-2}$ %

σ_Y $\frac{\Delta R}{R} = 1.2 \times 10^{-2}$ %

σ_{XB} $\frac{\Delta R}{R} = 1.67 \times 10^{-2}$ %

σ_Z $\frac{\Delta R}{R} = 1.97 \times 10^{-2}$ %

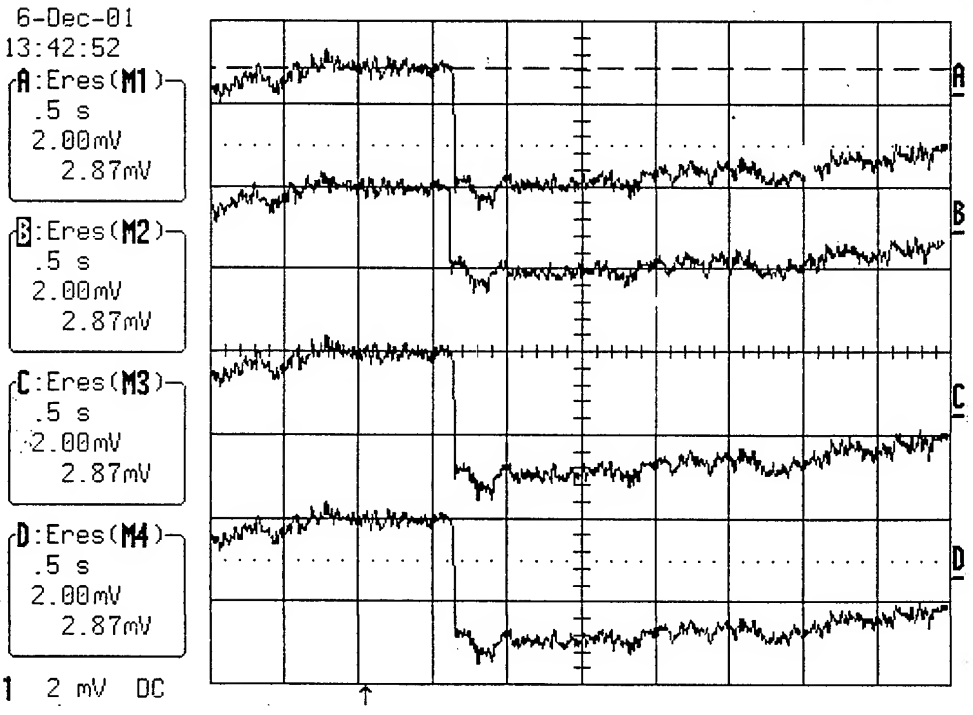

Fig. 27

H.V.D.R STATIC CAL. TEST

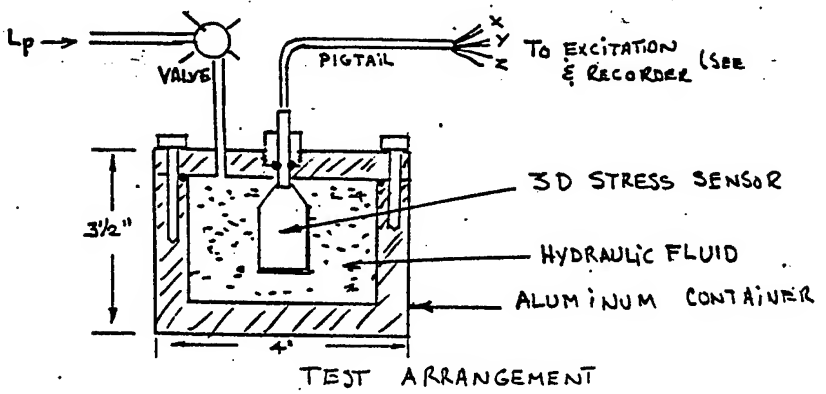

TEST ARRANGEMENT

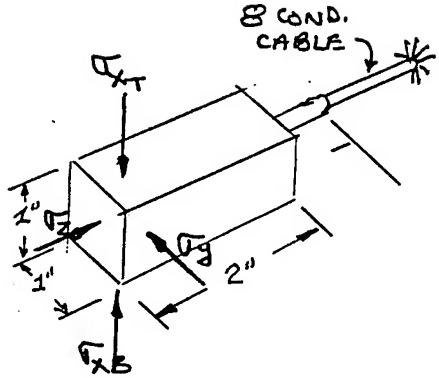

3D SENSOR FLUID-COUPLED #1

σy GAUGE DAMAGED

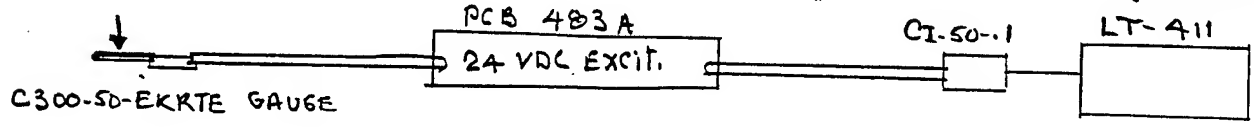

EXCITATION & RECORDING

DATE 12/06/01 TEST # 12/06/01 T3 TEST PRESS 75 PSI

GAUGE	R, Ω BEFORE TEST	R, Ω AFTER TEST	ΔV, EXCIT. BEFORE TEST	ΔV, EXCIT. AFT. TEST	ΔV, SIGNAL	
σ_{xT} BLACK-WHITE			17.576	17.573	.0046	
σ_y BLUE/LAVENDER			17.064	17.069	.0034	
σ_{xB} YELLOW/ORANGE			17.739	17.746	.0046	
σ_z GREEN/RED			15.965	15.871	.0046	

$$\frac{\Delta R}{R} = \frac{\Delta V_S}{\Delta V_E} \times 100\ \%$$

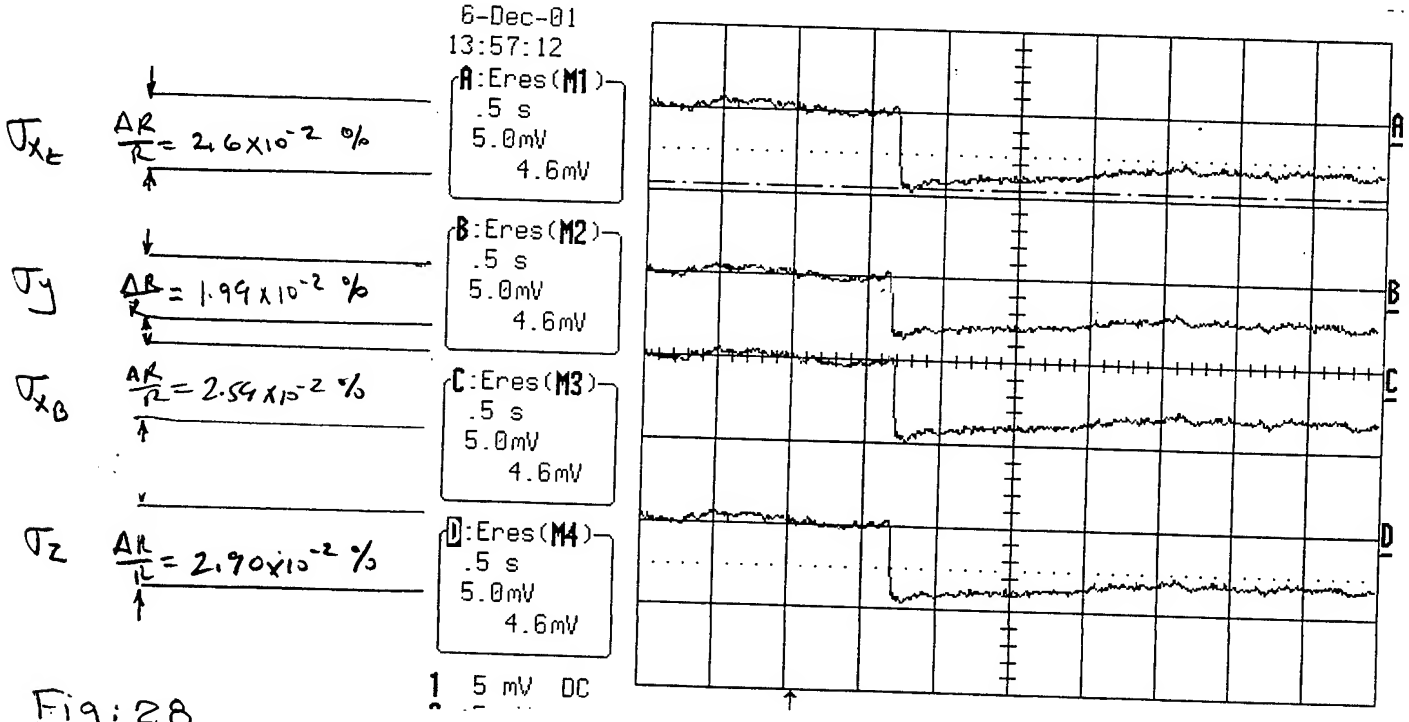

Fig: 28

HYDR STATIC CALIBRATION (12/06/01)

FLUID-COUPLED #1 3D SENSOR 17°C (σ_y GAUGE DAMAGED)

σ_{x_L}: ○ σ_y: X σ_{x_B}: ■ σ_z: ▲

Cal Date: 12/06/01

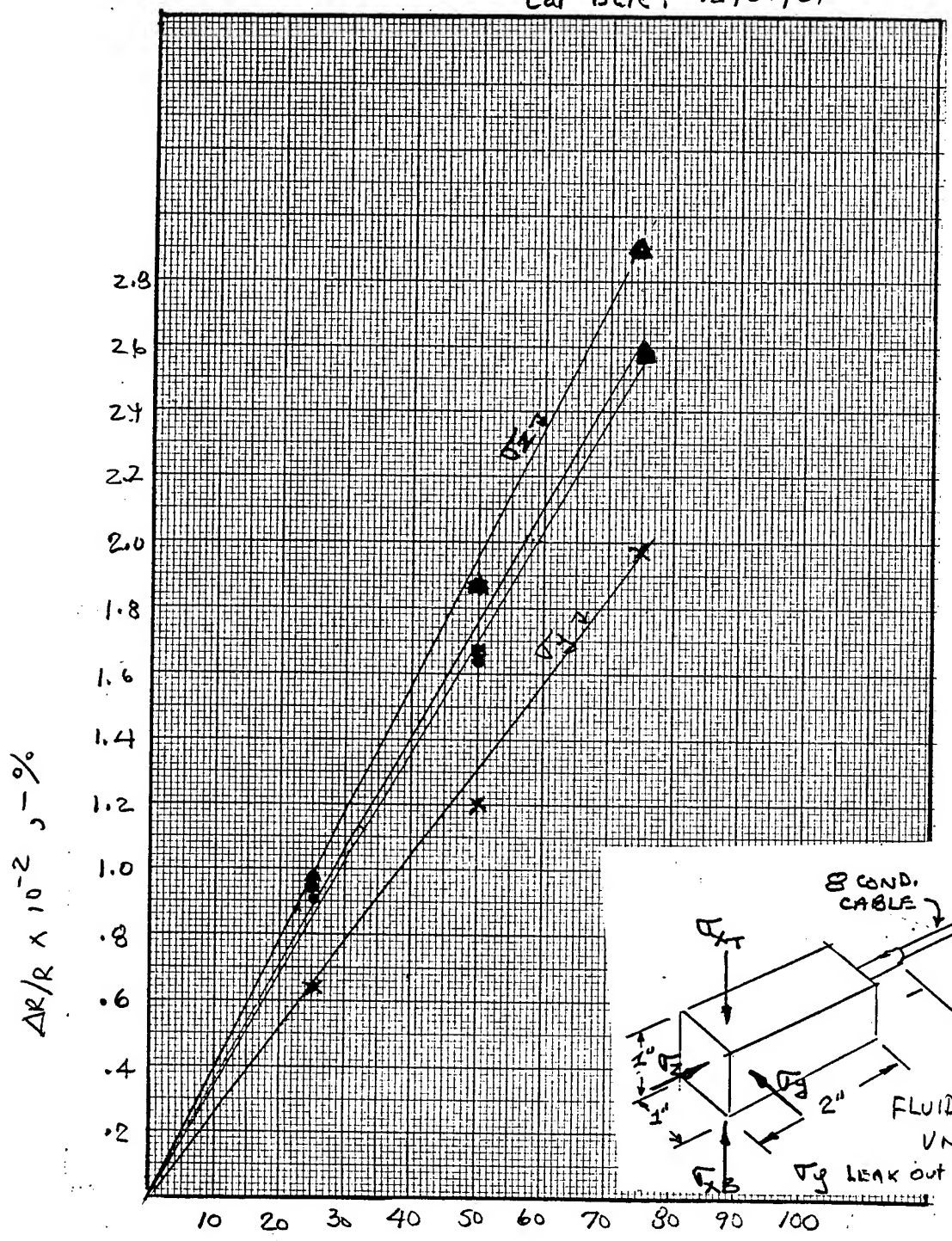

Fig. 29

SOIL TRANSDUCER TESTING

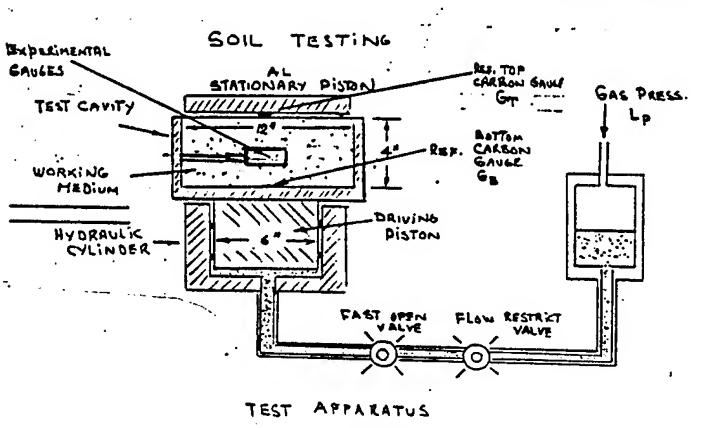

TEST APPARATUS

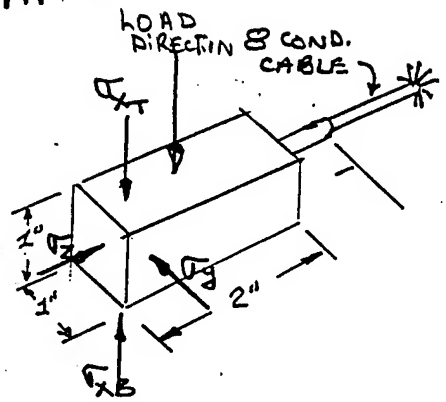

3D SENSOR

FLUID-COUPLED #1

σ_y GAUGE DAMAGED

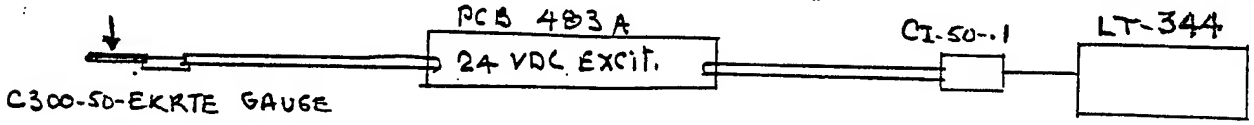

EXCITATION & RECORDING

DATE 12/06/01 TEMP. 19°C TEST #: 12/06/01 T1 TEST PRESS L_p: 200 PSI

1ST TEST AFTER INSTALLING GAUGE

GAUGE	R, Ω BEFORE TEST	R, Ω AFTER TEST	ΔV, EXCIT. BEFORE TEST	ΔV, EXCIT. AFT. TEST	ΔV, SIGNAL	
σ_{XT} BLACK/WHITE	1,834.4		17.627	17.663	.00305	
σ_y BLUE/LAVENDER	1,766.8		17.111	17.157	.00091	FLUID ESCAPED FROM σ_y NO GOOD
σ_{XB} YELLOW/ORANGE	1,846.0		17.734	17.830	.0036	
σ_z GREEN/RED	1,640.8		15.901	15.94	.00141	

$$\frac{\Delta R}{R} = \frac{\Delta V_s}{\Delta V_e} \times 100, \%$$

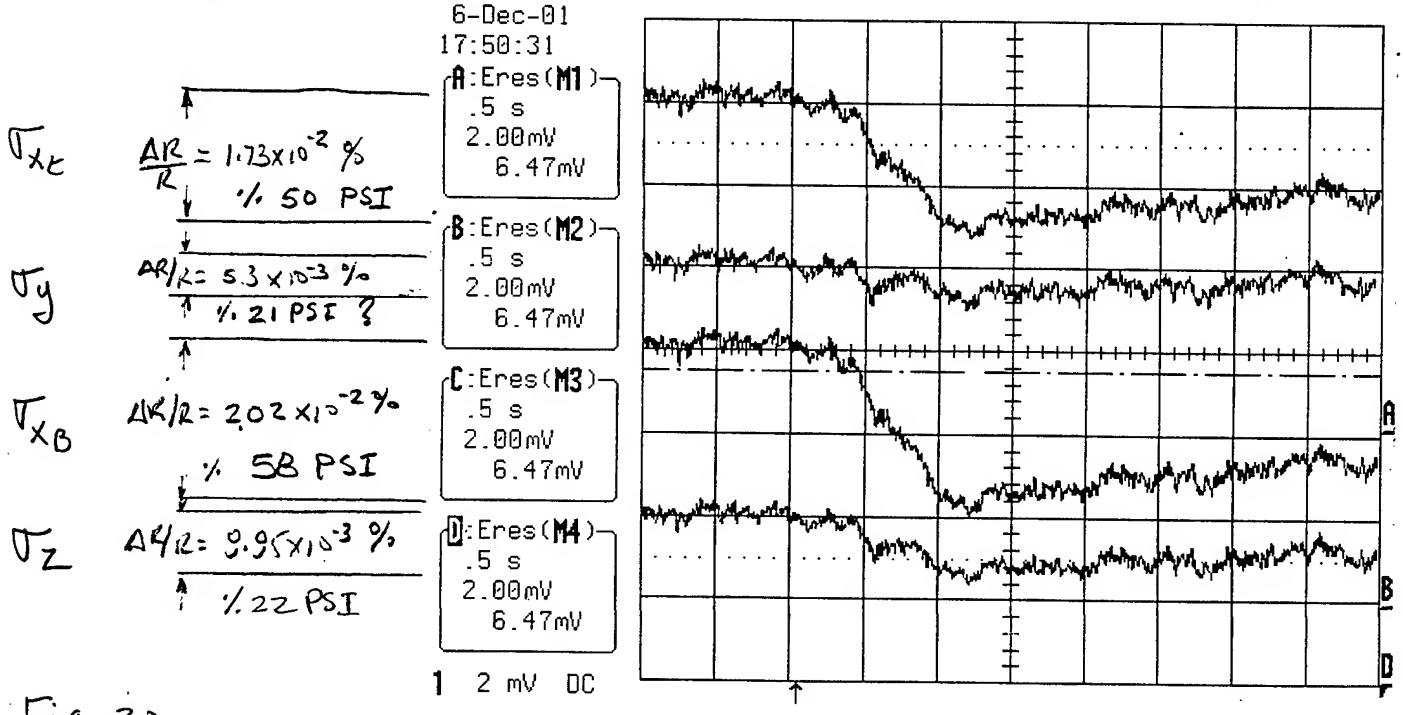

Fig. 30

SOIL TRANSDUCER TESTING

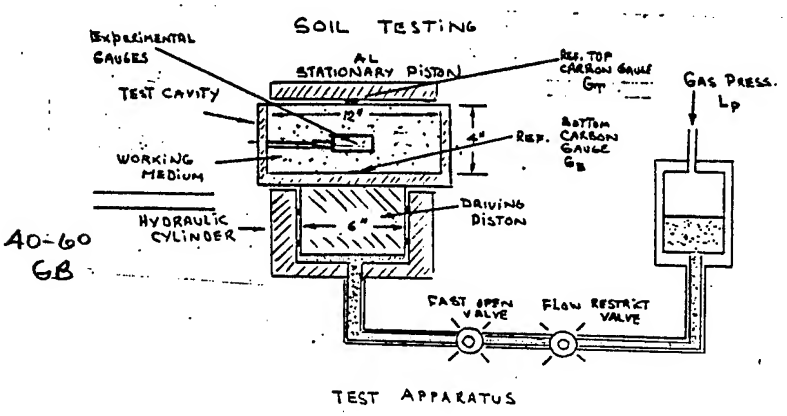

TEST APPARATUS

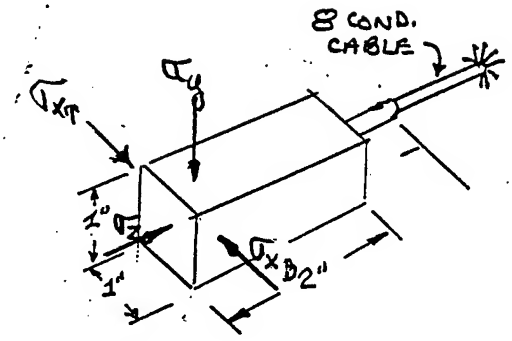

3D SENSOR

FLUID-COUPLED #1

σ_y Gauge DAMAGED

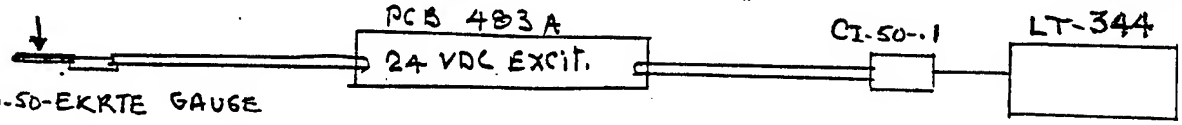

EXCITATION & RECORDING

DATE 12/07/01 TEMP. 16°C TEST #: 12/07/01 T1 TEST PRESS L_P: 200 PSI

1st TEST AFTER RE-DOING WORK BED

GAUGE	R, Ω BEFORE TEST	R, Ω AFTER TEST	ΔV, EXCIT. BEFORE TEST	ΔV, EXCIT. AFT. TEST	ΔV, SIGNAL	
σ_{XT} BLACK-white	1838.2	1,833.8	17.185	17.26	.00196	
σ_y BLUE/LAVENDER	1,7707	1,766.7	16.686	16.77		σ_y LEAKED FLUID DOES NOT WORK.
σ_{XB} YELLOW/ORANGE	1,849.9	1,845.7	17.337	17.43	.00178	
σ_z GREEN/RED	1,644.0	1,640.3	15.493	15.57	.00182	

$\frac{\Delta R}{R} = \frac{\Delta V_S}{\Delta V_E} \times 100\ \%$

SEE Cal. of 12/06/01 For FLUID-Coupled #1

σ_{XT} $\frac{\Delta R}{R} = 1.14 \times 10^{-2}\ \%$ ~ 32 PSI

σ_y No Data BECAUSE of LEAK

σ_{XB} $\frac{\Delta R}{R} = 1.02 \times 10^{-2}\ \%$ ~ 30 PSI

σ_z $\frac{\Delta R}{R} = 1.17 \times 10^{-2}\ \%$ ~ 29 PSI

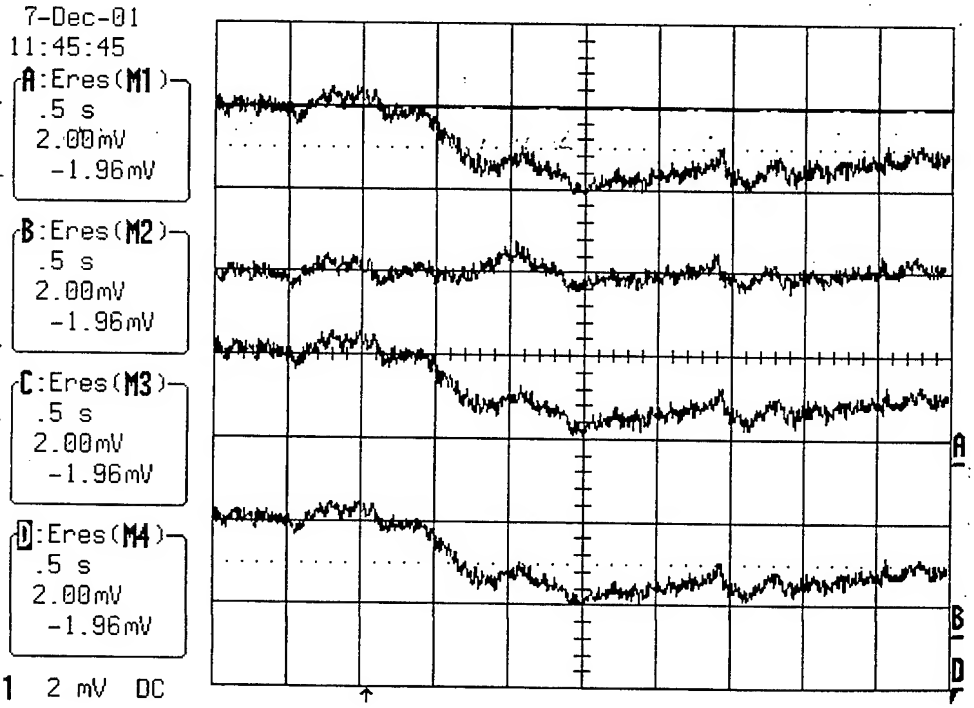

Fig. 31

SEE OTHER SIDE for SUPERIMPOSED DATA of σ_{XT}, σ_{XB} & σ_z

H.1 # H.V.D.R STATIC CAL. TEST

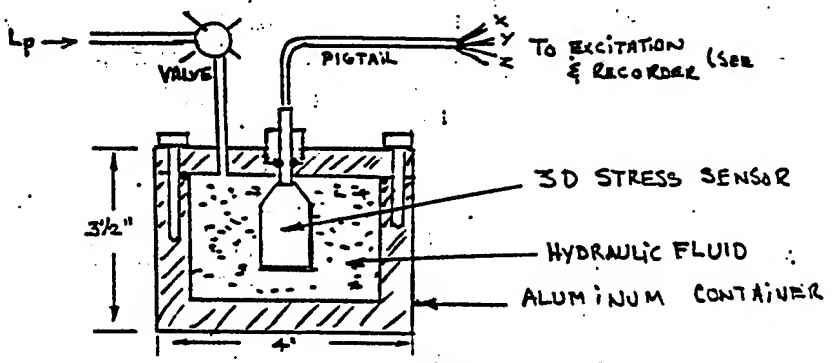

TEST ARRANGEMENT

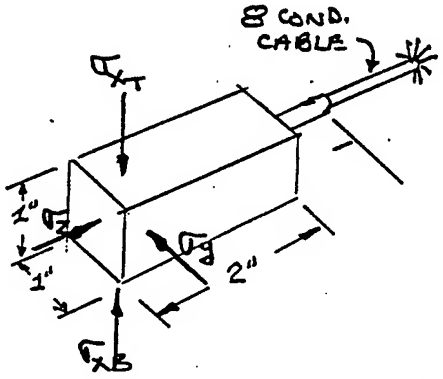

3D SENSOR FLUID-COUPLED #1
AFTER RE-Built σy & σz

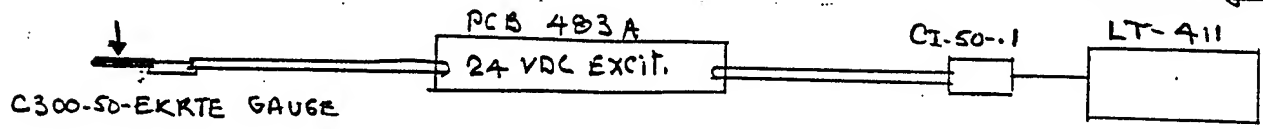

EXCITATION & RECORDING

DATE 12/17/01 14°C TEST #: 12/17/01 T1 TEST PRESS 25 PSI

GAUGE	R, Ω BEFORE TEST	R, Ω AFTER TEST	ΔVε EXCIT. BEFORE TEST	ΔV, EXCIT. AFT. TEST	ΔVs SIGNAL	
σXT BLACK-WHITE	1841.0		17.300 V	17.360 V	.00132 V	
σy BLUE/LAVENDER	1,773.0		16.840 V	16.900 V	.00128 V	
σXB YELLOW/ORANGE	1,855.0		17.480V	17.540 V	.00141 V	
σZ GREY/RED	1648.0		15.620 V	15.67 V	.00137 V	

$\frac{\Delta R}{R} = \frac{\Delta V_s}{\Delta V_\varepsilon} \times 100$; %

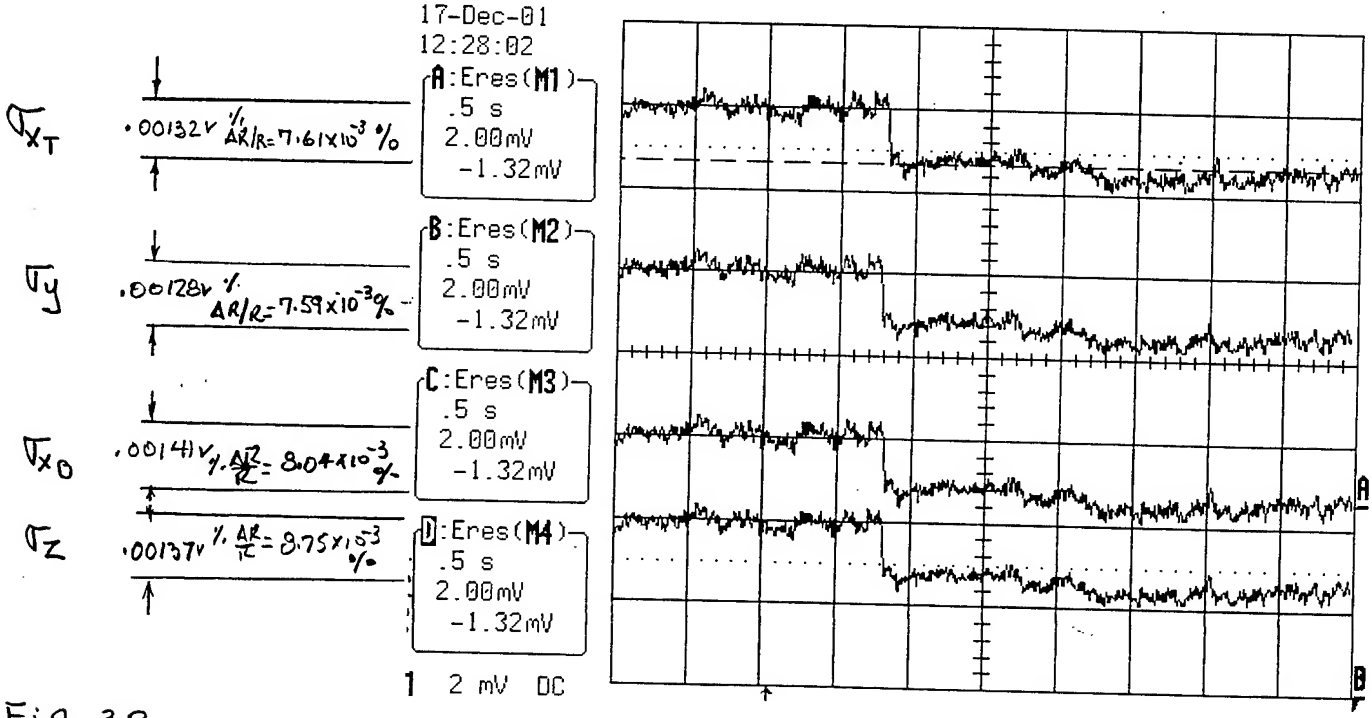

Fig. 32

SEE OTHER SIDE FOR SUPER IMPOSED TRACES

H.V.DR STATIC CAL. TEST

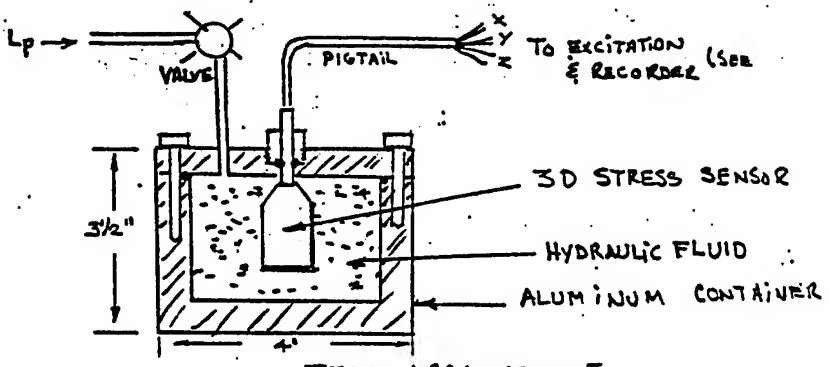

TEST ARRANGEMENT

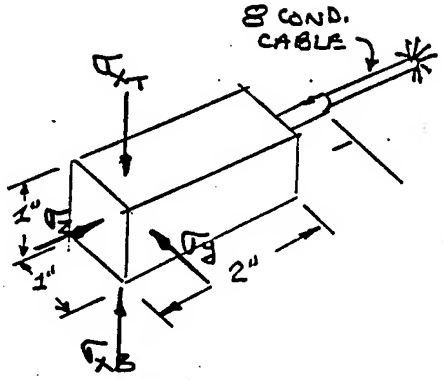

3D SENSOR FLUID-COUPLED #1
RE-Built σ_y, σ_z

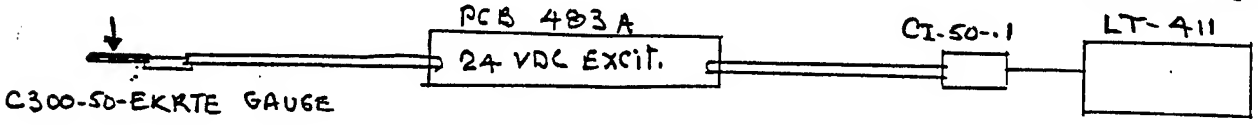

EXCITATION & RECORDING

DATE 12/17/01 14°C TEST #: 12/17/01 T2 TEST PRESS 50 PSI

GAUGE	R, Ω BEFORE TEST	R, Ω AFTER TEST	ΔV_E, EXCIT. BEFORE TEST	ΔV_E, EXCIT. AFT. TEST	ΔV_S, SIGNAL	
σ_{xT} BLACK-WHITE	1841.0		17.43 V		.00237 V	
σ_y BLUE/LAVENDER	1,773.0		16.97 V		.00237 V	
σ_{xB} YELLOW/ORANGE	1,855.0		17.61 V		.00251 V	
σ_z GREEN/RED	1,648.0		15.74 V		.00260 V	

$\frac{\Delta R}{R} = \frac{\Delta V_S}{\Delta V_E} \times 100_3$ %

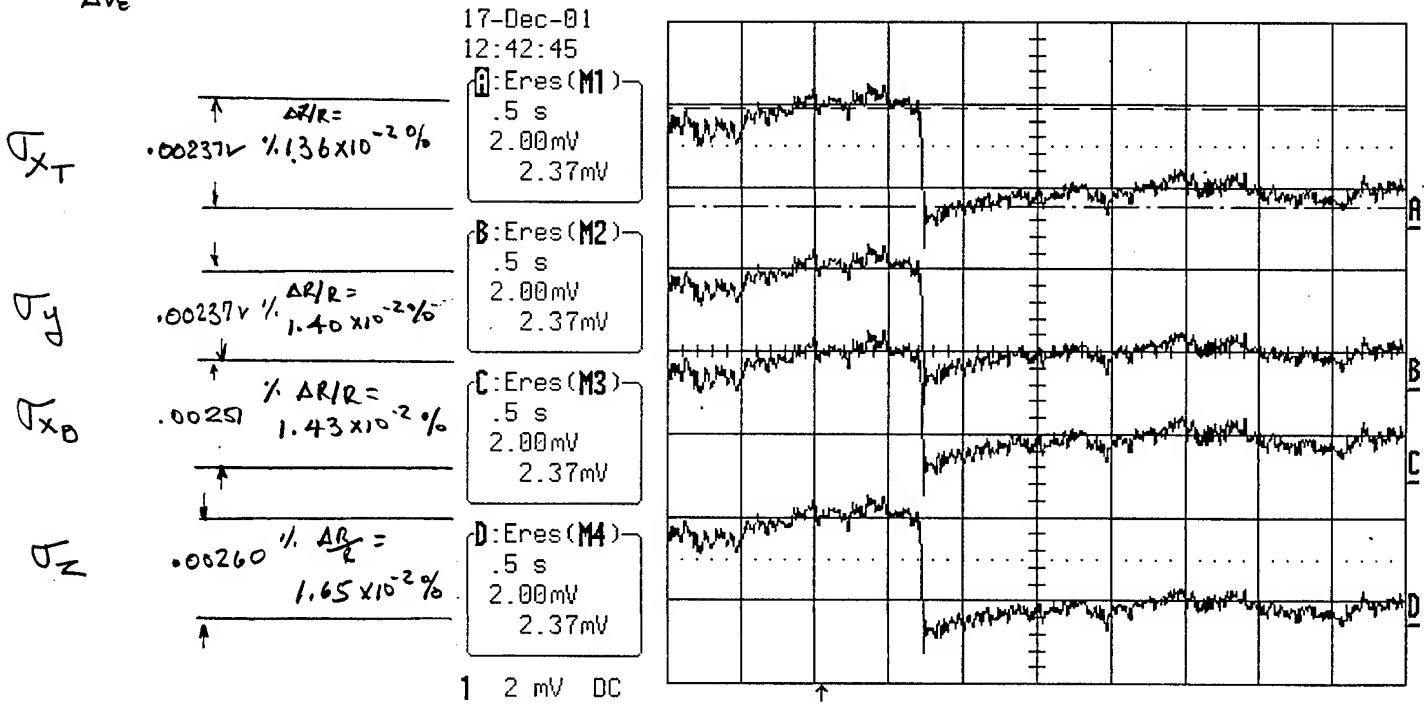

Fig. 33

SEE OTHER SIDE FOR SUPERIMPOSED TRACES

H.V.DR STATIC CAL. TEST

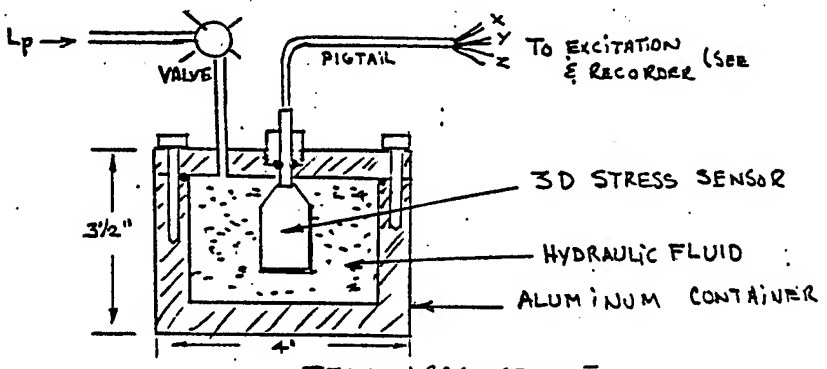

TEST ARRANGEMENT

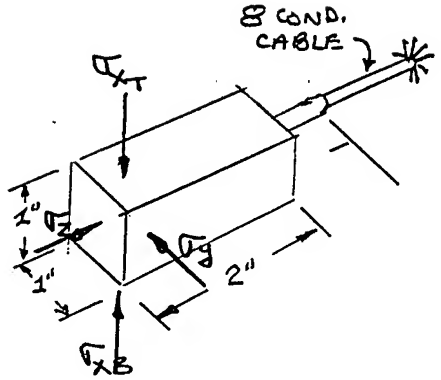

3D SENSOR FLUID—COUPLED #1

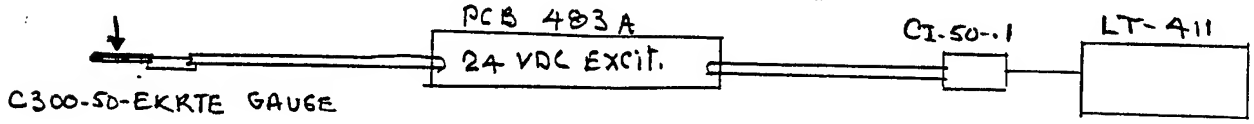

EXCITATION & RECORDING

DATE 12/17/01 14°C TEST#: 12/17/01 T3 TEST PRESS 75 PSI

GAUGE	R, Ω BEFORE TEST	R, Ω AFTER TEST	ΔV, EXCIT. BEFORE TEST	ΔV, EXCIT. AFT. TEST	ΔV, SIGNAL	
σ_{xT} BLACK-WHITE	1,841.0		17.47		.00383	
σ_y BLUE/LAVENDER	1,723.0		17.00		.00383	
σ_{xB} YELLOW/ORANGE	1,855.0		17.65		.00383	
σ_z GREEN/RED	1,648.0		15.78		.00383	

$$\frac{\Delta R}{R} = \frac{\Delta V_S}{\Delta V_E} \times 100, -\%$$

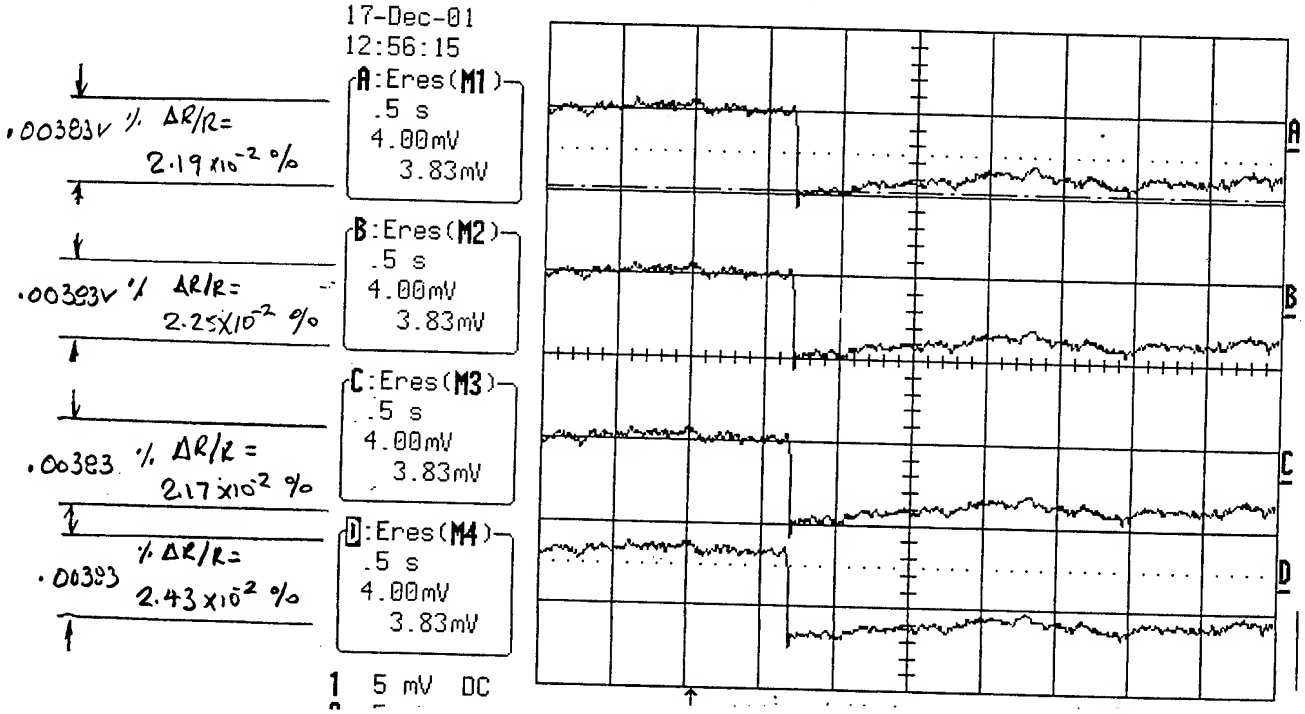

Fig. 34

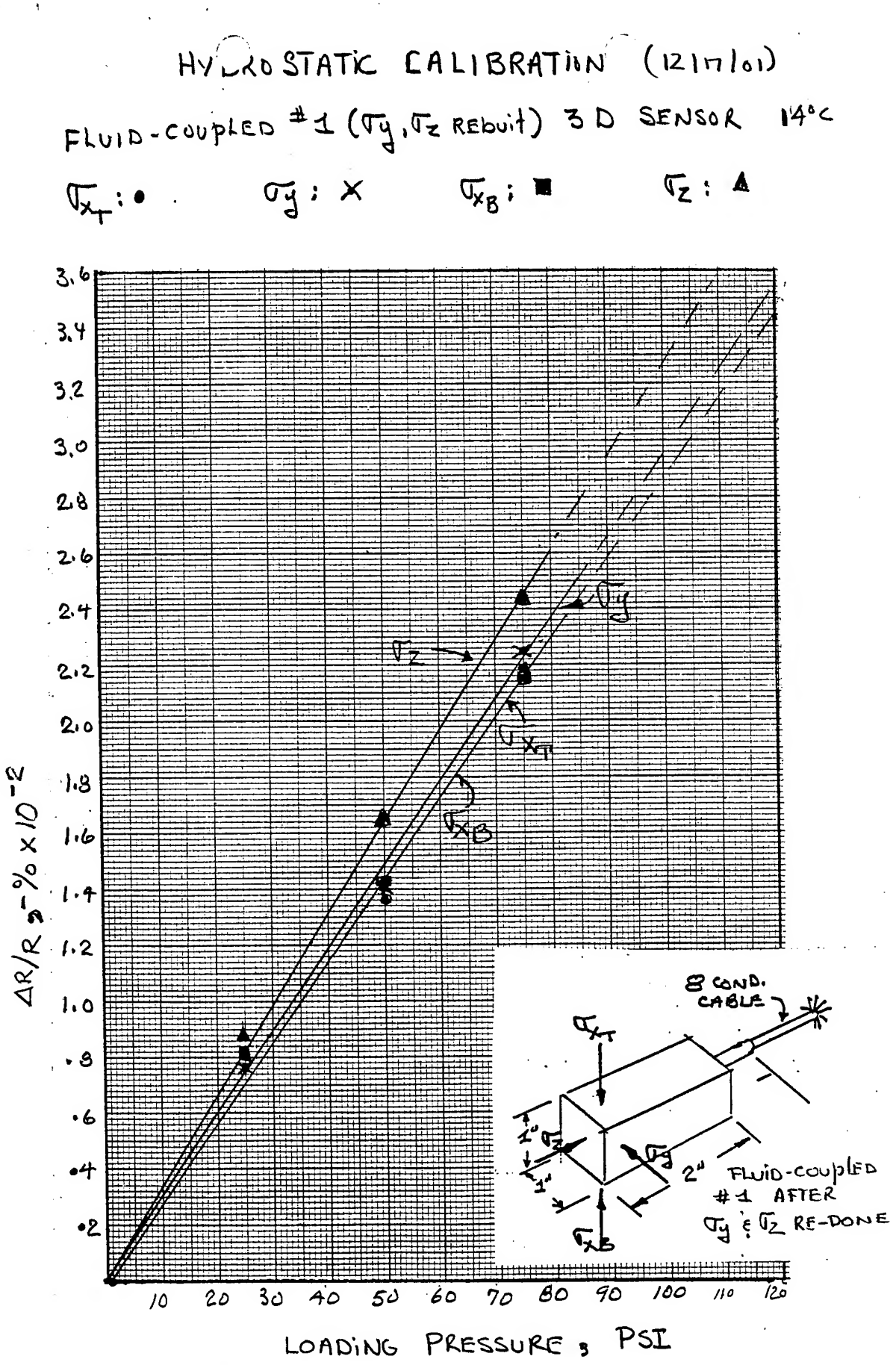

Fig. 35. Hydro-Static Calibration of Repaired 3D Fluid-Coupled Sensor

SOIL TRANSDUCER TESTING

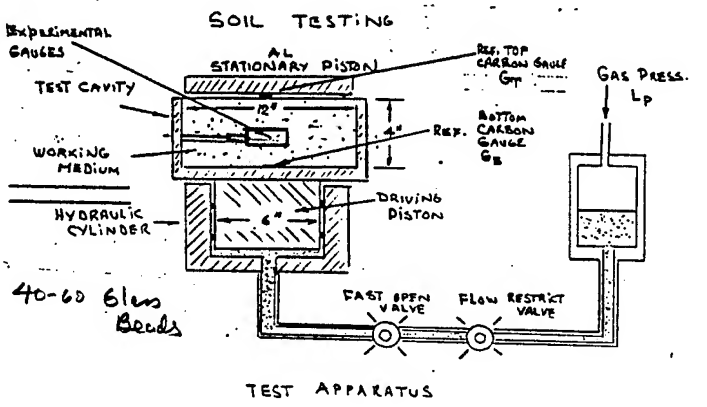

TEST APPARATUS

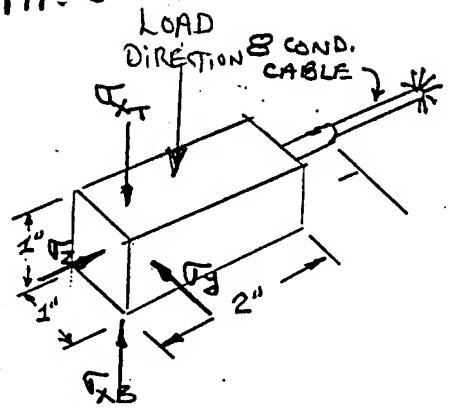

3D SENSOR FLUID-COUPLED #1

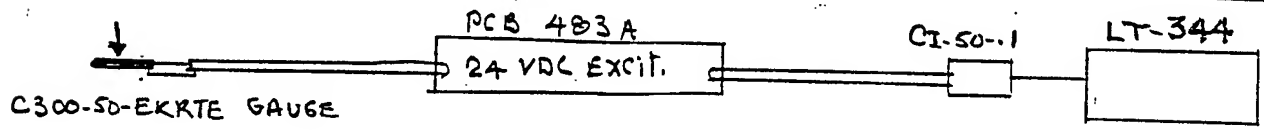

EXCITATION & RECORDING

DATE 12/17/01 TEMP. 17°C TEST #: 12/17/01 T2 TEST PRESS L_P: 200 PSI

GAUGE	R, Ω BEFORE TEST	R, Ω AFTER TEST	ΔV, EXCIT. BEFORE TEST	ΔV, EXCIT. AFT. TEST	ΔV, SIGNAL	TEST FOLLOWS TEST 12/17/01 T1 without
σ_{xT} Black-White	1,843.6	1840.9	17.67 v		.00287	DISTURBING TEST BED
σ_y Blue/Lavender	1,779.6	1,777.1	17.19 v		.00150	
σ_{xB} Yellow/Orange	1,856.6	1,853.9	17.84 v		.00383	
σ_z Grey/Red	1,648.7	1,646.6	15.94		.00146	

$\Delta R/R = \frac{\Delta V_S}{\Delta V_E} \times 100, \%$

σ_{xT}: $\frac{\Delta R}{R} = \frac{.00287}{17.67} = 1.62 \times 10^{-2}\%$ ≈ 56 PSI

σ_y: $\frac{\Delta R}{R} = \frac{.0015}{17.19} = 873 \times 10^{-3}\%$ ≈ 29 PSI

σ_{xB}: $\frac{\Delta R}{R} = \frac{.00383}{17.84} = 215 \times 10^{-2}\%$ ≈ 74 PSI

σ_z: $\frac{\Delta R}{R} = \frac{.00146}{15.94} = 916 \times 10^{-3}\%$ ≈ 29 PSI

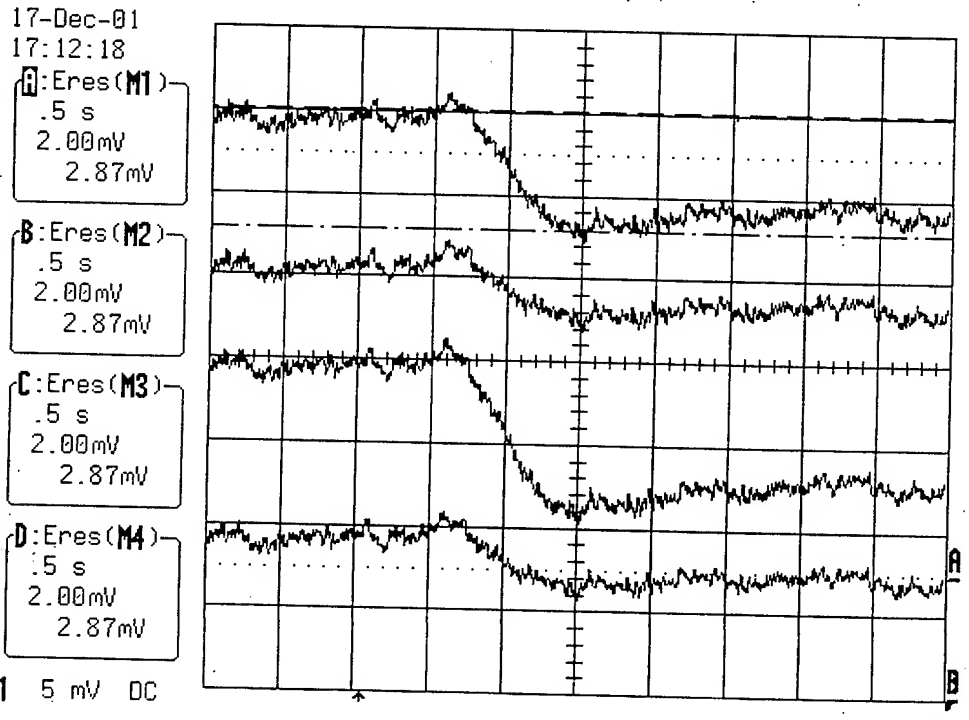

Fig. 36

SEE OTHER SIDE FOR SUPERIMPOSED TRACES

SOIL TRANSDUCER TESTING

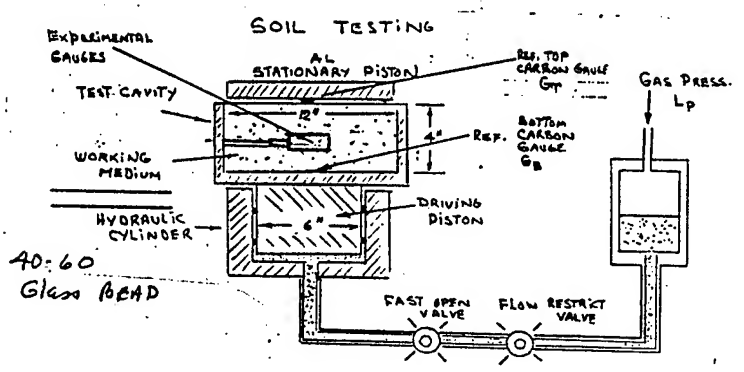

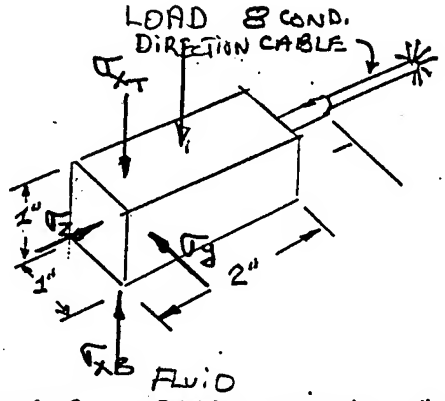

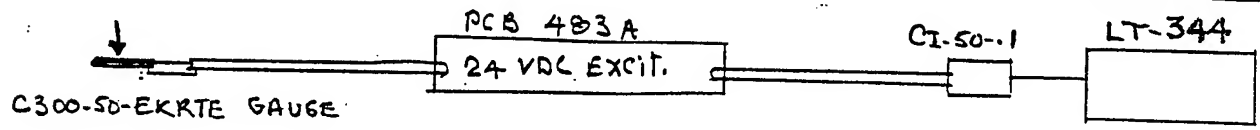

EXCITATION & RECORDING

DATE 12/17/01 TEMP. ~16 °C TEST #: 12/17/01 T1 TEST PRESS, L_P: 200 PSI

GAUGE	R, Ω BEFORE TEST	R, Ω AFTER TEST	ΔV, EXCIT. BEFORE TEST	ΔV, EXCIT. AFT. TEST	ΔV, SIGNAL	1ST TEST AFTER MAKING
σ_{xT} Black-White	1844.3	1841.0	17.63		.00246	TEST BED
σ_y Blue/Lavender	1,780.4	1777.4	17.16		.00114	with 40-60 GB.
σ_{xB} Yellow/Orange	1,857.3	1,854.4	17.80		.00356	
σ_z Grey/Red	1649.7	1647.0	15.91		.00109	

$$\frac{\Delta R}{R} = \frac{\Delta V_S}{\Delta V_E} \times 100, \%$$

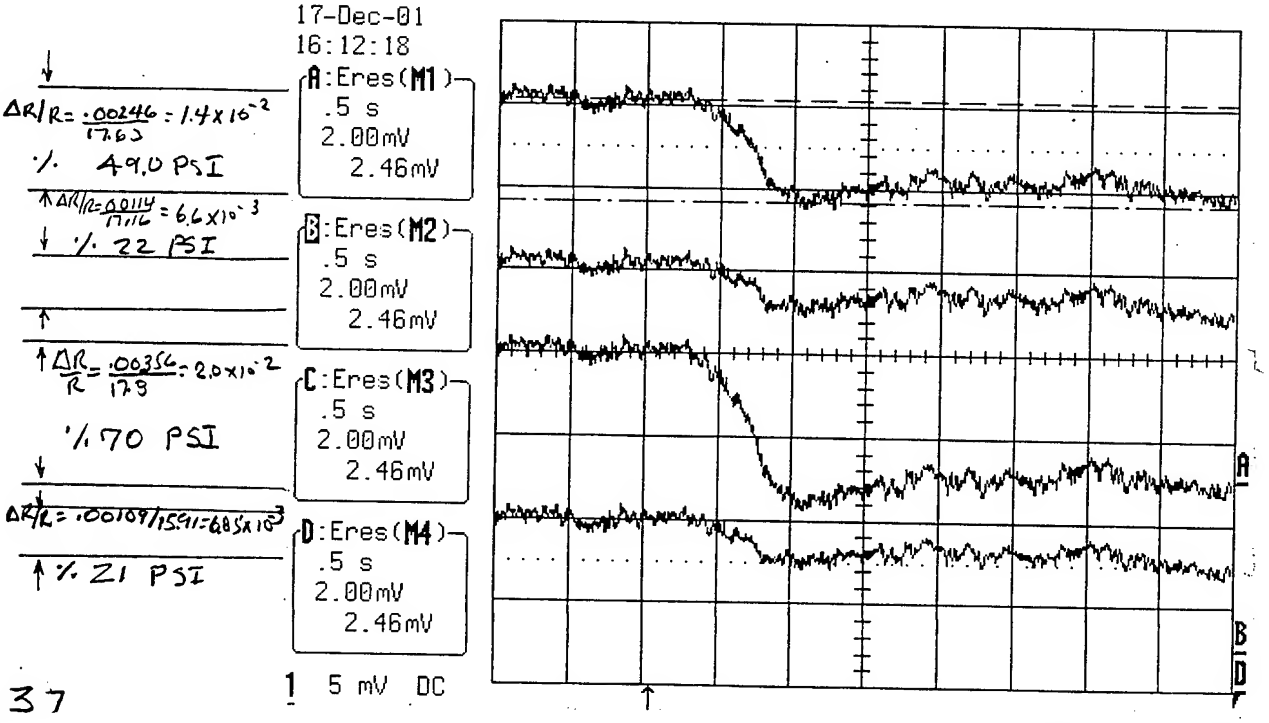

Fig. 37

SEE OTHER SIDE FOR SUPERIMPOSED TRACES

SOIL TRANSDUCER TESTING

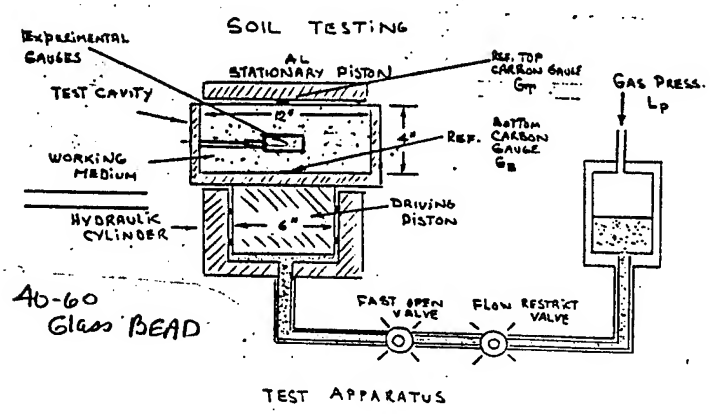

TEST APPARATUS

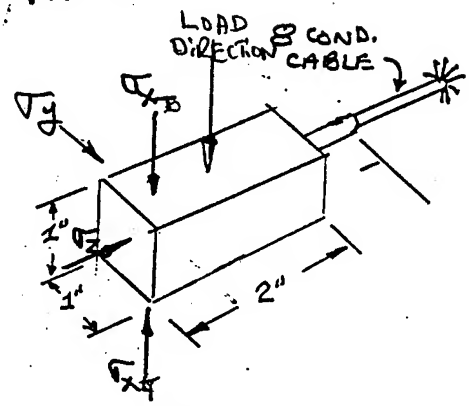

3D SENSOR

FLUID-COUPLED #1
σy & σz REBUILT

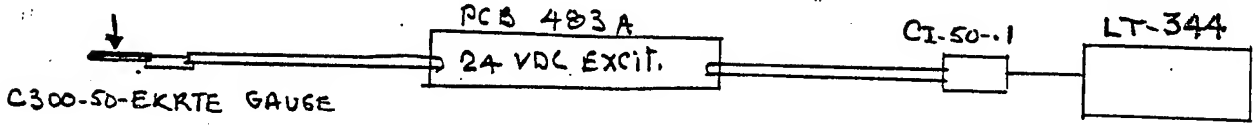

EXCITATION & RECORDING

DATE 12/18/01 15°C TEST#: 12/18/01 T1 TEST PRESS 200 PSI

GAUGE	R, Ω BEFORE TEST	R, Ω AFTER TEST	ΔV, EXCIT. BEFORE TEST	ΔV, EXCIT. AFT. TEST	ΔV SIGNAL	1ST TEST AFTER
σ_{xT} BLACK-WHITE	1844.7	1,841.7	17.100	17.16 V	.00392	MAKING TEST
σ_y BLUE LAVENDER	1780.6	1,777.8	16.64	16.70 V	.00146	WORKING BED
σ_{xB} YELLOW ORANGE	1,857.7	1,854.8	17.07	17.13 V	.00305	
σ_z GREEN RED	1649.4	1,646.5	15.42	15.48 V	.00109	

$$\frac{\Delta R}{R} = \frac{\Delta V_S}{\Delta V_E} \times 100, \%$$

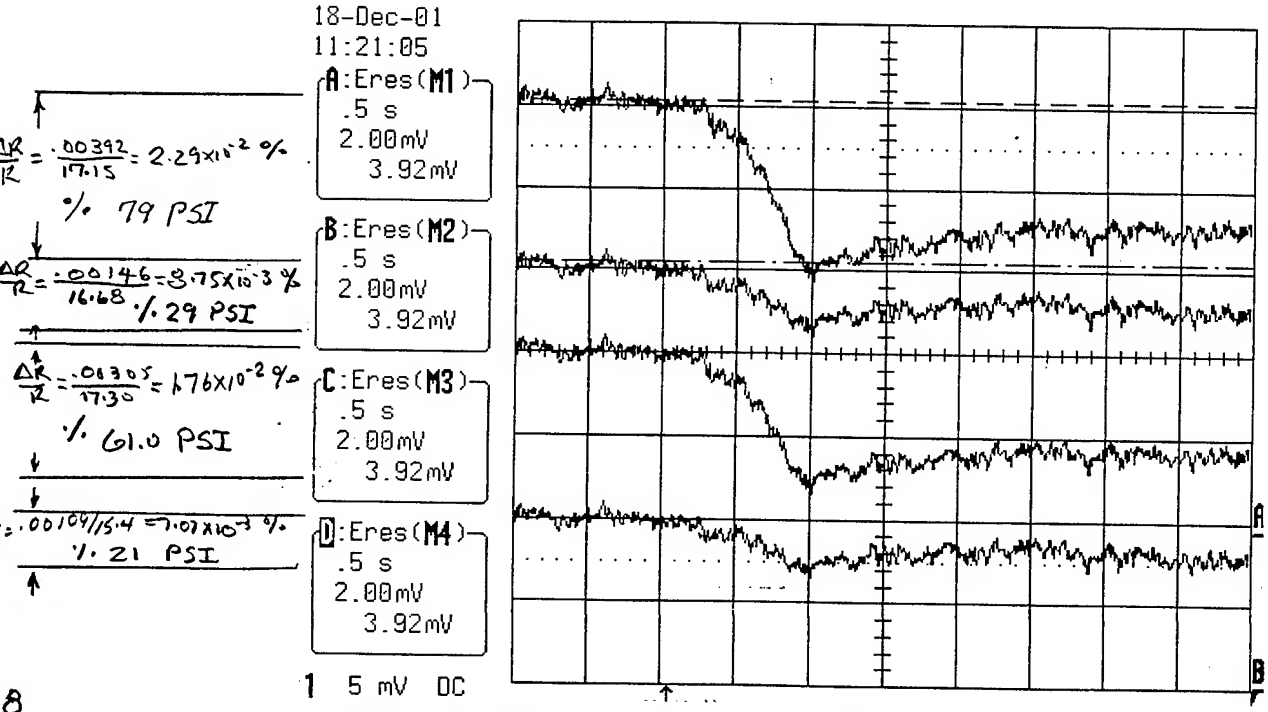

σ_{xT}: $\frac{\Delta R}{R} = \frac{.00392}{17.15} = 2.29 \times 10^{-2}$ % ≈ 79 PSI

σ_y: $\frac{\Delta R}{R} = \frac{.00146}{16.68} = 8.75 \times 10^{-3}$ % ≈ 29 PSI

σ_{xB}: $\frac{\Delta R}{R} = \frac{.00305}{17.30} = 1.76 \times 10^{-2}$ % ≈ 61.0 PSI

σ_z: $\frac{\Delta R}{R} = .00109/15.4 = 7.07 \times 10^{-3}$ % ≈ 21 PSI

Fig. 38

SEE OTHER SIDE FOR SUPERIMPOSED TRACES

SOIL TRANSDUCER TESTING

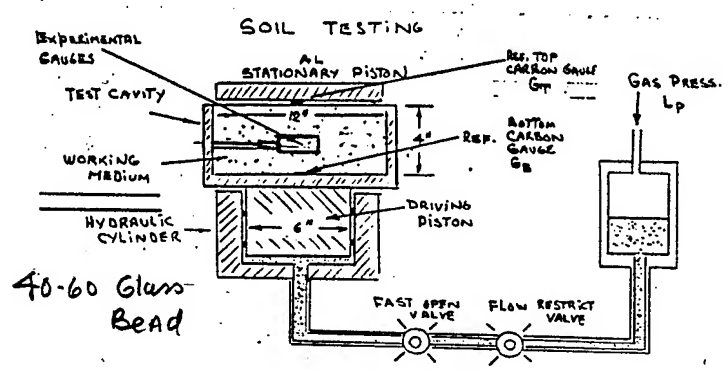

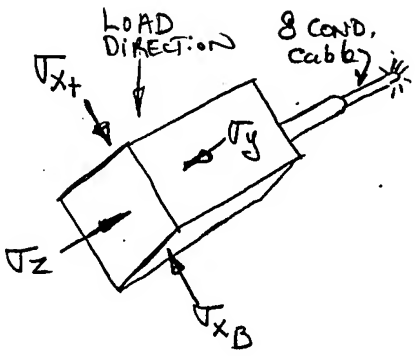

3D SENSOR FLUID-COUPLED #1

σ_y & σ_z REBUILT

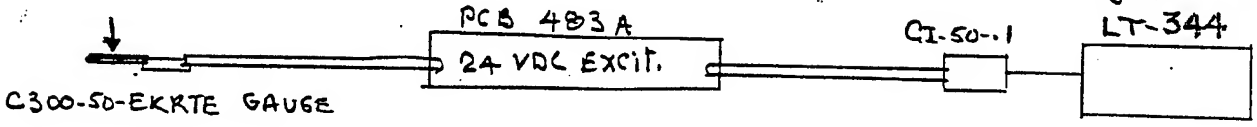

EXCITATION & RECORDING

DATE 12/18/01 TEMP. 17°C TEST #: 12/18.01 T1 TEST PRESS L_P: 200 PSI

GAUGE	R, Ω BEFORE TEST	R, Ω AFTER TEST	ΔV_E EXCIT. BEFORE TEST	ΔV_E EXCIT. AFT. TEST	ΔV_S SIGNAL	1ST TEST AFTER MAKING
σ_{XT} BLACK-WHITE	1,843.3	1840.0	17.65 V	17.70	.00242	TEST BED
σ_y BLUE/LAVENDER	1,779.3	1,776.3	17.17	17.22	.00182	
σ_{XB} YELLOW/ORANGE	1,856.4	1853.0	17.82	17.88	.00246	
σ_z GREEN/RED	1,649.1	1,645.4	15.91	15.98	.00114	

$$\frac{\Delta R}{R} = \frac{\Delta V_S}{\Delta V_E} \times 100, \%$$

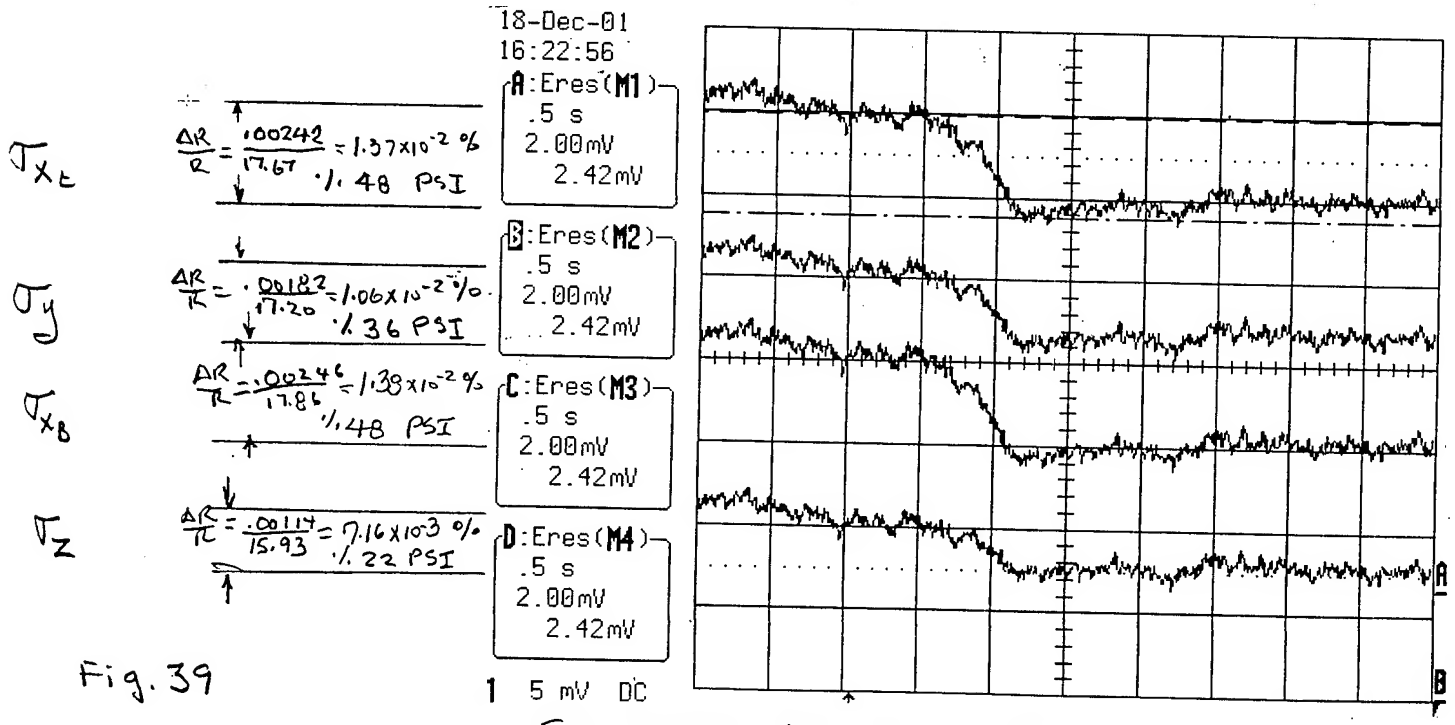

σ_{XT}: $\frac{\Delta R}{R} = \frac{.00242}{17.67} = 1.37 \times 10^{-2}\%$ ≈ 1.48 PSI

σ_y: $\frac{\Delta R}{R} = \frac{.00182}{17.20} = 1.06 \times 10^{-2}\%$ ≈ 1.36 PSI

σ_{XB}: $\frac{\Delta R}{R} = \frac{.00246}{17.86} = 1.38 \times 10^{-2}\%$ ≈ 1.48 PSI

σ_z: $\frac{\Delta R}{R} = \frac{.00114}{15.93} = 7.16 \times 10^{-3}\%$ ≈ 1.22 PSI

Fig. 39

SEE OTHER SIDE FOR SUPERIMPOSED DATA

SOIL TRANSDUCER TESTING

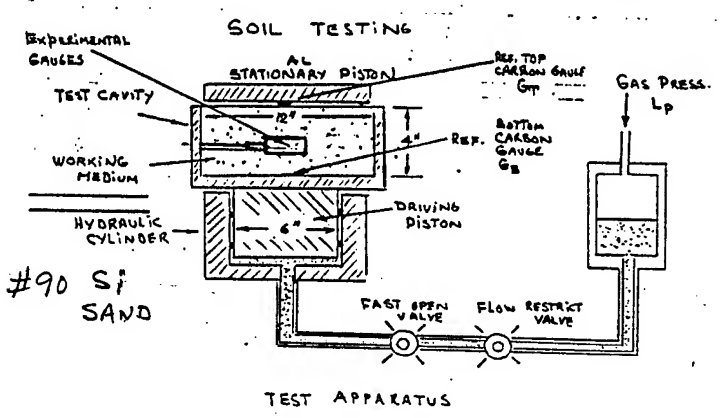

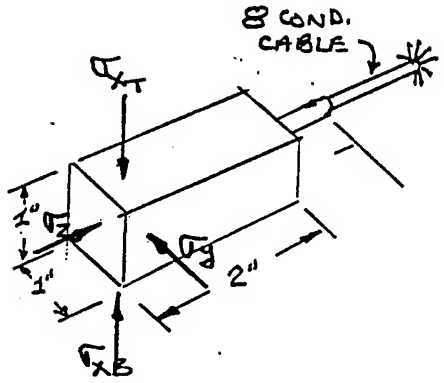

3D SENSOR FLUID-COUPLED #1

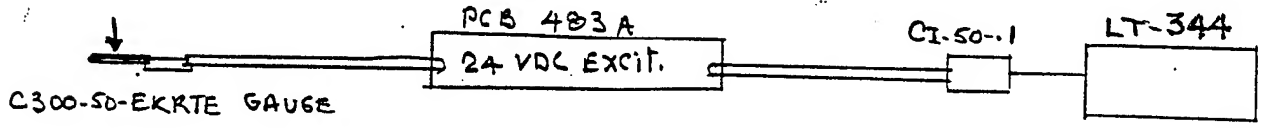

EXCITATION & RECORDING

DATE 12/19/01 TEMP. 17°C TEST #: 12/19.01 T7 TEST PRESS L_P: 200 PSI

GAUGE	R, Ω BEFORE TEST	R, Ω AFTER TEST	ΔV, EXCIT. BEFORE TEST	ΔV, EXCIT. AFT. TEST	ΔV. SIGNAL	1ST TEST AFTER DOING
σ_{XT} BLACK-WHITE	1,845.6	1,842.0	17.49	17.51	.00611	WORK BED IN
σ_y BLUE/LAVENDER	1,781.8	1,778.2	17.01	17.02	.00182	#90 SI SAND
σ_{XB} YELLOW/ORANGE	1,858.9	1,855.7	17.67	17.70	.00802	
σ_Z GREEN/RED	1,650.2	1,647.1	15.78	15.81	.00191	

$\frac{\Delta R}{R}$ =

σ_{XT} $\frac{\Delta R}{R} = \frac{.00611}{17.50} = 3.49 \times 10^{-2}$ % ≈ 122 PSI

σ_y $\Delta R/R = \frac{.00183}{1702} = 1.07 \times 10^{-2}$ % ≈ 36 PSI

σ_{XB} $\frac{\Delta R}{R} = \frac{.00802}{17.70} = 4.53 \times 10^{-2}$ % ≈ 167 PSI ESTIMATED

σ_Z $\Delta R/R = \frac{.00191}{15.80} = 1.21 \times 10^{-2}$ % ≈ 37 PSI

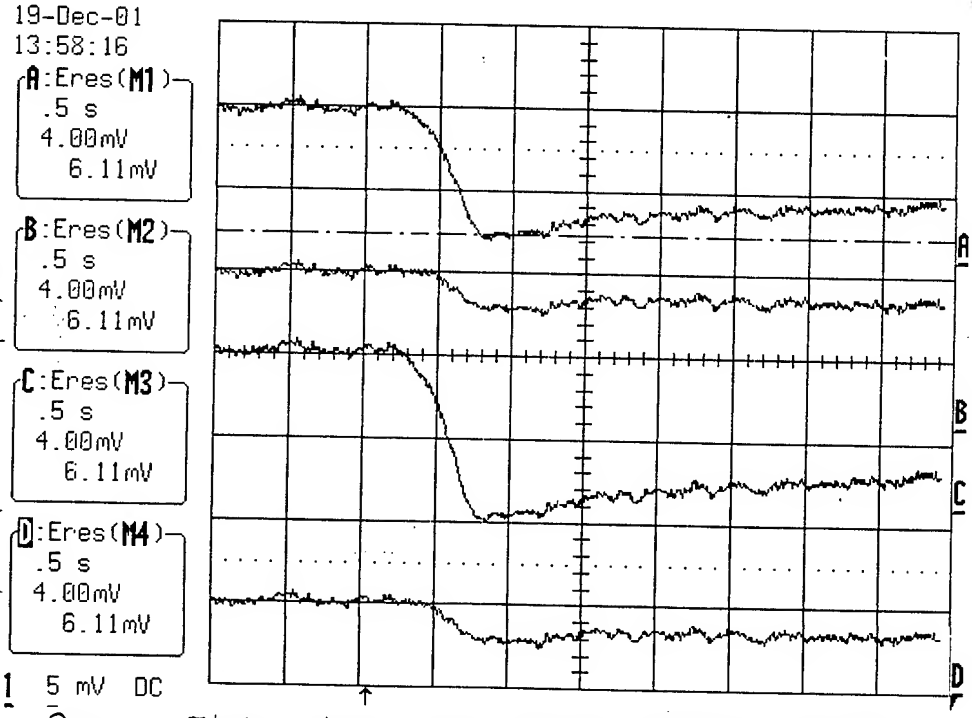

Fig. 40

SEE OTHER SIDE FOR SUPERIMPOSED TRACES

SOIL TRANSDUCER TESTING

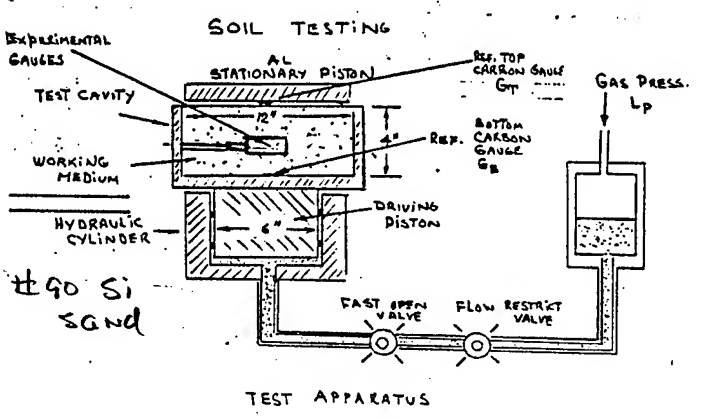

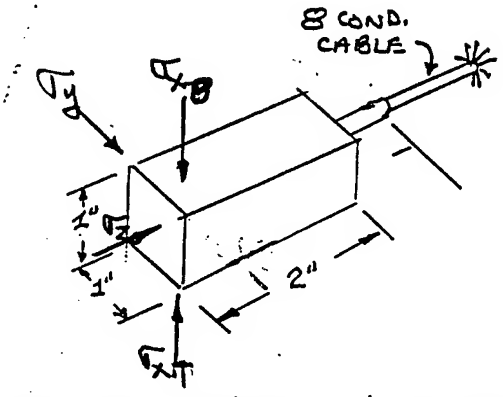

FLUID-COUPLED #1

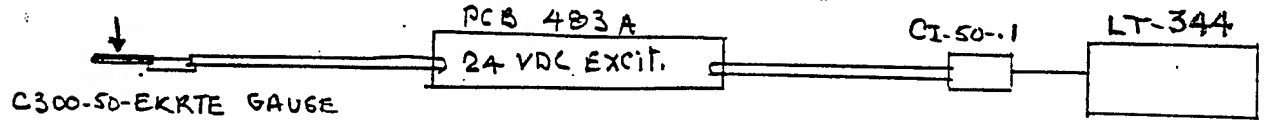

EXCITATION & RECORDING

DATE 12/19/01 TEMP. 18°C TEST #: 12/19/01 T2 TEST PRESS L_P: 200 PSI → 150

GAUGE	R, Ω BEFORE TEST	R, Ω AFTER TEST	ΔV, EXCIT. BEFORE TEST	ΔV, EXCIT. AFT. TEST	ΔV, SIGNAL	
σ_{xT} BLACK-WHITE	1,843.8	1840.3	17.64	17.67	.00839	1ST TEST AFTER
σ_y BLUE/LAVENDER	1,780.0	1776.3	17.16	17.20	.00229	RE DOING TEST BED
σ_{xB} YELLOW/ORANGE	1,857.1	1,853.2	17.81	17.86	.00638	WITH Si SAND #90
σ_z GREEN/RED	1,648.5	1,644.3	15.99	15.95	.00201	

$$\frac{\Delta R}{R} = \frac{\Delta V_S}{\Delta V_E} \times 100, \%$$

σ_{xt}: $\left(\frac{\Delta R}{R}\right) = \frac{.00839}{17.64} = 4.76 \times 10^{-2}\%$ ↓ 1.175 PSI

σ_y: $\frac{\Delta R}{R} = \frac{.00229}{17.16} = 1.33 \times 10^{-2}\%$ ↓ 1.47 PSI

σ_{xB}: $\frac{\Delta R}{R} = \frac{.00638}{17.85} = 3.57\%$ ↓ 123 PSI

σ_z: $\Delta R/R = \frac{.00201}{15.95} = 1.25 \times 10^{-2}\%$ ↓ 1.37 PSI

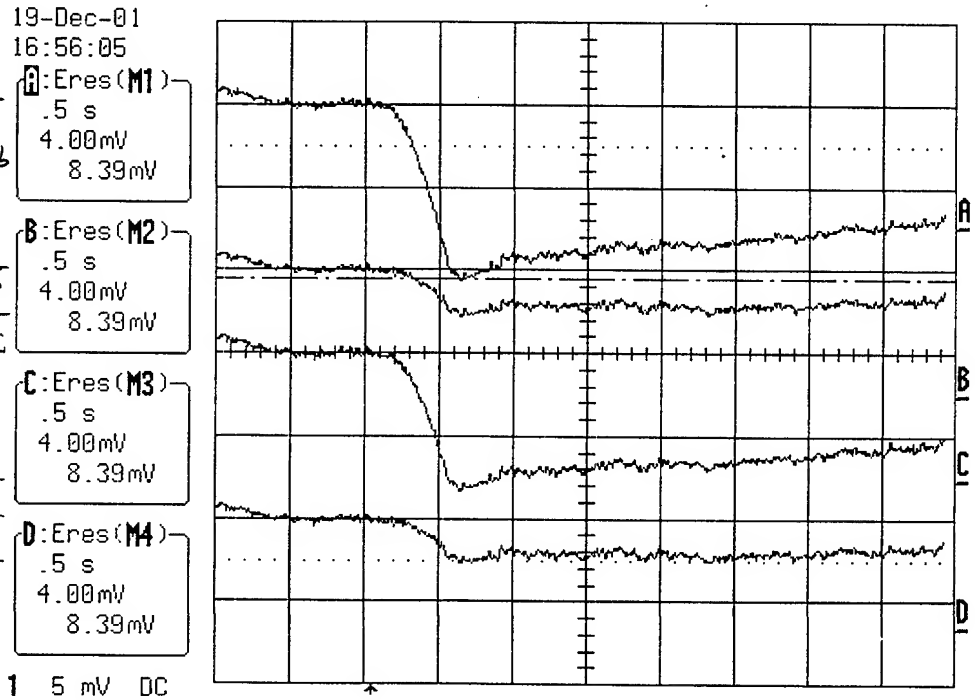

Fig. 41

SEE OTHER SIDE FOR SUPER-IMPOSED DATA